Negative microfilm
received from university

Mic 61-1726

BURNSTEIN, Raphael Aaron. THE PRODUCTION AND INTERACTION OF STRANGE PARTICLES PRODUCED BY 1.0-1.1 Bev π^- MESONS IN A XENON BUBBLE CHAMBER.

University of Michigan, Ph.D., 1961
Physics, nuclear

University Microfilms, Inc., Ann Arbor, Michigan

THE PRODUCTION AND INTERACTION OF STRANGE PARTICLES PRODUCED BY 1.0 - 1.1 Bev π^- MESONS IN A XENON BUBBLE CHAMBER

by
Raphael Aaron Burnstein

A dissertation submitted in partial fulfillment
of the requirements for the degree
of Doctor of Philosophy in
The University of Michigan
1960

Doctoral Committee:

Professor Donald A. Glaser, Chairman
Professor Kenneth M. Case
Assistant Professor Bernard A. Galler
Professor Wayne E. Hazen
Associate Professor George H. Trilling

ACKNOWLEDGEMENTS

Since this was a group endeavor, the author wishes to thank the many people who participated in this effort. He wishes to acknowledge the assistance of his colleagues, Howard Bryant, Richard Hartung, and James Van Putten.

In addition, the efforts of the following in the preparation of this dissertation were most helpful: Dr. John Brown, Dr. John Kadyk, Dolores Moebs, La Vaughn Karapostoles, and especially, Howard Bryant. The generous help of Professor George Trilling was most essential.

The author wishes to acknowledge the stimulating influence of Professor Donald Glaser and to thank him for his guidance.

TABLE OF CONTENTS

	Page
ACKNOWLEDGEMENTS	ii
LIST OF TABLES	vi
LIST OF FIGURES	vii
LIST OF APPENDICES	ix
CHAPTER I INTRODUCTION	1
1.1 Background	1
1.2 Rationale of Experiment and This Thesis	3
1.3 Strange Particle Production and Interactions	4
CHAPTER II APPARATUS AND THE EXPERIMENT	6
2.1 Xenon Bubble Chamber Design	6
2.2 Experimental Arrangement and the Run	14
CHAPTER III REDUCTION OF DATA	16
3.1 Description of Overall Procedure	16
3.2 Scanning of Film	18
3.3 Measurement	20
3.4 Computation	22
3.5 Analysis	24
3.6 Analysis Rules and Background Estimates	27

TABLE OF CONTENTS (Continued)

Page

CHAPTER IV DETERMINATION OF THE BASIC PARAMETERS OF THE EXPERIMENT AND CORRECTION FACTORS..... 29

4.1 Total Length of Pion Track..... 29

4.1.1 Beam Orientation..... 29
4.1.2 Beam Track Count Rules and Recount Procedure..... 31
4.1.3 Corrections for the Number of Good Pictures. 32
4.1.4 Corrections for Spatial Distribution of Beam..... 34
4.1.5 Average Length of Pion Track..... 36

4.2 Estimation of the Muon Contamination in Beam..... 37

4.2.1 Measurement of the Attenuation Length of the Beam in Xenon..... 37
4.2.2 Independent Pion Attenuation Length Measurement..... 38
4.2.3 Calculation of Muon Contamination..... 39
4.2.4 Lower Limit on Muon Contamination from Beam Geometry..... 39

4.3 Density of Xenon..... 41

4.4 Beam Energy Determination..... 42

4.5 Attenuation of Beam..... 50

4.6 Summary of Beam Properties and Corrections..... 51

4.7 Scanning Efficiency Corrections..... 52

4.7.1 Single Λ_+ and K^0_{1+} Efficiency..... 52
4.7.2 $\Lambda_+ K^0_{1+}$ Efficiency..... 52
4.7.3 $\Lambda_+ K^+$ Efficiency..... 53
4.7.4 Scanning Efficiency as a Function of the Track Count..... 53

4.8 Geometrical Corrections..... 54

4.9 Conversion Efficiency of γ From $\Sigma^\circ \rightarrow \Lambda + \gamma$..... 56

4.10 Correction for Σ° Contamination of ΛK° Events..... 58

4.11 Correction for Scattered V°..... 59

4.12 Correction for One-Legged Λ_+..... 60

TABLE OF CONTENTS (Continued)

Page

CHAPTER V EXPERIMENTAL RESULTS 62

5.1 Total Absolute Cross Sections 62

5.2 Corrected ΛK_1° and ΛK^+ Distributions 75

5.2.1 Corrected Momentum and Angular Distributions of ΛK_1° 75

5.2.2 Corrected Momentum and Angular Distributions of ΛK^+ 80

5.3 Energy and Momentum Balance in ΛK_1° and ΛK^+ 83

5.4 Interactions of K° Mesons 89

5.5 Polarization of Λ from ΛK_1° and ΛK^+ 102

APPENDIX A DENSITY OF LIQUID XENON 107

A.1 Direct Measurement of the Density 107

A.2 Measurements of the Critical Density 111

A.3 Range Energy Relations and the Density of Xenon 113

APPENDIX B $K_1^\circ - K_2^\circ$ MASS DIFFERENCE CALCULATION 115

APPENDIX C LISTS OF DATA 118

BIBLIOGRAPHY 124

LIST OF TABLES

Table	Title	Page
1	Masses and Mean Lives of Elementary Particles.....	2
2	Xenon Bubble Chamber Properties.....	8
3	Prongness of Neutral Stars.....	28
4	Distribution of Space Angles for Beam Tracks.....	30
5	Frames 4,000 - 67,119 (1.0 Bev π^-). Beam Count	33
6	Frames 67,200 - 139,999 (1.1 Bev π^-) Beam Count	33
7	Measurements of the Density of Xenon.....	41
8	Summary of Beam Properties and Corrections.....	51
9	Λ - K° Cross Section at 0.96 Bev.....	69
10	Λ - K° Cross Section at 1.05 Bev.....	70
11	Σ° - K° Cross Section at 0.95 Bev.....	71
12	Σ° - K° Cross Section at 1.05 Bev.....	72
13	Λ - Total K^+ Cross Section at 0.96 Bev.....	73
14	Expected Number of $\bar{K}^\circ$ Interactions.....	100
15	Asymmetry Parameter Determinations.....	106
16	π^+ Range From $K_{\pi 2}$ Decay.....	113
17	K° Interaction Data.....	118
18	Cross Section Samples.....	119

LIST OF FIGURES

Figure	Title	Page
1	Schematic Drawing of Xenon Bubble Chamber.....	7
2	Photograph of Gas Handling System Panel of Xenon Bubble Chamber.....	11
3	Photograph of Bevatron Experimental Area.....	15
4	Beam Energy Determination - Results of Experiment and Results of Monte Carlo Calculation.....	44
5	Corrected Λ Momentum Distributions for ΛK_1^0 from 1.0 and 1.1 Bev π^- Mesons.....	76
6	Corrected K_1^0 Momentum Distributions for ΛK_1^0 from 1.0 and 1.1 Bev π^- Mesons.....	77
7	Corrected Λ Angular Distributions for ΛK_1^0 from 1.0 and 1.1 Bev π^- Mesons.....	78
8	Corrected K_1^0 Angular Distributions for ΛK_1^0 from 1.0 and 1.1 Bev π^- Mesons.....	79
9	Corrected Λ and K^+ Momentum Distributions for ΛK^+ from 1.0 Bev π^- Mesons.....	81
10	Corrected Λ and K^+ Angular Distributions from ΛK^+ for 1.0 Bev π^- Mesons.....	82
11	Corrected ΔE Distributions for ΛK_1^0 for 1.0 and 1.1 Bev π^- Mesons.....	84
12	Corrected ΔE Distribution for ΛK^+ from 1.0 Bev π^- Mesons.	85
13	Corrected $\lvert\vec{p}_F\rvert$ Distributions from ΛK_1^0 for 1.0 and 1.1 Bev π^- Mesons.....	87

LIST OF FIGURES (Continued)

Figure	Title	Page
14	Corrected $\vec{p}_F \cdot \hat{x}$ Distributions from ΛK_1° for 1.0 and 1.1 Bev π^- Mesons	88
15	K° Interaction as Seen on Film	90
16	$\bar{K}^\circ$ Interaction as Seen on Film	91
17	$\bar{K}^\circ$ Amplitude as Function of Distance from Beam Origin	96
18	Likelihood Functions for Observed $\bar{K}^\circ$ Interactions	98

LIST OF APPENDICES

		Page
APPENDIX A	DENSITY OF LIQUID XENON.....	107
A.1	Direct Measurement of the Density.....	107
A.2	Measurements of the Critical Density.....	111
A.3	Range Energy Relations and the Density of Xenon.....	113
APPENDIX B	K_1° - K_2° MASS DIFFERENCE CALCULATION.....	115
APPENDIX C	LISTS OF DATA.....	118

CHAPTER I

INTRODUCTION

1.1 Background

A list of elementary particle properties has been reproduced in order to present the values of some of the physical constants used in the calculations. In addition, this list summarizes current experimental information on the different types of particles that have been observed. Data on anti-baryons has not been tabulated here nor have recent suggestions about other new particles been included.[1, 2]

Values of a new quantum number called "strangeness" have been inserted in Table 1. This quantity has been included because of its success in predicting allowed elementary particle reactions. The "strangeness" or S has been observed to take on the values 0, 1, -1, -2. Those particles for which $|S| > 0$ form a subclass of elementary particles called the "strange particles".

TABLE 1

MASSES AND MEAN LIVES OF ELEMENTARY PARTICLES[1]

CLASS	PARTICLE	SPIN	MASS (Mev)	MEAN LIFE (Sec)	STRANGENESS
PHOTON	γ	1	0.	Stable	0
LEPTONS	ν	1/2	0.	Stable	0
	e^+, e^-	1/2	0.510976 $\pm$ 0.000007	Stable	0
	μ^+, μ^-	1/2	105.70 $\pm$ 0.06	$(2.261 \pm 0.007) \times 10^{-6}$	0
MESONS	π^+, π^-	0	139.63 $\pm$ 0.06	$(2.56 \pm 0.05) \times 10^{-8}$	0
	π°	0	135.04 $\pm$ 0.16	$< 4 \times 10^{-16}$	0
	K^+, K^-	0	494.0 $\pm$ 0.2	$(1.224 \pm 0.13) \times 10^{-8}$	+1, -1
	K°, $\bar{K}^\circ$	0	497.9 $\pm$ 0.6	K_1°: $(1.00 \pm 0.38) \times 10^{-10}$ K_2°: $(6.1\ ^{+1.6}_{-1.1}) \times 10^{-8}$	+1, -1
BARYONS	p	1/2	938.213 $\pm$ 0.01	Stable	0
	n	1/2	939.506 $\pm$ 0.01	$(1.04 \pm 0.13) \times 10^{3}$	0
	Λ	1/2	1115.45 $\pm$ 0.12	$(2.505 \pm 0.086) \times 10^{-10}$	-1
	Σ^+	1/2	1189.55 $\pm$ 0.21	B. Chamber $(0.75 \pm 0.1) \times 10^{-10}$ Emulsion $(0.93 \pm 0.09) \times 10^{-10}$	-1
	Σ^-	1/2	1196.39 $\pm$ 0.34	$(1.59\ ^{+0.1}_{-0.09}) \times 10^{-10}$	-1
	Σ°	1/2	1191.94 $\pm$ 0.53	$< (0.1) \times 10^{-10}$	-1
	Ξ^-	?	1319.1 $\pm$ 0.5	$(1.9\ ^{+0.6}_{-0.4}) \times 10^{-10}$	-2
	Ξ°	?	1311 $\pm$ 8	1.5×10^{-10} (1 event)	-2

[1] Kiev Conference, July 1959; all the anti-particles have not been observed but the spin, masses and mean lives are assumed to be the same; errors represent a standard deviation.

1.2 Rationale of Experiment and This Thesis

The use of xenon as a bubble chamber liquid presented certain advantages over other materials. In this dense medium we expected to produce large numbers of strange particles and, in addition, the increased density made it more likely for particles in flight to interact. In the volume of high Z liquid available, it was possible to observe with high probability the conversion of γ rays into electron pairs and thereby gain information about the neutral decay modes of strange particles.

The experiment, performed in the 1.0 - 1.1 Bev Bevatron π^- meson beam in the summer of 1958, made use of some of the special properties of a xenon-filled bubble chamber.

Information has been acquired on the following topics which are the subjects of this thesis.

(1) Absolute cross sections for strange particle production in the complex nucleus of xenon and corrected angular and momentum distributions in the laboratory.

(2) The study of the interactions of K° particles in xenon which result in hyperon production and the interpretation of this data.

Additional results of the analysis of this experiment have been discussed elsewhere.[3,4]

1.3 Strange Particle Production and Interactions

It is important to predict the various allowed strange particle production and scattering reactions. The situation is complicated by the experimental result that not all of the possible strange particle production interactions are observed even though conventional conservation laws are obeyed. The application of the selection rule $\Delta S = 0$ for strong interactions, together with the strangeness assignments of Table 1, results in clear predictions that certain reactions violate this rule while others do not violate this rule. For example,

$$\pi^- + p \rightarrow \Lambda + \pi^\circ$$

has been searched for but not found.[5] By the $\Delta S = 0$ rule, it is not allowed as a strong interaction.

For our experiment, we can list the allowed strange particle production reactions for 1.0 - 1.1 Bev kinetic energy π^- mesons incident on nucleons.

$$\pi^- + p \rightarrow \Lambda + K^\circ$$

$$\pi^- + p \rightarrow \Sigma^\circ + K^\circ$$

$$\pi^- + p \rightarrow \Sigma^- + K^+$$

$$\pi^- + n \rightarrow \Sigma^- + K^\circ$$

This list contains the important elementary strange particle production interactions occurring in this experiment. Measured cross sections for strange particles emerging from the xenon nucleus are presented in Section 5.1.

Again utilizing the simple strangeness selection rule, the following elementary $\bar{K}^\circ$ meson interactions could be expected to occur if a source of $\bar{K}^\circ$ particles was present

$$\bar{K}^\circ + \binom{n}{p} \rightarrow Y^{\circ}_{\mp} + \pi^{\circ}_{\pm}$$

where Y is the general symbol for a hyperon. On the other hand, a reaction such as

$$K^\circ + \binom{n}{p} \rightarrow Y^{\circ}_{\mp} + \pi^{\circ}_{\pm}$$

is forbidden since $\Delta S = 2$. In this experiment, only K° particles were produced and yet reactions where hyperons were produced by $\bar{K}^\circ$ have been observed. An explanation of this phenomenon will be the subject of Section 5.4.

CHAPTER II

APPARATUS AND THE EXPERIMENT

2.1 Xenon Bubble Chamber Design

The particle detecting instrument of this experiment was a xenon filled bubble chamber. A side cross section view of the chamber is shown in Figure 1. In addition, some of the details of the chamber and its associated equipment are listed in Table 2.

Although the basic operation of the chamber was similar to earlier models[6], significant differences and improvements in design were incorporated in this equipment. Many of these design characteristics were due to safety considerations and also reflected concern over possible loss of the valuable chamber contents. One noticeable example was that the bubble chamber windows were not directly in contact with the external environment but were each enclosed by large aluminum "hats." One hat was called the "light source hat" and the other the "camera hat." The camera hat had two viewing ports and two ports through which the camera lenses viewed the chamber at 90° by means of a front surfaced mirror. Each port hole contained two 3/4 in. pieces of glass cemented together with Canada balsam. The first piece was laminated to stop shrapnel from a possible window failure and the second was tempered for maximum strength. The hats were pressurized with 140 pounds of helium to reduce the load on

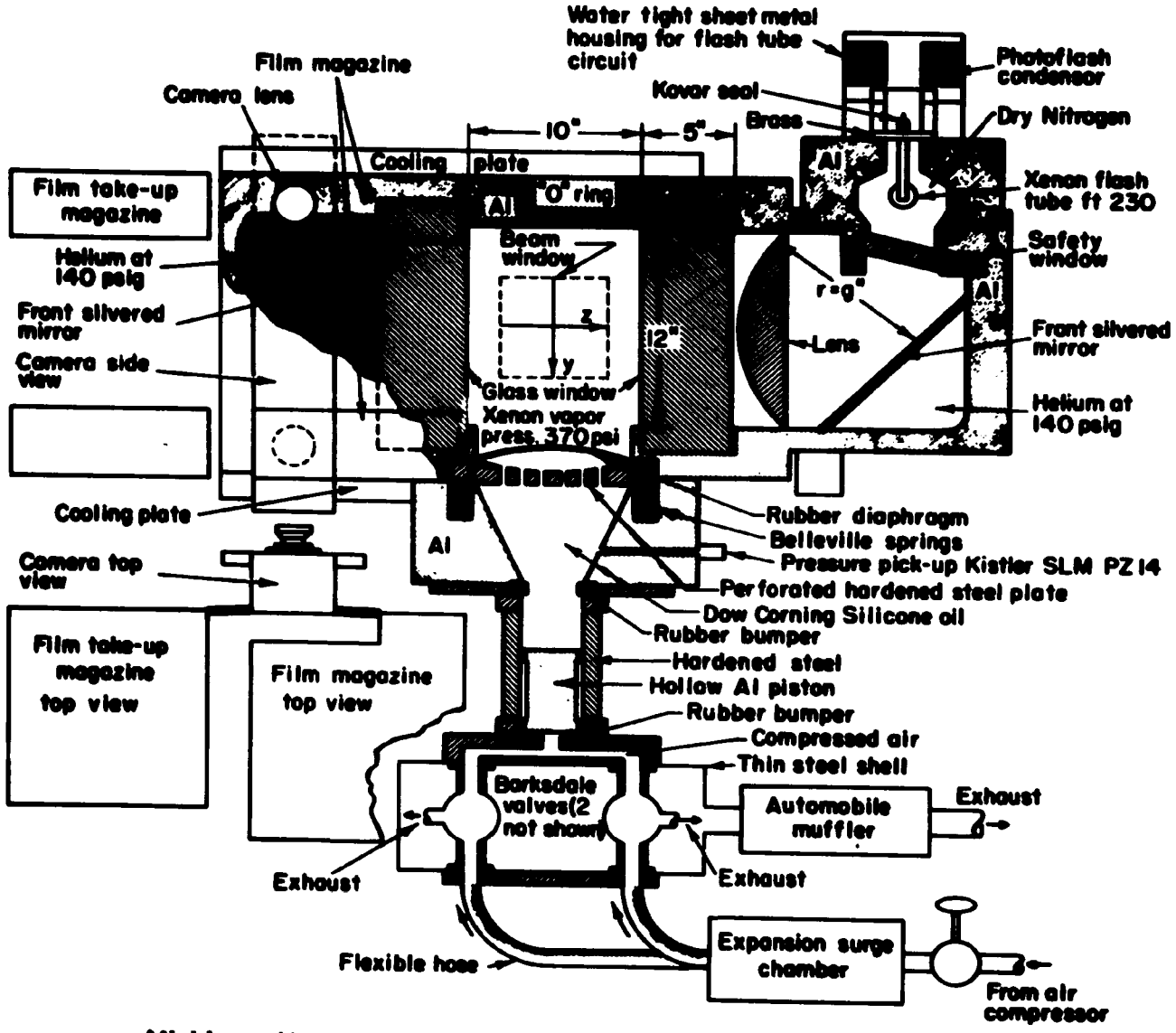


Figure 1. Schematic Drawing of Xenon Bubble Chamber

TABLE 2

XENON BUBBLE CHAMBER PROPERTIES

Sensitive Liquid at Operating Conditions

Composition - (99.48 ± 0.02)% xenon by weight
(0.52 ± 0.02)% ethylene by weight

Density - 2.23 ± 0.07 gms/cm^3

Vapor Pressure - 370 psig (measured)

Temperature - (-21.5 ± 0.1) °C

Chamber Properties

Dimensions of illuminated volume - 12 in. diameter x 10 in. deep

Volume of xenon mixture required to fill chamber - 21 liters

Chamber body material - aluminum forging, Alloy 2024, machined and heat treated

Glass windows - 15 in. diameter x 5 in. thick, borosilicate crown glass

Expansion System

Diaphragm material - Raybestos - Manhattan, 2 ply nylon cord, low temperature flexible Buna N rubber, 1/8 in. thick

Diaphragm supporting fluid - Dow Corning "200" silicone oil

Piston cylinder diameter - 3.9940 ± 0.0005 in.

Piston travel distance - 3.970 in.

Piston displacement - 0.82 liters

Chamber free volume - 2.7 - 3.0%

Compressed air expansion valves - four 3/4 in. port Barkesdale valves

TABLE 2 (Continued)

Compressor pressure - 430 psig

Pressure sensing elements - SLM PZ-14, Kistler Instrument Company

Cooling System

Type - Coolant mixture circulated around body of bubble chamber

Coolant - 50 - 50 mixture of ethylene glycol and water

Refrigerator - 2 ton Frigidaire unit designed by Mr. Hugh J. Scullen of Detroit

Optical System

Distance from lenses of camera to center of chamber - 26 in.

Distance between camera lenses - 14-3/8 in.

Camera lenses - Two 65 mm Schneider Super Angulon wide-angle lenses - matched focal lengths to 0.1 mm, stopped down to f/45

Cameras - 70 mm film, vacuum backs, 800 ft film storage magazines

Film - Kodak linagraph pan, very fast panchromatic film of medium contrast, blue-grey acetate base, resolving power 70 lines per mm

Chamber illumination optics - dark field

Light source - General Electric FT 230 lamp (discharged at 1500 volts and capacitance of 45 microfarads)

Duration of light flash - 100 microseconds

Time delay for bubble growth - 1500 microseconds

Camera hat mirrors - 1/4 in. thick, front surfaced

Camera peepholes - 3/4 in. thick - 3 ply laminated water white glass and 3/4 in. thick water white Herculite glass

the main bubble chamber windows. No window failures were ever experienced in the operation of the bubble chamber. However, window failure tests were conducted first at the Quonset Hut Laboratory and subsequently at the Willow Run Rocket Bunker. These tests indicated that the failure of an unprotected bubble chamber window would be a very grave personnel hazard.

The bubble chamber expansion system will serve as another illustration of careful design. The piston whose motion was actuated by compressed air was not in direct contact with the xenon but acted on an intermediate hydraulic fluid which in turn moved a rubber diaphragm. This eliminated the problem of piston seals and in addition prevented a large heat leak. In the event of hydraulic fluid loss, a perforated, hardened steel plate was present to support the rubber diaphragm and thereby prevent its rupture.

The front panel of the xenon gas handling system is shown in Figure 2. The entire supply of 10,000 liter-atmospheres of the xenon gas mixture[1] was stored in a 300 liter tank at 500 psig behind the panel. A spare storage tank sat next to the filled tank and was connected to the blow-out disk of the xenon bubble chamber. If the pressure in the chamber rose to 600 ± 30 lbs, the blow-out disk ruptured and the contents of the chamber were to be dumped into this dummy storage tank. Both storage tanks were rolled from 3/4 in. thick sheets of stainless steel plate

[1] Xenon gas and xenon gas mixture are being used interchangeably.

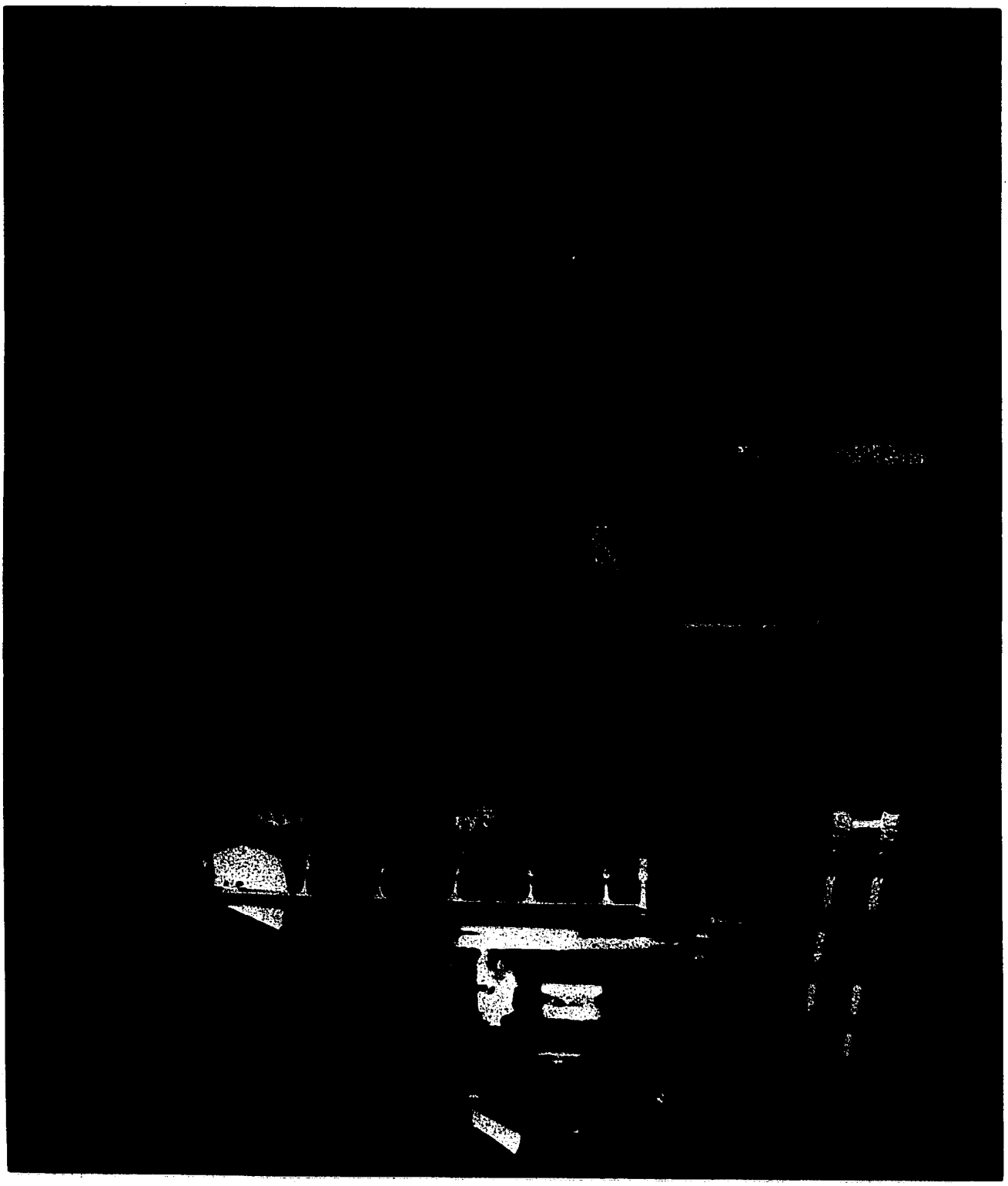


Figure 2. Photograph of Gas Handling System Panel of Xenon Bubble Chamber

which were then welded together. The tanks were subsequently cleaned and helium leak tested. Stainless steel was used since the tensile strength of this material did not fall off rapidly at high temperatures. Consequently, the storage tanks were designed to safely contain the xenon gas through a normal fire. These stainless steel tanks could also be immersed in liquid nitrogen so that the xenon could be transferred from one tank to the other.

The filling of the bubble chamber with xenon was accomplished by condensing the xenon from the main storage tank into a unit of three one-gallon stainless steel cylinders (tri-tanks) which were immersed in a liquid nitrogen bath. The large cylindrical metal Dewar in the photograph holds this liquid nitrogen bath. Heating elements were clamped around the tri-tanks to warm up the xenon from its frozen state to the point where it could be either transferred into the chamber as a liquid at approximately the operating temperature, or else distilled into the chamber. The distillation procedure, while slower, was found necessary in order to purify the xenon. It was found that elastomers and particles of carbon black, necessary ingredients of the low temperature Buna N rubber compound, contaminated the liquid xenon. Some of this dirt was deposited in the tri-tanks and distillation was used to transfer xenon from the tri-tanks to the bubble chamber. Included in the gas handling system was a scavenger which was designed for use in

the chamber emptying process. This scavenger was a one-liter stainless steel cylinder which was immersed in a liquid nitrogen bath; it removed the last traces of xenon from the tri-tanks. The scavenger operated quite efficiently since the vapor pressure of xenon at liquid nitrogen temperature was 25 microns. When the scavenging process was completed, the valve between the scavenger and tri-tanks was closed and the scavenger became a permanent part of the gas storage system.

In the xenon gas plumbing system, double wall thickness 3/8 in. outside diameter copper tubing was used. Tubing was joined by first threading the tubing into couplings machined from solid brass bar stock and then by silver soldering the units. The entire gas handling system was pressure tested and helium leak tested.

Since the completion of the xenon bubble chamber unit in April 1958, three Bevatron runs have been performed. The Bevatron exposure described in this thesis was but the first of these experiments. To date there has been no detectable change in the contents of the xenon reservoir. In addition, these runs have been carried out with only a small running time loss due to bubble chamber equipment breakdown. This was a benefit of careful design, which although not tangible in the early design stages, has proven worthwhile.

2.2 Experimental Arrangement and the Run

Figure 3 is a photograph taken during the summer of 1958 showing a section of the experimental area on the floor of the Bevatron. The xenon bubble chamber unit is enclosed by the concrete block house in the foreground. The beam enters the block house after passing through the apparatus of Cool, Cork, Cronin, and Wenzel (not shown in photograph), and then a focusing magnet and a momentum analyzing magnet. The distance from the bending magnet to the target in the south straight section of the Bevatron was approximately 112 feet.

A run of 160,000 stereo photographs was performed with this beam geometry. The nominal beam energy was 1.0 Bev for the first 67,000 photographs and 1.1 Bev for the remainder of the pictures. Only minor changes were made to the apparatus during the run. The beam collimation was changed slightly at frame 37,000 and additional shielding was included starting at frame 70,500.

The photographs were quite uniform in quality. A slight darkening was noted in the photographs due to clouding of the xenon by rubber diaphragm extract. The xenon was cleaned twice during the run by distillation to minimize this effect.

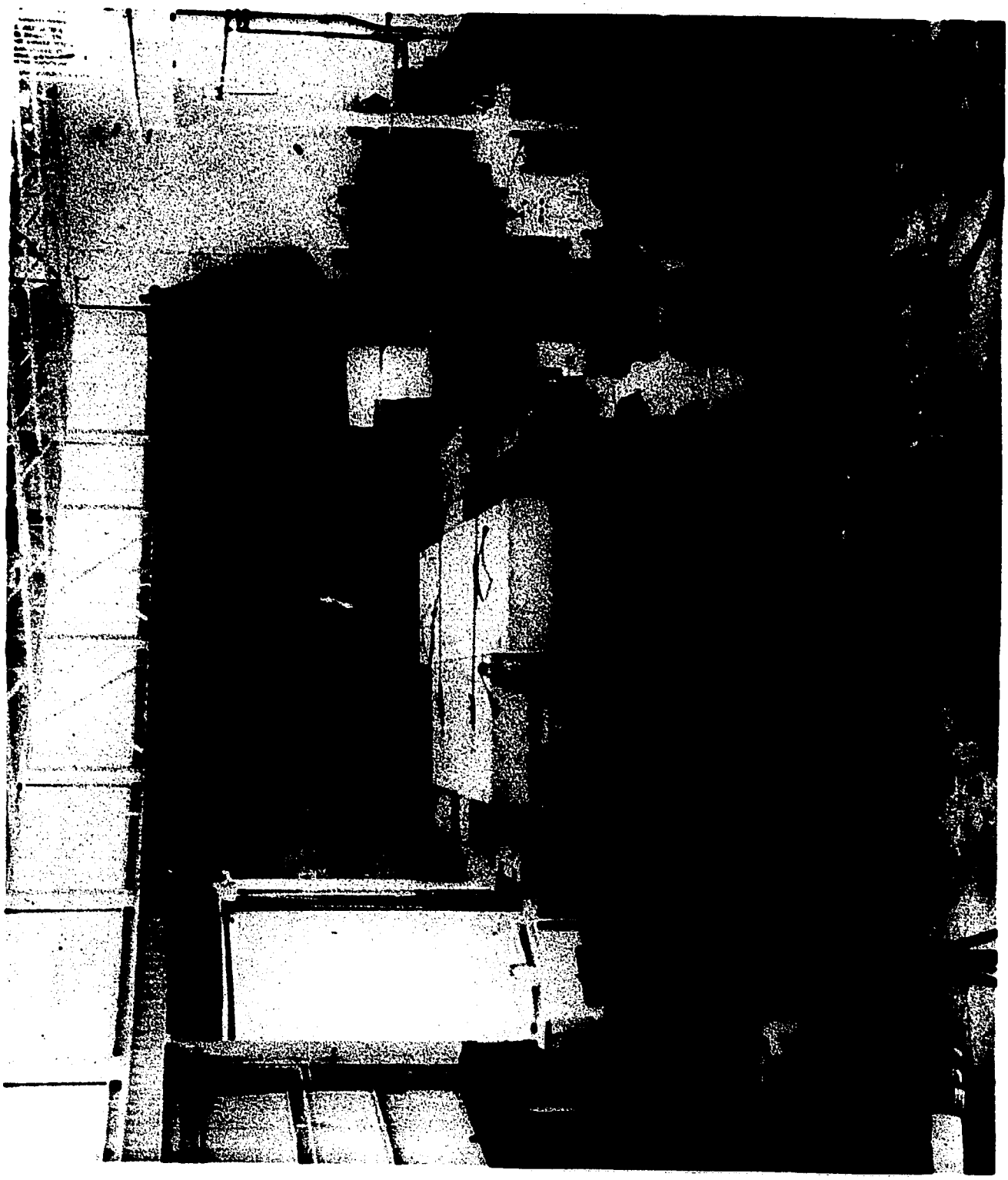


Figure 3. Photograph of Bevatron Experimental Area

CHAPTER III

REDUCTION OF DATA

3.1 Description of Overall Procedure

In the fall of 1958, the raw data of the experiment had become available - 400 pairs of rolls of film with each roll containing 400 bubble chamber photographs.

The overall procedure of data handling consisted of progressing through four phases - scanning, measurement, computation, and analysis. We will very briefly describe a few essential characteristics of each phase and then in succeeding sections proceed to repeat the discussion of each of these stages in the reduction of data in much greater detail.

Scanning

This phase of the data handling consisted of looking at an approximately life-size projected image of each frame of film on specially constructed viewers for preselected categories of bubble chamber track configurations and making sketches or noting those events of interest.

Measurement

In the measurement phase, each entry either sketched or noted by the scanners was looked at on optical devices which could project an image of magnification 1.75:1 or 4.25:1 onto a green transmission viewing screen. The stages which moved the film were digitized so that the

measured coordinates of points on the film could be transferred directly onto IBM cards. Provision was also made for including coding remarks along with the coordinate measurements.

Computation

The transformation from the measurements of coordinates on each of the stereo views of the film to the true space coordinates of the points was done by IBM electronic computer. Roughly one-half the measurements were processed by the IBM 650 computer, while for the other half the IBM 704 computer was used. After the space coordinates of the points were computed, geometric quantities such as angles and lengths were derived from these computed spatial coordinates.

Analysis

The analysis phase consisted of deciding on the basis of the computed space coordinates, geometrical quantities, and kinematic tests whether the object measured in the photograph was or was not a strange particle and, in addition, whether the strange particle decay was a charged Λ or a charged K_1°.[1]

---

[1] Frequently the charged Λ decay is written Λ_+ and the charged K_1° decay is written K_{1+}° where

$$\Lambda_+ \rightarrow p + \pi^-$$

$$K_{1+}^\circ \rightarrow \pi^+ + \pi^-$$

3.2 Scanning of Film

The scanning process was carried out in the Quonset Hut Laboratory. Four film scanning instruments were constructed. Each of these film viewers consisted of a white Formica viewing surface at normal desk level, but slightly inclined. The film projectors were mounted overhead on a second level above the white viewing surface. The projected image from each stereo view was reflected onto the viewing surface by means of a front surfaced mirror. One of the mirrors and one of the projectors had levers attached to it so that one view of the film could be moved independently of the other in two directions. The projected images were only slightly larger than 1:1 and events of interest were conveniently drawn on sheets of 8-1/2 x 11 in. looseleaf paper and stored in large three-ring binders. Once the adjustment levers and film advance controls were set, a scanner would proceed through a roll of film in the automatic film advance mode. A hand-held control box enabled the scanner to advance frames or alternate rapidly between stereo views. These automatic features made it possible to scan both views of 400 pictures in from 4 to 6 hours with a minimum of fatigue.

The scanning of the film was done in two large sections - frames 0 - 86,000 and frames 86,000 - 160,000. In the first section of the scan, only the staff and thesis students participated. While specific scanning instructions were formulated, it was the practice for each scanner to understand each photograph. Those events which were

not clearly understood were noted, as well as the events of interest. In this way we were in a position to detect any strange processes occurring in the experiment which ordinarily would have escaped a less thorough scanning procedure.

When the results of the 0 - 86,000 section of the data were evaluated, it was decided to employ three scanners to view the remainder of the film. They were instructed to search for specific types of events and, in addition, note events not understood. In general, they were given a more restrictive list of things to search for. For example, they were not explicitly instructed to look for K^+ or Σ^- decays.

For the purposes of the experiment treated in this thesis, the scanning consisted in looking for V-like bubble chamber track configurations which were associated with beam tracks interacting or disappearing within the illuminated volume of the bubble chamber. All V-like objects in the chamber were noted,[1] although the V's of primary importance were those called "V° to origin", which satisfied the requirement that a line from the end of the pion track to the vertex of the V fell between the legs of the V. When one V° to origin was found by a scanner, he was instructed to search the photograph for another V° with or without origin and also search for electron pairs coming from the origin producing the V°.[2]

---

[1] Some limitations were made on this rule for frames above 86,000.

[2] We are not including the scanning rules for neutral Λ and neutral K_1° decays. We frequently use the notation $\Lambda_\circ$ for neutral Λ and $K_{1\circ}^\circ$ for neutral K_1° where

$$\Lambda_\circ \rightarrow n + \pi^\circ$$
$$K_{1\circ}^\circ \rightarrow \pi^\circ + \pi^\circ$$

3.3 Measurement

Each entry on the scanner's list was examined on optical devices capable of performing measurements on the film. These instruments projected the film in a choice of two magnifications onto a large transmission screen.[1] The transmission screen was backed with an emulsion of green hue which dispersed the light efficiently enough to provide good images at wide angles of view. Two of these green screen instruments were constructed differing considerably in appearance and design. They were similar in that the stages were digitized, although the digitizing units themselves were different. In the one device used for making most of the measurements for this thesis, the digitizing units were Wang encoders which were attached to the ends of the lead screw shafts and which transmitted their information in binary form. After passing through a binary to decimal conversion circuit, the data was fed into an IBM card punch. An extra checking circuit was provided to verify the binary to decimal conversion. The positions of the film stages gave a 5 digit decimal number for each of the x and y coordinates of the stage. An extra 6 digits were affixed to this number to label the measurements. One digit was a code for the computer, the next three digits specified the stereo view and the point type of the measurement, i.e., whether the point was a beam origin or a V° apex, etc.; and finally, the last two digits served as measuring remarks and also signaled the end of a

---

[1] The magnifications were approximately 1.75:1 and 4.25:1.

particular measurement by the use of the numbers 00. The information for the computer was therefore contained in fields 16 columns wide on the IBM card with four or five fields punched onto a card depending on the computing facility used.

The first 16 columns of the IBM card contained the following information: frame number, date, operator number, and type of event. The image of the point being measured was centered on a reticle cemented to the rear surface of the green screen. The measuring commenced when the coordinates of the center grid mark[1] together with the 6 numerical remarks were read out onto the IBM card. The corresponding point, the front center grid mark on the other stereo view, was measured next. Then other points relevant to the event of interest were coded and read out. Finally, the four corner grid marks were measured to check for possible rotations of one film view with respect to the other. Film shrinkage was checked by determining the absolute distance between the corner grid marks.

An actual measurement took from 15 - 25 minutes. Perhaps 10 minutes of this time was spent in the actual measuring process, while the remainder of the time was required for the inspection of the photograph.

---

[1] A rectangular array of grid marks 2 cm apart was deposited on the inside surfaces (in contact with xenon) of the main bubble chamber windows. In addition to serving as reference and check points for each measurement, the absolute spacing of the grid marks on the film enabled the determination of constants for the stereo formulas, e.g., lens magnifications.

3.4 Computation

The IBM cards containing the coordinates and code numbers of corresponding points on each of the two stereo views were processed for the first half of the experiment by the IBM 650 computer. From these data cards, a stereo program transformed the measurements on each of the film views into the true space coordinates of the points. The results of this program were obtained from the computer as cards and the listed cards contained the computed space coordinates. The card output of this program was fed back into the computer and by means of an additional program various geometrical quantities were computed. A list of some of these quantities will be given.[1]

Origin Data

Direction cosines of the primary beam track

Distance from origin to first measured point on beam track

V° Particle Data

Direction cosines of each V° leg

Length of segment from apex of V° to first point on each V° leg

Range of each V° leg and opening angle Θ

V° Origin Data

Direction cosines of V° with respect to origin

Path length of V° with respect to origin and production angle ω

Angles between V° particle and legs of V° (Θ_1, Θ_2)

Angle between V° particle and decay plane (coplanarity angle, δ)

[1] Gamma ray data is not included in this list.

Error Data

The variations in δ, θ_1 and θ_2, were listed for separate 0.01 cm changes in the space coordinates of the origin, V° apex, etc. For example, quantities such as $\frac{\partial \delta}{\partial x}_{origin}$, $\frac{\partial \delta}{\partial y}_{origin}$, $\frac{\partial \delta}{\partial z}_{origin}$ were computed. In all, twelve such triplets were computed.

The use of the IBM 650 was entirely satisfactory except that the output was not in the most convenient form – English text could not be printed along with the numbers. The installation of the IBM 704 computer on The University of Michigan campus in the late summer of 1959, furnished improvements in this respect and also resulted in some program modifications.

In the final IBM 704 program written by Mr. Richard Hartung, the basic stereo program and geometry program coded by him for the previous computer were retained. An additional input checking program was included. This program reproduced the IBM card input data in a convenient form so that point coding errors and encoder errors could be quickly located. The program also detected double punches in input cards and noted obvious measuring errors such as the absence of corner grid mark measurements. Events were not computed unless the predetermined distances between three grid marks agreed to within ± 0.01 cm. The printed output of this program contained the reproduced input data, the space coordinates of the measured points, and the computed geometrical quantities with appropriate English text introducing the numbers. This convenient format decreased the time required to analyze events and also reduced the number of errors in the transcription of data.

3.5 Analysis

From the sketches and the computed results of the measurements, the events were separated into various categories. Usually in the classification of V° events, information about the momenta of the V° legs is useful. For this reason bubble chambers with magnetic fields have been constructed. In our experiment the xenon bubble chamber did not have a magnetic field. However, very accurate momentum estimates for the V° legs could be made for those legs which stopped in the chamber by ionization. Since we found that approximately 89% of the charged Λ had one or both legs stopping in the chamber and approximately 28% of the charged K_1^0 had one leg brought to rest in the chamber,[1] it was a frequent occurrence to have information concerning the momentum of one or even both of the V° legs. It was natural therefore to carry out the analysis in terms of the observed range of the V° legs. Three classifications were made:

(1) Both V° legs stop in the chamber

(2) One V° leg stops in the chamber

(3) Neither V° leg stops in the chamber

For each of these three alternatives, printed analysis sheets were prepared. On each of these sheets, there was space for transcribing certain data from the computer, as well as space for data derived from the graphical analysis of the event.

---

[1] For frames 0 - 86,000 only. For frames 86,000 - 140,000 similar results were found.[7]

Both V° Legs Stop in the Chamber

The measured ranges of the two legs implied two values for the predicted V° opening angle Θ'. If the measured opening angle Θ was such that

$$\frac{|\Theta - \Theta'|}{\Theta'} \leq 0.15$$

then the V° was considered to be a Λ_+.[1,3] In this way, a Λ_+ could be identified independently of the presence of an interaction origin. In most instances there was an interaction origin, but for scattered Λ_+ this was not the case. Of course in this identification of Λ_+ without origin, the choice of legs implied by the analysis had to be in agreement with the observed bubble density and multiple scattering of the legs.[4] When an interaction origin was present, then the predicted Λ_+ angles, Θ_p' and Θ_π', had to be in agreement with the measured angles Θ_1 and Θ_2. Charts of expected errors in measurement due to multiple scattering were useful in evaluating these results. A coplanarity angle, δ, of less than 7° was usually required for identification except in configurations where larger measuring errors were implied.[2]

---

[1] It was impossible for both pion legs from the charged K_1° decay to stop by ionization within the 30 cm diameter xenon bubble chamber. The energy release, or Q, of a K_{1+}° decay at rest implied a range of approximately 23 cm for each leg.

[2] Large measuring errors occurred for events where corresponding points could not be accurately found or cases where the initial direction of the V° leg could not be well determined.

[3] The $\left|\frac{\Theta - \Theta'}{\Theta'}\right| \leq 0.15$ was an empirical rule.

[4] This also applies to the identification of Λ_+ to origin and K_{1+}° to origin.

One V° Leg Stopped in the Chamber

The analysis proceeded for those V° whose coplanarity was $\leq 7°$.[1] Since only one leg stopped, both the Λ_+ and K°_{l+} strange particles were possible. If the stopping leg of the V° showed a $\pi\mu e$ decay, then identification of the V° as a K°_{l+} was virtually certain. In other cases, we assumed that the V° was a Λ and that the stopping leg was first a proton. The resulting Θ_p' was compared with the measured Θ_1. If agreement was not satisfactory then the stopping leg was assumed to be a pion and the analysis proceeded to compare Θ_π' and Θ_1. In a similar way, the analysis was carried through under the assumption the V° was a K°_{l+}. Usually the measurements and predictions for one of the V° would be inconsistent and it was possible to identify the V° as either a Λ_+ or K°_{l+}. However, there were some ambiguous single V° cases.[2]

Neither V° Leg Stopped in the Chamber

The analysis proceeded for only those V° whose coplanarity was $\leq 7°$.[1] The measured angles Θ_1 and Θ_2 implied for Λ_+ or K°_{l+} predicted ranges for the V° legs. In cases where the observed ranges were inconsistent then the events were thrown out. The number of ambiguous single V° cases was greatest for this category. Frequently K°_{l+} could be ruled out because the predicted momentum was greater than that allowed by the application of energy and momentum conservation to the production process.

[1] At this stage a decision concerning remeasurement was made. If $\delta > 7°$, and an identified charged V° was present, a remeasurement was made.

[2] When an associated identified charged V° was present, the ambiguity was removed. We did not find an example of $\Lambda_+ K^\circ_{l+}$ where the assignments of Λ_+ and K°_{l+} were interchangeable.

Once a tentative identification of a strange particle was made, the predicted angles θ_1' and θ_2' were used to determine the momentum of the V° and the center of mass decay angles.

3.6 Analysis Rules and Background Estimates

The rules of Section 3.5 were oriented primarily toward the identification of single V°. In the cases where two associated strange particles were present, the analysis and identificationof events became considerably easier. The rules for the acceptance of events into the various cross section samples were therefore made less stringent than for single V°. This was necessary in order not to remove otherwise good events from the cross section sample.

On the other hand, it was necessary to demonstrate that this did not introduce "fake events" into the cross section sample.[1]

We determined that the background of events simulating double V was small and that the use of relatively loose criteria for accepting double V events was fully justified. This result was obtained by re-scanning the pictures in the region 0 - 86,000. In this determination, one inspected the sample of known double V and noted neutral stars in each double V picture and the number of prongs per star. Table 3 presents the results of this study for 122 double V events with $\leq$ 15 tracks per picture.

---

[1] A fake event is an event which passes the existing criteria for a real event, but would have been rejected if the criteria were made sufficiently precise.

TABLE 3

PRONGNESS OF NEUTRAL STARS[1]

NUMBER OF PRONGS	% OF DOUBLE V PICTURES
0	73.0
1	18.8
2	3.2
3	2.5
4	2.5

Of the 122 pictures, only four two prong stars were observed ($3.2 \pm 1.6\%$ where the error was statistical). Of these stars none could possibly have been classified as a real Λ_+ or K^0_{1+}.

This result gives confidence that the background of fake double V's was negligible.

[1] One prong stars with secondaries < 1.0 cm in length are not included in this tabulation.

CHAPTER IV

DETERMINATION OF THE BASIC PARAMETERS OF THE EXPERIMENT AND CORRECTION FACTORS

The measurement of an absolute cross section required the knowledge of certain constants of the experiment. Quantities such as the length of pion track scanned, the density of liquid xenon and purity of the pion beam had to be determined. These constants as well as correction factors applied to our measurements will be discussed in this chapter.

4.1 Total Length of Pion Track

The data for this determination was the beam track count registered by the scanners during the original scan of the film. Each scanner had counted the number of beam tracks per picture once every 50 frames of film. However, the rules for this track counting procedure were never formalized and consequently the possibility of systematic errors could not be ruled out. An example of a possible biased count would occur when a picture of poor photographic quality was used for a beam track count. For this reason we undertook an independent beam track count.

4.1.1 Beam Orientation

In order to provide background information for setting up rules for beam track counting, the angular spread of the beam pions was studied.

The direction cosines of the incident pion which produced $\Lambda_+ K^o_{1+}$ were measured for 74 events.[1] The average beam direction with respect to a right-handed cartesian coordinate system with the x (beam) axis chosen parallel to the line of front center grid marks[2] was

$$\langle \hat{\pi} \rangle = 0.9973\ \hat{x} + 0.0137\ \hat{y} + 0.0104\ \hat{z}$$

$$\sqrt{1 - (\hat{\pi} \cdot \hat{x})^2} = \sqrt{(\hat{\pi} \cdot \hat{y})^2 + (\hat{\pi} \cdot \hat{z})^2}$$

Table 4 displays the distribution of $\sqrt{(\hat{\pi} \cdot \hat{y})^2 + (\hat{\pi} \cdot \hat{z})^2}$.

In our beam track count we would then want to accept beam tracks which made space angles of $\leq 8°$ to the x axis so that all possible events would be included. Since the beam counting was done on projected views of the film, the angular requirement for the beam was taken as $\leq 5°$ on one projected camera view.

TABLE 4

DISTRIBUTION OF SPACE ANGLES FOR BEAM TRACKS

ANGULAR INTERVAL (Space Angles)	NUMBER OF EVENTS
0° - 1.2°	19
1.2° - 2.4°	23
2.4° - 3.6°	14
3.6° - 4.8°	6
4.8° - 6.0°	8
6.0° - 7.2°	2
7.2° - 8.4°	2
8.4° -	0

[1] These events were for frames in the range 86,000 - 140,000. Similar results for 40 events are available for frame numbers 4,000 - 86,000.

[2] The coordinate system was defined as follows: the x (beam) axis was parallel to line of front center grid marks, the y (camera) axis was perpendicular to the x axis and in the plane of the front window, and the z depth axis was orthogonal to both the x and y axes and positive z was in the direction from the front window to the rear window.

4.1.2 Beam Track Count Rules and Recount Procedure

The selection of the frame numbers of film in the beam track recount was determined in a random fashion. A random number table generated ten digit numbers. The last six digits of this random number were used to specify the frame numbers of the 100 pictures which were to be recounted in the region 4,000 - 139,999.

The following rules were used for this beam track count and these same rules were again used when track counts were made on pictures containing strange particles.

(1) Count as beam track if there was a minimum ionizing track which made a projected angle $\leq 5°$ to the x axis of grid marks.

(2) Count as beam track if a 2 cm piece of track was visible in the chamber before interacting[1].

(3) Old tracks or tracks of low bubble density were not to be included in the track count.

In order to have these results in a useful form, we defined a "good" picture as

(1) Number of tracks ≤ 15 but not equal to zero

(2) Picture not torn, fogged, missing or double exposed

---

[1] This track count was later corrected for the attenuation of the pions in the distance to the beginning of the 10 cm radius fiducial volume. This correction factor was

$$C_\pi = e^{-\chi/\lambda'} \cong 1 - \frac{\chi}{\lambda'} = 0.96 \pm 0.00$$

where

λ' = attenuation length of beam = 84.3 cm

χ = average distance to the fiducial volume = 3.35 cm

The results of the recount are presented in Tables 5 and 6. The original beam track count results are included. In addition, the beam track count as inferred from $\Lambda_+ K^\circ_{1+}$ pictures is also included.[1] The average track count for these pictures was computed from the relation

$$< n > \;=\; \frac{N}{\sum_{i=1}^{N} \frac{1}{n_i}}$$

where

N = total number of pictures

n_i = number of tracks on the i^{th} picture.

The errors in Tables 5 and 6 are the statistical errors.

The track count values that were used in computing the length of pion track was the average of the recount and double V results.[2] The fraction of good pictures was taken to be the average of the values determined by the recount and the original count.

4.1.3 Corrections for the Number of Good Pictures

The number of good pictures was corrected to eliminate those frames which fell in the range 30,892 - 31,820 (1.0 Bev π^+) or in the

[1] The track count for an equally weighted sample of pictures is

$$\bar{n} \;=\; \frac{\sum_{i=1}^{N} n_i}{N}$$

[2] In those cases where $\bar{n}$ was compared with $< n >$ then pictures of zero track count were not included in the $\bar{n}$ sample.

TABLE 5 Beam Count

FRAMES 4,000 - 67,119 (1.0 Bev π^-)

Sample	Fraction "Good" Pictures	No. Tracks in Good Pictures / No. Good Pictures	No. Tracks in Good Pictures / Total No. Pictures
Original Count	0.75 ± 0.01	6.65 ± 0.07	4.95 ± 0.06
Recount	0.73 ± 0.06	6.80 ± 0.42	4.96 ± 0.31
Double V $\Lambda_+ K^\circ_{1+}$	1.00 (by definition)	6.92 ± 0.44	

TABLE 6 Beam Count

FRAMES 67,200 - 139,999 (1.1 Bev π^-)

Sample	Fraction "Good" Pictures	No. Tracks in Good Pictures / No. Good Pictures	No. Tracks in Good Pictures / Total No. Pictures
Original Count	0.75 ± 0.01	7.18 ± 0.08	5.74 ± 0.06
Recount	0.75 ± 0.06	7.14 ± 0.44	5.21 ± 0.32
Double V $\Lambda_+ K^\circ_{1+}$	1.00 (by definition)	7.18 ± 0.32	

range 104,037 - 106,606 (0.8 Bev π^-). In addition, there was a 0.4% correction for the removal of the first and last pictures of each roll of film from the "good" picture sample.

4.1.4 Corrections for Spatial Distribution of Beam

To ensure high detection efficiency for strange particle productions, the origins for events were limited to a fiducial volume of radius $R \leq 10$ cm where $R = \sqrt{x^2 + y^2}$ and $3 \leq z \leq 22$ cm. The beam track count, which did not take into account any kind of fiducial volume limitations in the y and z directions, was therefore overestimated slightly.

Two factors were required

f_z = fraction of beam tracks for which ($z \geq 3$ and $z \leq 22$)

$n(y)$ = distribution of beam tracks along y axis

This determination was done by randomly selecting pictures and recording the y and z coordinates of beam tracks which made interactions. For reasons of speed and convenience, measurements were made with a ruler on projected views of the film. An empirical formula was set up relating the projected to the real-space coordinates by using events already accurately measured as data. Beam tracks with interactions were used because the interaction marked the beam track clearly. This gave the spatial distribution of pions in the y and z directions. The momentum spread of the beam occurs along the z axis and therefore the properties of the beam and the properties of the pions were not necessarily identical along the

z axis. However, possible differences along the z axis were considered negligible. The beam and the pion spatial distributions along the y axis were also assumed similar.

$f_z \cong f_z'$ = fraction of pion tracks for which ($z \geq 3$ and $z \leq 22$)

$n(y) \cong n(y)'$ = distribution of pion tracks along y axis

We needed to know n(y) for the computation of the average beam track length inside the fiducial volume

$$\bar{l} = \frac{2\int_{-R}^{R} n(y)\sqrt{R^2 - y^2}\, dy}{\int_{-R}^{R} n(y)\, dy}$$

This result was not sensitive to details of the n(y) distribution for beams with collimation. A rough model of our beam and one convenient for calculational purposes was

$n(y) = 0.9\ N$ for $|y| \leq 4$

$n(y) = 0.1\ N$ for $8 \leq |y| \leq 4$

$n(y) = 0$ for $|y| \geq 8$

The $\bar{l}$ could be calculated exactly for this assumed beam shape:

$$\bar{l} = \frac{1}{4N}\left\{0.9N\left[y\sqrt{R^2 - y^2} + R^2 \sin^{-1}\frac{y}{R}\right]_0^4 + 0.1\ N\left[y\sqrt{R^2 - y^2} + R^2 \sin^{-1}\frac{y}{R}\right]_4^8\right\}$$

$\bar{l} = 19.1$ cm

The fraction of pions for which $z \geq 3$ and $z \leq 22$ was

$$f_z' = 0.97 \pm 0.02$$

4.1.5 Average Length of Pion Track

We obtained a result for $\bar{\ell}$ by performing a graphical numerical integration of the expression

$$\bar{\ell} = \frac{2\int_{-10}^{+10} n(y)' \sqrt{R^2 - y^2}\, dy}{\int_{-10}^{+10} n(y)'\, dy}$$

We took $n(y)'$ to be the distribution of 100 observed pion tracks which were selected at random [1]

$$\bar{\ell} = 19.3 \text{ cm}$$

1. The frame numbers of the film to be observed were generated by a random number table.

4.2 Estimation of the Muon Contamination in Beam

Two estimates of the muon contamination were made. One method was based on a direct measurement of the observed attenuation length of the beam in the xenon bubble chamber. The other method was based on the geometry of the beam set up.

4.2.1 Measurement of the Attenuation Length of the Beam in Xenon

Rolls of film were selected and the beam was scanned "along the track" for inelastic interactions or scatters with greater than 5° projected angles. To ensure a high efficiency for detecting scatters, photographs were rejected before the scan if the contrast was poor or if the track count exceeded 9. Those interactions occurring within a volume whose length was 20 cm were recorded. The volume was not bounded in the z direction but was limited approximately to $|y| \leq 5$. The projected angles of all pions scattered greater than 5° were recorded. The attenuation length for pion scatters of various angles could be computed. The results are presented for scatters of greater than 7° projected angle. This angle was chosen so that the results would be in a convenient form for comparison with already published data. This determination was performed with the beam of pions of 1.0 Bev (nominal) kinetic energy.

Total number of beam tracks followed	= 4253
Number which interacted	= 874
Attenuation length of beam [1]	= 84.3

[1] Attenuation length is equivalent to an interaction mean free path.

where the error was due to the statistics. The average path length, $\bar{x}$, of those tracks which interacted was:

$$\bar{x} = \frac{\int_0^{\bar{l}} x \; e^{-x/\lambda} \; dx}{\int_0^{\bar{l}} e^{-x/\lambda} \; dx}$$

$$\bar{x} = \frac{\lambda \left[\left(\frac{\bar{l}}{\lambda} + 1 \right) e^{-\bar{l}/\lambda} - 1 \right]}{e^{-\bar{l}/\lambda} - 1}$$

Using $\bar{l} \cong 20$ cm and for the attenuation length of pions in xenon obtained in Section 4.2.2, $\lambda \cong 75$ cm, one gets

$$\bar{x} = 9.7 \text{ cm}$$

4.2.2 Independent Pion Attenuation Length Measurement

We have examined the data of Cronin, Cool, and Abashian[8] on the attenuation cross sections of 0.97 Bev π^- mesons. Their measured attenuation cross section for tin, Z = 50, was sufficiently close to xenon, Z = 54, so that an extrapolation could be made. We have taken the results for the attenuation cross section of negative pions by tin for scatters of $\geq 10°$ space angle.

The measured cross section for tin = (1175 ± 20) mb. The error was the statistical error and did not include a further 3% uncertainty in the muon contamination of their beam.

By assuming the cross section varied as $A^{2/3}$ and using an average value of the density of xenon as 2.23 ± 0.07 gm/cm^3,[1] we found

Attenuation length of 100% pion beam = 77.9 ± 3 cm

where the error was the result of compounding the uncertainties in the cross section for tin and the density of xenon.

4.2.3 Calculation of Muon Contamination

The average muon contamination, f_μ, would then be related to the ratio of the attenuation lengths listed:

$$f_\mu = 1 - \frac{\lambda'}{\lambda} = 1 - \frac{77.9}{84.3} = 0.08 \pm 0.05$$

The errors were the compounded errors.

4.2.4 Lower Limit on Muon Contamination from Beam Geometry

An estimate of the lower limit on the average muon contamination in the chamber could be understood if we follow the beam along from the target to the bubble chamber. The geometry of the experimental set up was reconstructed from the log books of the run and the schematic drawing of Cool, Cork, Cronin, and Wenzel[9]. In the 112 feet from the Bevatron target to the last bending magnet, 43% of all pions decayed. Most of the muons generated, however, were rejected by the momentum analyzing magnets. A certain fraction, ϵ, of these muons was not rejected. This fraction, in general, was expected to be small and of the

---

[1] Measurements of the density of xenon are discussed in Section 4.3 and Appendix A.

order of a few per cent but it could not be estimated unless the momentum resolution of the system was precisely known. Most of the muon contamination occurred from decays between the last bending magnet and the chamber. In this 15.8 foot length, 7.5% of the pions decayed. These muons contaminate the beam incident on the bubble chamber.

The attenuation of pions in the beam window and in the 15 cm of xenon to the center of the chamber further enhanced the μ contamination. At the center of the chamber, the fraction of pions which remained was

$$f_{\pi^-} = e^{-t_{Al}/\lambda_{Al}} \; e^{-t_{xe}/\lambda_{xe}}$$

where

t_{Al} = thickness of beam window in grams

= 5.98

λ_{Al} = attenuation length of pions in aluminum in grams

= 100.2

t_{xe} = 15 cm of xenon

λ_{xe} = attenuation length of pions in xenon

= 77.9 ± 3 cm

$$f_\mu = (0.075)\left(\frac{1}{0.77}\right) + \epsilon$$

$$f_\mu > 0.097$$

This is in reasonable accord with the estimate of $f_\mu = 0.08 \pm 0.05$ from Section 4.2.3.

4.3 Density of Xenon

The density of xenon was a parameter which was essential to a cross-section determination. Two values for the density of xenon are presented in Table 7. In Appendix A the details of the direct measurement of the density of xenon are described. In addition, other measurements of the density of xenon are discussed.

In Table 7 only the results of measurements performed in connection with this experiment are listed. The agreement between the direct measurement and the density of xenon based on the ranges of the π^+ from five $K_{\pi 2}$ decays was not good. The cause of this discrepancy is not clear at the present time. For this reason the value of the density of xenon was taken to be the average of these two different type determinations, namely,

$$\rho = 2.23 \pm 0.07 \text{ gm/cm}^3$$

where the error was obtained from the spread of the values.

TABLE 7

MEASUREMENTS OF THE DENSITY OF XENON

METHOD	VALUE OF DENSITY
Direct measurement of density	2.17 ± 0.03
Comparison of observed range of $5\pi^+$ from $K_{\pi 2}$ decay with predicted range calculated from Bethe-Bloch energy loss formula with an ionization potential of 702 ev	2.30 ± 0.03

4.4 Beam Energy Determination

Since this experiment was performed with pions of two different kinetic energies, it was of interest to measure the two different beam energies.

The xenon bubble chamber was downstream in the π^- beam used by another group of experimenters. Cool, Cork, Cronin, and Wenzel determined the mean value of the kinetic energy of the beam incident on their apparatus as 1.00 ± 0.01 Bev and 1.10 ± 0.01 Bev and have published these results.[9][1]

When the pions were incident on the xenon bubble chamber, their energy may have been slightly different. There was some degradation in energy when the beam traversed the apparatus of Cool, Cork, Cronin, and Wenzel and, in addition, our beam collimation did not accept the central portion of the energy spectrum of beam pions. For these reasons we have independently determined the beam energy of the incident pions.

One approach to this problem was to apply energy conservation to the reaction

$$\pi^- + p \rightarrow \Lambda + K^\circ$$

with the assumption that each of the strange particles did not interact after production and with the neglect of coulomb and nuclear potentials

$$E_{\pi'} = (E_\Lambda + E_{K^\circ}) - E_p$$

---

[1] The momentum spread of the beam was ± 4% according to reference [9].

where

$E_{\pi'}$ = total energy of the π^- meson in Mev

$E_\Lambda + E_K$ = sum of the total external energies of the Λ hyperon and the K° meson in Mev

E_p = total energy of struck bound proton in Mev

= rest of energy of proton in Mev - binding energy of proton in Mev

$\approx$ 930 Mev

The kinetic energy of the pion that interacted could be computed in this way. Furthermore, if the energy loss of the pion in the 5.98 gms aluminum beam window as well as the ionization loss in the length of xenon traversed, was taken into account, the original incident beam kinetic energy could be found.

When these resulting computed incident pion kinetic energies were plotted for all $\Lambda_+ K^\circ_{1+}$ events in the range 4,000 - 67,118, we found the plot reproduced in Figure 4. The observed distribution in energy was a spread throughout the range 0.60 - 1.00 Bev. It might have indicated that the beam energy was varying, but the threshold for ΛK° production was 0.75 Bev. Therefore below 0.75 Bev, we would expect the number of ΛK° to decrease rapidly with beam energy. On the other hand, it was more reasonable to suppose that the strange particles whose energies were being added together, had lost some energy due to interactions inside the parent nucleus after production. With this explanation in mind, the beam energy could be estimated by selecting that fraction of

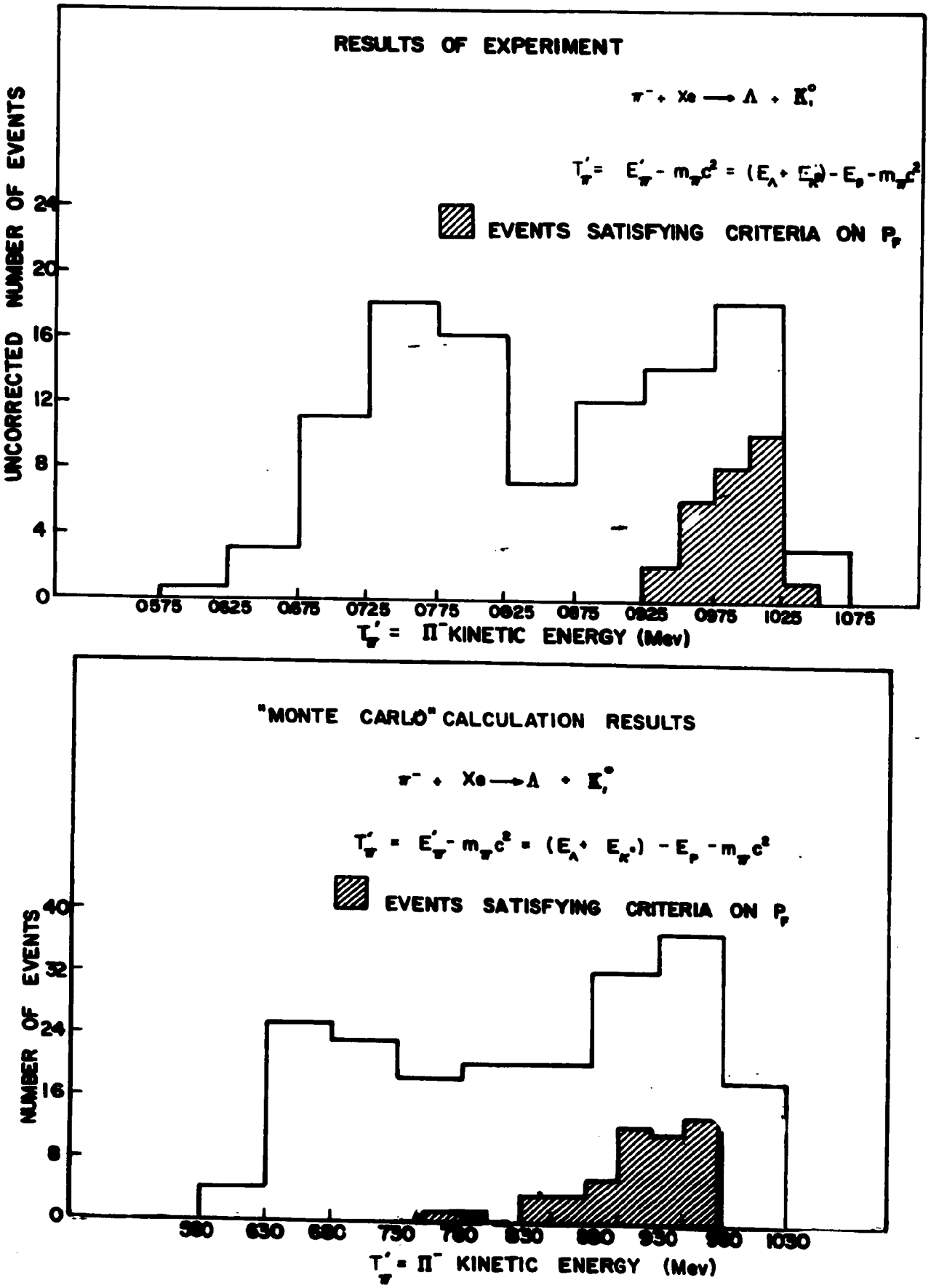


Figure 4. Beam Energy Determination - Results of Experiment and Results of Monte Carlo Calculation

strange particle productions where both the strange particles escaped from the parent nucleus with small energy losses. Those events were objectively selected from the entire sample by requiring that the components of the momentum of the struck nucleon along three suitably chosen axes have values typical of the nucleon momentum.

We computed $\vec{p}_F$, the momentum of the struck nucleon,

$$\vec{p}_F = \vec{p}_\pi - \vec{p}_\Lambda + \vec{p}_{K^\circ}$$

where we set $\vec{p}_\pi$ equal to the approximate incident beam momentum but with corrections for the momentum losses in beam window and the xenon traversed.

We required that each component of $\vec{p}_F$ be no larger than 0.144 Bev/c which was the RMS value of the assumed Gaussian nucleon momentum distribution.[10]

The three components of $\vec{p}_F$ together with the criteria were

$$|\vec{p}_{Fx}| = \left| \vec{p}_F \cdot \frac{\vec{p}_\pi}{|\vec{p}_\pi|} \right| \leq 0.144 \text{ Bev/c}$$

$$|\vec{p}_{F2}| = \left| \vec{p}_F \cdot \frac{\vec{p}_\pi \times (\vec{p}_\Lambda \times \vec{p}_K)}{|\vec{p}_\pi \times (\vec{p}_\Lambda \times \vec{p}_K)|} \right| \leq 0.144 \text{ Bev/c}$$

$$|\vec{p}_{F3}| = \left| \vec{p}_F \cdot \frac{\vec{p}_\pi \times [\vec{p}_\pi \times (\vec{p}_\Lambda \times \vec{p}_K)]}{|\vec{p}_\pi \times [\vec{p}_\pi \times (\vec{p}_\Lambda \times \vec{p}_K)]|} \right| \leq 0.144 \text{ Bev/c}$$

The application of these criteria changed the total sample of Figure 4 to the shaded events. By looking at the distribution of these events, we found the beam energy by examining the upper end of this

spectrum for that energy for which the number of events started to drop off sharply. The cutoff, of course, was spread out by measuring errors. In fact, for these V° particles of higher energy, the momentum estimates were based more on angular measurements than range measurements, which increased the errors. Our final estimate of the beam energy was obtained by averaging events in a region 30 Mev downward from the apparent cutoff. The results were

$$1.00 \text{ Bev (nominal) } \pi^- \text{ Beam Energy} = 1.01_4 \text{ Bev} \quad (8 \text{ events})$$

The choice of 30 Mev was somewhat arbitrary. If the width of this energy band was decreased further then the number of events would have been correspondingly decreased. On the other hand, a wider region would have systematically lowered the beam energy estimate. This can be understood by an inspection of Figure 4.

A similar plot to Figure 4 has been made for the 1.1 Bev (nominal) kinetic energy π^- beam and estimates of the beam energy were made in the same way with the results:

$$1.10 \text{ Bev (nominal) } \pi^- \text{ Beam Energy} = 1.10_3 \text{ Bev}$$

This discussion did not attempt to decide whether these strange particles were "truly" unscattered. Of course, this would be interesting

information but for the purposes of estimating the beam energy, it was important to assume that it was possible for pairs of strange particles to escape from the nucleus either unscattered or with small energy losses and that kinematic tests would sensitively reveal this.

In order to test the accuracy of this method of predicting beam energies, a model of strange particle production in complex nuclei was examined. [11] This was not an analytic calculation since the type of reactions that might have occurred were large in number and complicated in nature. The calculation made use of the Monte Carlo technique which determined the choice of a series of alternative reactions by the use of random numbers. At each decision making stage, a random number was generated which determined the particular choice In this way, long and complicated sequences of processes could be followed. By many repetitions of the same program, distributions of events were obtained.

In the particular model we examined, π^- mesons of 0.980 Bev were assumed to interact with individual nucleons in a xenon nucleus to produce strange particles. The nucleon distribution was assumed to be a Gaussian with an RMS value for each component of 162 Mev/c. However, the tails of this distribution were cut off and values of the nucleon momenta were restricted to the range 20 Mev/c $\leq |\vec{p}| \leq$ 380 Mev/c.

Once the strange particles were produced, they were followed until they escaped or were captured by the nucleus. Known K° nucleon interaction data, as well as assumed hyperon nucleon interaction parameters, were inserted in the program so that detailed predictions were made.

For the purposes of this discussion, we were interested in estimating the known 0.980 Bev beam energy by the application of the identical criteria used to estimate the unknown beam energy of our experiment. This comparison was accomplished by looking at all ΛK° which emerged from the nucleus. The momenta were recorded and the data was handled in the same manner as were the "real" observed $\Lambda_+ K^\circ_{1+}$. The details of what happened inside the nucleus were not considered since this was not relevant to determining the beam energy.

Twelve events from the Monte Carlo calculation were found to satisfy our criteria, the average was

$$0.980 \text{ Bev } \pi^- \text{ Beam Energy} = 0.978 \text{ Bev}$$

Figure 4 presents a graph of the beam energy as inferred from the Monte Carlo calculation data. The events which satisifed the criteria on the components of $\vec{p}_F$ are shaded.

The fiducial volume of the chamber for cross-section measurements was 10 cm in radius. Pions which interacted within the fiducial region would have energies in the range 0.93 - 0.99 Bev for the lower beam energy and 1.02 - 1.08 Bev for the higher beam energy.[1]

The average interaction energies of this experiment were therefore taken as 0.96 and 1.05 Bev.

---

[1] This was the value at the center of the chamber. This was not exactly correct but valid to within 2 Mev.

4.5 Attenuation of Beam

The total length of pion track had to be corrected for the attenuation of pions in traversing the fiducial volume.

The fraction of pions surviving after a distance $\bar{l}$ was

$$f_\pi = e^{-\bar{l}/\lambda}$$

where

λ = attenuation length of pions in cm

$\bar{l}$ = average length of fiducial region in cm

The total length of track traversed by non-interacting pions, L_π', was

$$L_\pi' = N_T P_x f_g f_z' C_\pi (1 - f_\mu) \; f_\pi \; \bar{l}$$

The symbols and constants found in this expression are defined and evaluated in Table 8.

The total length of track traversed by the pions which interacted, L_π'', was

$$L_\pi'' = N_T P_x f_g f_z' C_\pi (1 - f_\mu) \; (1 - f_\pi) \; \bar{x}$$

$$L_\pi = L_\pi' + L_\pi''$$

$$L_\pi = N_T P_x f_g f_z' C_\pi \; (1 - f_\mu) \; [\bar{l} \, f_\pi + \bar{x} \, (1 - f_\pi)]$$

where

$$\bar{x} = \frac{\int_0^{\bar{l}} x \, e^{-x/\lambda} \, dx}{\int_0^{\bar{l}} e^{-x/\lambda} \, dx}$$

The errors for L_π and L_π' were assumed to be independent and were so compounded. The symbols and constants used above are also defined in Table 8.

4.6 Summary of Beam Properties and Corrections

TABLE 8

SUMMARY OF BEAM PROPERTIES AND CORRECTIONS

PROPERTY	CORRECTION OR FACTOR	
	1.0 Bev π^- Beam	1.1 Bev π^- Beam
Average no. tracks no. "good" pictures	$N_T = 6.86 \pm 0.3$	$N_T = 7.16 \pm 0.3$
Fraction "good" pictures	$f_g = 0.74 \pm 0.03$	$f_g = 0.75 \pm 0.03$
Total number of pictures including subtraction frames of π^+ pictures, 0.8 Bev π^-, and loss of first and last pictures on roll	$P_x = 6.20 \times 10^4$	$P_x = 7.03 \times 10^4$
f_z' = fraction of pions in side of fiducial volume $z \geq 3$ $z \leq 22$	$f_z' = 0.97 \pm 0.02$	
$\bar{l}$ = average length of pion track in fiducial volume	$\bar{l} = 19.3 \pm 0.2$ cm	
Attenuation length of beam	$\lambda' = 84.3 \pm 3$ cm	
Attenuation length of pions	$\lambda = 77.9 \pm 3$ cm	
Muon contamination	$f_\mu = 0.08 \pm 0.05$	
Density of xenon	$\rho = 2.23 \pm 0.07$ gm/cm^3	
Beam Energy	1.01 Bev	1.10 Bev
Average interaction energy	0.96 Bev	1.05 Bev
"Survival" of beam after pion interactions	0.77 ± 0.03	
Total track length of non-interacting pions in cm	$(4.0 \pm 0.4) \times 10^6$	$(4.8 \pm 0.5) \times 10^6$
Total track length of interacting pions in cm	$(0.59 \pm 0.06) \times 10^6$	$(0.72 \pm 0.07) \times 10^6$
Total pion track length in cm	$(4.6 \pm 0.5) \times 10^6$	$(5.5 \pm 0.5) \times 10^6$
C_π = correction for attenuation of beam before fiducial volume	0.96 ± 0.00	
$\bar{x}$ = average interaction length in cm	$\bar{x} = 9.7$	

4.7 Scanning Efficiency Corrections

4.7.1 Single Λ_+ and K°_{1+} Efficiency

Rolls of film were randomly selected and carefully scanned for a second time. Possible V° events that were missed on the first scan were measured. The fraction of real V° events that were missed lead to the following estimate of scanning efficiency.

$$\text{for single } \Lambda_+ - \quad p(\Lambda_+) \quad = \quad 0.87 \pm 0.05$$

$$\text{for single } K^\circ_1 - \quad p(K^\circ_{1+}) \quad = \quad 0.89 \pm 0.11$$

4.7.2 $\Lambda_+K^\circ_{1+}$ Efficiency

The $\Lambda_+K^\circ_{1+}$ scanning efficiency was computed from a knowledge of the single V° scanning efficiencies.

$$p(\Lambda_+K^\circ_{1+}) \quad = \quad 1 - [1 - p(\Lambda_+)]\ [1 - p(K^\circ_{1+})]$$

$$= \quad 0.99 \pm 0.01$$

In the direct rescan of the film for frames 0 - 86,000, no examples of missed $\Lambda_+K^\circ_{1+}$ were recorded. This implied a value of 100% for the double V scanning efficiency as determined by the direct method.

In another direct rescan of the film for frame numbers > 86,000, a check was made on the efficiency of a group of newly hired scanners. They were found to miss only one $\Lambda_+K^\circ_{1+}$ in 48 events. Since pictures of varying quality were included in this rescan, this result was also consistent with a value of 0.99 for the scanning efficiency for $\Lambda_+K^\circ_{1+}$.

4.7.3 Λ_+K^+ Efficiency

In the absence of an accurate measurement of the scanning efficiency for K^+, we assumed that the efficiency for Λ_+K^+ was given by the scanning efficiency for Λ_+.

4.7.4 Scanning Efficiency as a Function of the Track Count

There was no statistically significant evidence that the scanning efficiencies varied as a function of the beam track count in the region $0 \leq 15$ tracks. But this possible effect was taken into account by considering that the scanning efficiencies for the various strange particle events were values averaged over the track count distribution for ≤ 15 tracks. There was evidence, however, that in the region of 20 - 25 tracks, the scanning efficiency for single V° dropped to ~0.5. It was reasonable to exclude from a cross-section determination events occurring in pictures of ≥ 16 tracks if only because of the difficulty in determining suitable scanning efficiency correction factors.

4.8 Geometrical Corrections

The probability of observing a V° particle, of mean life τ, decay in dt at a time t is exp $(-t/\tau)\ \frac{dt}{\tau}$.

$$F(t,\tau) = e^{-t/\tau}\ \frac{dt}{\tau}$$

The normalized probability function for apparatus of finite resolution is

$$p(t,\tau) = \frac{e^{-t/\tau}\ dt \cdot \frac{1}{\tau}}{\int_{t_{min}}^{t_{max}} e^{-t/\tau}\ dt \cdot \frac{1}{\tau}}$$

This equation contains the corrections to an exponential decay caused both by the escape of particles from a finite sized chamber and the failure to observe particles whose decay time was short.

Since

$$t = \frac{\ell}{pc/M}$$

where

M = rest mass of particle in Mev

p = momentum of particle in Mev/c

ℓ = decay length of particle in cm

c = velocity of light in cm/sec

The short cutoff and escape correction factor is

$$\frac{1}{e^{-\frac{\ell_{mn}}{pc\tau/M}} - e^{-\frac{\ell_{mx}}{pc\tau/M}}}$$

The short decay length, ℓ_{mn}, was chosen to be 0.5 cm for the cross-section samples and was taken to be 0.2 cm for the ΛK° angular and momentum distribution samples.

The potential path, ℓ_{mx}, was determined for each individual event.

4.9 Conversion Efficiency of γ From $\Sigma^\circ \rightarrow \Lambda^\circ + \gamma$

The Σ° decays that were observed, where $\Sigma^\circ \rightarrow \Lambda^\circ + \gamma$, were weighted by the reciprocal of the probability of observing the conversion of the γ ray. This probability was a function of the potential path of the γ ray and the mean conversion distance of the γ ray, λ_γ. The relation was

$$\lambda_\gamma = 4.94 + \frac{153.6}{E_\gamma} - \frac{165.2}{E_\gamma^2}$$

where

λ_γ = distance in cm

E_γ = energy in Mev

This was a simple and convenient analytical representation of the results of the Bethe-Heitler formula corrected for the use of the Born approximation, screening, and the effect of pair production in the field of atomic electrons. The density of xenon used in the expression for λ_γ was 2.23 gm/cm^3. This was the same value of the density of xenon as was used for the cross-section determinations.

The energy of the γ ray in a Σ° decay was found by the application of energy and momentum conservation

$$\vec{p}_{\Sigma^\circ} = \vec{p}_{\Lambda^\circ} + \vec{p}_\gamma$$

$$E_{\Sigma^\circ} = E_\Lambda + E_\gamma$$

with the result that

$$E_\gamma = \frac{M_{\Sigma^\circ}^2 - M_\Lambda^2}{2\left(E_\Lambda - \vec{p}_\Lambda \cdot \frac{\vec{p}_\gamma}{|\vec{p}_\gamma|}\right)}$$

where

p = momentum of particle in Mev/c

E = total energy of particle in Mev

M_{Σ° = mass of Σ° hyperon in Mev

M_Λ = mass of Λ hyperon in Mev

Once E_γ was known, the energy and momentum of the Σ° could be calculated.

The average energy of γ rays from twelve Σ° decay events was 77 Mev. For this average energy, the conversion distance was 6.90 cm.

The escape correction for γ rays was computed for each Σ° decay event and was

$$\frac{1}{1 - e^{-\ell_{mx}/\lambda_\gamma}}$$

where

ℓ_{mx} = potential path of γ ray in cm

λ_γ = conversion distance of γ ray in cm

4.10 Correction for Σ° Contamination of ΛK° Events

We have found in Section 4.9 that the escape correction, $\frac{1}{C_\gamma}$, for γ rays from Σ° decays was

$$\frac{1}{C_\gamma} = \frac{1}{1 - e^{-\left(\frac{l_{max}}{\lambda_\gamma}\right)}}$$

where the notation of Section 4.9 is followed.

The average probability that the γ rays from the Σ° did not convert was

$$\frac{\sum_{i=1}^{N}\left(\frac{1 - C_{\gamma_i}}{C_{\gamma_i}}\right)}{\sum_{i=1}^{N}\frac{1}{C_{\gamma_i}}}$$

The factor which corrects for the Σ° contamination of the ΛK° sample, due to failure of γ ray from Σ° to convert, was

$$1 - \frac{\sum_{i=1}^{N}\left(\frac{1 - C_{\gamma_i}}{C_{\gamma_i}}\right)}{\sum_{i=1}^{N}\frac{1}{C_{\gamma_i}}} \cdot \text{("true" fraction of double V being } \Sigma^\circ)$$

$$1 - \frac{\sum_{i=1}^{N}\left(\frac{1 - C_{\gamma_i}}{C_{\gamma_i}}\right)}{\sum_{i=1}^{N}\frac{1}{C_{\gamma_i}}} \cdot \left(\frac{N_T(\Sigma^\circ K_1^\circ)}{N_T(\Lambda K_1^\circ)}\right)$$

where

N = total number of observed Σ°

$N_T(\Sigma^\circ K_1^\circ)$ = total corrected number of Σ° K_1°[1]

$N_T(\Lambda K_1^\circ)$ = total corrected number of ΛK_1°

[1] This in principle includes a correction for Σ° escape as well as other factors.

4.11 Correction for Scattered V°

A certain fraction of ΛK° events were rejected because one of the V° was scattered. We have estimated the Λ correction factor to be the following

Scattered Λ correction = 1.02 ± 0.01

This correction was obtained by inspecting a sample of 96 $\Lambda_+ K^\circ_{1+}$ for scattered Λ°. In a total Λ decay path length of 321 cm, two scattered Λ's were found. This corresponds to a scattering length in xenon of 161 ± 114 cm.

The K° scattering correction factor was obtained from K^+ emulsion cross-section data after corrections for the density of xenon. For an average K°_{1+} momentum of 421 Mev/c a cross section of 12 mb per nucleon was used[12].

Scattered K° correction = 1.01 ± 0.01

4.12 Correction for One-Legged Charged Λ

Λ decays in the charged mode occasionally had secondaries whose range was too short to be visible in the bubble chamber. Usually, the one visible leg was the pion and consequently some of these events were identified.

In order to ensure an accurate cross-section measurement, we rejected events if either of the Λ decay secondaries had a range of less than 0.2 cm and corrected the accepted sample for the loss of these events.

For the proton from the Λ decay, one can calculate by relativistic kinematics

$E_p = \gamma (E_p^* + \beta p^* \cos \Theta^*)$ = proton energy in the laboratory

E_p^* = proton total energy in the Λ center of mass

p^* = proton momentum in the Λ center of mass

similarly for the pion from the Λ decay, one can calculate

$E_\pi = \gamma (E_\pi^* - \beta p^* \cos \Theta^*)$

E_π^* = pion total energy in the Λ center of mass

p^* = pion momentum in the Λ center of mass

where

$\beta = \frac{v}{c}$, where v = velocity of the Λ in the laboratory coordinate system

$\gamma = \frac{1}{\sqrt{1 - \beta^2}}$

Θ^* = angle between proton and Λ line of flight in the Λ center of mass

The requirement that both proton and pion ranges had to be greater than 0.2 cm implied that

$$E_\pi \geq 146 \text{ Mev}$$

$$E_p \geq 951.2 \text{ Mev}$$

let

$$C_\Lambda = \frac{1}{\text{fraction of } \Lambda \text{ with both legs} > 0.2 \text{ cm}}$$

for $p_\Lambda < 67$ Mev/c

$$C_\Lambda = 0$$

for $67 \leq p \leq 308$ Mev/c

$$C_\Lambda = \frac{2}{1 - \cos \Theta^* (0.2 \text{ cm})}$$

where

$$\cos \Theta^* (0.2 \text{ cm}) = \frac{951.2 - 943.5\ \gamma}{99.4\ \beta\gamma}$$

for $308 \leq p_\Lambda \leq 400$ Mev/c

$$C_\Lambda = 1.00$$

for $400 \leq p_\Lambda \leq 1200$ Mev/c

$$C_\Lambda = \frac{2}{1 + \cos \Theta^* (0.2 \text{ cm})}$$

where

$$\cos \Theta^* (0.2 \text{ cm}) = \frac{171.7\ \gamma - 146.0}{99.4\ \beta\gamma}$$

In the actual practice of computing corrections the factors were multiplied together by the computer, so it was not ordinary procedure to separate out the corrections. But for purposes of orientation, the one-legged Λ correction was 1.07 on the average.

CHAPTER V

EXPERIMENTAL RESULTS

5.1 Total Absolute Cross Sections

The absolute cross sections for the following strange particle production reactions are discussed in this subchapter.

$$\pi^- + Xe \rightarrow \Lambda + K^\circ \qquad (1)$$

$$\pi^- + Xe \rightarrow \Sigma^\circ + K^\circ \qquad (2)$$

$$\pi^- + Xe \rightarrow \Lambda + K^+ \qquad (3)$$

$$\pi^- + Xe \rightarrow \Sigma^- + K^\circ \qquad (4)$$

The cross sections for reactions (1) and (2) are given for negative pions of two different kinetic energies 0.96 Bev and 1.05 Bev.[1] For reaction (3) the cross section is given for a beam energy 0.96 Bev. For reaction (4) the lower limit is given for the cross section at 0.96 Bev.

The cross sections were evaluated from the relation

$$\sigma = \frac{N_{TC}}{L_\pi X}$$

where

N_{TC} = total number of corrected events,

L_π = total length of pion track scanned, and

X = number of xenon atoms/cm^3

[1] Details of beam energy determination are discussed in Section 4.4.

The determination of X and L_π is discussed in Sections 4.3 and 4.5

In this section the criteria used in the selection of the various strange particle production samples are given, and as a summary, for each cross section determination, the uncorrected data, corrections, and parameters are listed in tabular form.

5.1.1 Criteria Suitable for Cross-Section Measurement

It was important in this experiment to devise rules or criteria for the separation of events into the various categories. The presence of formal criteria allows reproducibility of separations and permits the introduction of cutoffs and the use of the corresponding correction factors. The criteria decided upon were related to the type of measurement required. A branching ratio determination was a relative measurement and one could deliberately exclude events in each of two samples as long as corresponding fractions of each population were rejected. A cross-section measurement, on the other hand, was an absolute measurement, and events could not be eliminated unless corrections for their losses were made. The importance and necessity of rejecting "fake" events increases as the background of "fake" events increases. Cross-section measurements are consequently difficult when the background is high.

In this experiment, it was determined empirically that the background of "fake" associated production events was negligible.[1]

---

[1] This is discussed in Section 3.6.

The criteria selected, therefore, did not sensitively affect the contamination of the samples. For an associated production event, one could relax, for example, the coplanarity requirements on the second V° without fear of introducing any "fake" events.

5.1.2 Strange Particle Production Criteria

A particular type of strange particle production was defined as one satisfying the following class of criteria:

		PIX, ORG, λ, Θ	Cross section sample
ΛK°	–	PIX, ORG', λ', Θ	
		PIX, ORG', λ, Θ'	Momentum and angular distribution sample
$\Sigma^\circ K^\circ$	–	PIX, ORG, λ, Θ, γ	Cross section sample
ΛK^+	–	PIX, ORG, λ, κ	Cross section sample
$\Sigma^- K^\circ$	–	PIX, ORG, σ, Θ	Cross section sample

PIX Criteria --

(1) The picture was not spliced, torn, double exposed, or badly fogged.

(2) The number of beam tracks was ≤ 15 with the definition of beam track conforming identically with the definition of beam track used in the beam track count (Section 4.1.2).

(3) The picture did not have a background of bubbles or electron tracks which obscured large regions of the chamber or rendered an event unmeasurable.

ORG Criteria

(1) The origin was inside a fiducial volume defined by $R \leq 10.0$ cm where $R = \sqrt{x^2 + y^2}$ and $3 \leq z \leq 22$ cm.

(2) The beam track which caused the interaction had to make a projected angle of less than 5° on one view with the x (beam) axis.

ORG' Criteria

(1') The origin was inside a fiducial volume defined by $R \leq 11.5$ cm where $R = \sqrt{x^2 + y^2}$ and $3 \leq z \leq 22$ cm.

(2') Same as (2) of ORG

λ Criteria

(1) The decay distance was ≥ 0.50 cm.

(2) Both legs of the V° ≥ 0.20 cm.

(3) The measured coplanarity $\leq 7°$ on a measurement or remeasurement.

(4) If the other V° passed Θ criteria and had a measured coplanarity $\delta \leq 6°$ on a measurement or remeasurement then the coplanarity requirement in (3) was relaxed so that δ could be $> 7°$ if this observed coplanarity was consistent

with measuring errors.

(5) The V° fit the kinematics curves of the Λ hyperon within expected errors, also observed bubble densities were in agreement with the predictions.

(6) The apex of the V° was within a fiducial volume defined by $R \leq 11.0$ cm and $2 \leq z \leq 23$.

λ' Criteria

(1') The decay distance was ≥ 0.20 cm.

(2') Same as (2) of λ

(3') Same as (3) of λ

(4') Same as (4) of λ

(5') Same as (5) of λ

(6') The apex of the V° was within a fiducial volume defined by $R \leq 12.5$ cm and $2 \leq z \leq 23$.

Θ Criteria

(1) The decay distance was ≥ 0.50 cm.

(2) The V° was inconsistent with being a scattered beam track, i.e., a scattered beam track was suggested if one of the V° legs was closely parallel to the beam direction and this leg also showed no detectable multiple scattering.

(3) The measured coplanarity ≤ 6° in a measurement or remeasurement

(4) If the other V° passed the λ criteria and had a measured δ ≤ 7° on a measurement or remeasurement then the coplanarity requirement in (3) was relaxed so that δ could be > 6° if this observed coplanarity was consistent with measuring errors.

(5) The V° fit the kinematics curves of the charged K_1^0 meson within expected errors and the observed bubble densities were in agreement with the predictions.

(6) The apex of the V° was within a fiducial volume defined by R ≤ 11.0 cm and 2 ≤ z ≤ 23 cm.

(7) There was no evidence of a charged K_2^0 decay or a regenerated charged K_1^0 — i.e., the observed ratio of the decay time to the lifetime, t/τ, was less than 5.

Θ' Criteria

(1') The decay distance was ≥ 0.20 cm.

(2') Same as (2) of Θ.

(3') Same as (3) of Θ.

(4') Same as (4) of Θ.

(5') Same as (5) of Θ.

(6') The apex of the V° was within a fiducial volume defined by R ≤ 12.5 and 2 ≤ z ≤ 23 cm.

(7') Same as (7) of Θ.

γ Criteria

(1) There was an electron pair in the picture which was consistent with having been produced at an origin satisfying λΘ criteria.

(2) An electron pair had at least 3 cm of track and was within a fiducial volume defined by $R \leq 13$ cm and $2 \leq z \leq 23$.

κ Criteria

(1) There was a V° present in the picture satisfying λ criteria.

(2) The primary had a multiple scattering consistent with a K^+.

(3) The secondary from the alleged K^+ decay showed a distinctly lower bubble density than the primary.

(4) The alleged K^+ decay point was consistent with having no visible interaction prongs or μ from $\pi - \mu$ decay.

(5) To be classified a K^+, a recognizable K^+ decay mode was not required, i.e., a τ decay or $K_{\pi 2}^{+-}$ decay.

(6) If the primary left the chamber before decaying it was called a K_1^+ which did not decay.[1]

σ Criteria

From an origin which satisfied Θ criteria there was a prong (primary) which was consistent with decaying into either a slow or fast π^-.

[1] No events were found in the $\Lambda_+ K_1^{\circ}{}_+$ cross-section sample where an origin prong left the chamber (this was for origins satisfying the fiducial volume requirement that $R \leq 10$ cm).

TABLE 9

Λ - K° CROSS SECTION AT 0.96 Bev

QUANTITY	FACTOR FOR Λ_+	FACTOR FOR K°_{1+}
Uncorrected number of events passing $\lambda\Theta$ criteria	39 ± 6	
Short cutoff and escape correction[1]	1.81	
One-legged Λ correction		
Σ° contamination correction	0.98 ± 0.01	
Scattered V° correction	1.02 ± 0.01	1.01 ± 0.01
Scanning efficiency correction	1.01 ± 0.01	
Branching ratio correction[2,3]	1.60 ± 0.08	2.90 ± 0.3
Corrected number of $\lambda\Theta$ events	333 ± 61	
Length of pion track in cm	$(4.6 \pm 0.5) \times 10^6$	
Xenon atoms/cm^3	$(1.02 \pm 0.03) \times 10^{22}$	
Total cross section in mb	7 ± 1	

[1] The correction factor listed was an average correction derived by dividing the total correction by the number of events. An estimate of error is obtained from the deviation of this average from the observed values listed in Appendix C.

[2] The values used were $\frac{\Lambda \text{ charged}}{\text{all } \Lambda} = 0.627 \pm 0.03$ [13]

[3] The values used were $\frac{K^\circ_1 \text{ charged}}{\text{all } K^\circ} = 0.345 \pm 0.03$ [7]

TABLE 10

Λ - K° CROSS SECTION AT 1.05 Bev

QUANTITY	FACTOR FOR Λ_+	FACTOR FOR K°_{1+}
Uncorrected number of events passing $\lambda\Theta$ criteria	72 ± 8.5	
Short cutoff and escape correction	2.15	
One-legged Λ correction		
Σ° contamination correction	0.99 ± 0.01	
Scattered V° correction	1.02 ± 0.01	1.01 ± 0.01
Scanning efficiency correction	1.01 ± 0.01	
Branching ratio correction	1.60 ± 0.08	2.90 ± 0.3
Corrected number of $\lambda\Theta$ events	742 ± 14	
Length of pion track in cm	$(5.5 \pm 0.5) \times 10^6$	
Xenon atoms/cm^3	$(1.02 \pm 0.03) \times 10^{22}$	
Total cross section in mb	13 ± 2	

TABLE 11

Σ° - K° CROSS SECTION AT 0.96 Bev

QUANTITY	FACTOR FOR Σ°	FACTOR FOR K°_{1+}
Uncorrected number of events passing $\lambda\Theta\gamma$ criteria	3 ± 1.7	
Short cutoff and escape correction One-legged Λ correction	1.64	
Scattered V° correction	1.02 ± 0.01	1.01 ± 0.01
Scanning efficiency correction	1.01 ± 0.01	
Correction for escape of γ ray	1.24	
Branching ratio correction	1.60 ± 0.08	2.90 ± 0.3
Corrected number of $\lambda\Theta\gamma$ events	33 ± 20	
Length of pion track in cm	$(4.6 \pm 0.5) \times 10^6$	
Xenon atoms/cm^3	$(1.02 \pm 0.03) \times 10^{22}$	
Total cross section in mb	0.7 ± 0.4	

TABLE 12

Σ° - K° CROSS SECTION AT 1.05 Bev

QUANTITY	FACTOR FOR Σ°	FACTOR FOR K°_{1+}
Uncorrected number of events passing $\lambda\Theta\gamma$ criteria	5 ± 2.2	
Short cutoff and escape correction	1.64	
One-legged Λ correction		
Scattered V° correction	1.02 ± 0.01	1.01 ± 0.01
Scanning efficiency correction	1.01 ± 0.01	
Correction for escape of γ ray	1.21	
Branching ratio correction	1.60 ± 0.08	2.90 ± 0.3
Corrected number of $\lambda\Theta\gamma$ events	48 ± 20	
Length of pion track in cm	$(5.5 \pm 0.5) \times 10^6$	
Xenon atoms/cm^3	$(1.02 \pm 0.03) \times 10^{22}$	
Total cross section in mb	0.9 ± 0.4	

TABLE 13

Λ - TOTAL K^+ CROSS SECTION AT 0.96 Bev

QUANTITY	FACTOR FOR Λ	FACTOR FOR K^+
Uncorrected number of events passing $\lambda\kappa$ criteria	26.0 ± 5.1	
Short cutoff and escape correction	1.36	
One-legged Λ correction		
Σ° contamination correction	0.99 ± 0.01	
Scattered Λ correction	1.02 ± 0.01	
Scanning efficiency correction	1.15 ± 0.06	
Correction for origin prongs leaving chamber that were mistaken for K^+	1.00 ± 0.00	
Branching ratio correction	1.60 ± 0.08	
Corrected number of $\lambda\kappa$ events	65.0 ± 13	
Length of pion track in cm	$(4.6 \pm 0.5) \times 10^6$	
Xenon atoms/cm^3	$(1.02 \pm 0.03) \times 10^{22}$	
Total cross section in mb	1.4 ± 0.3	

Σ^- - K° Cross Section

The $\sigma\Theta$ criteria of Section 5.1 were applied to the strange particle samples. We found three events which satisfied these criteria for the 1.0 Bev π^- beam. This resulted in a lower limit on the Σ^- - K° cross section of 0.2 ± 0.1 mb.[1]

---

[1] Data on cross sections for strange particle production in complex nuclei is given in reference [14]. However, the π^- beam energy for this reference was significantly higher (approximately 1.5 Bev).

5.2 Corrected ΛK_1° and ΛK^+ Distributions[1,2]

5.2.1 Corrected Momentum and Angular Distributions of ΛK_1°

The ΛK_1° sample used for the cross-section determination was a sample of limited size. The number of events in this sample has been increased by decreasing the short cutoff on the V° to 0.20 cm, increasing the radius of the fiducial volume for origins to 11.5 cm, and increasing the radius of the fiducial volume for V° to 12.5 cm. For this purpose, the ORG', λ' and Θ' criteria were introduced. These changes probably do not introduce biases, but if anything affect the absolute scanning efficiency. The requirements on the number of beam tracks ≤ 15 has not been changed.

The momentum distribution of the Λ from ΛK_1° are presented in Figure 5 at the two beam energies and similarly the momentum distribution of K_1° from ΛK_1° are plotted in Figure 6. All geometric and one-legged Λ corrections were included.

The angular distribution of Λ and K_1° from ΛK_1° at the two beam energies is displayed in Figures 7 and 8. All geometric corrections and the correction for one-legged Λ decays were included.

In all angular distributions histograms, the assumption was made that the beam was parallel to the x axis. This introduced a negligible error.[3]

---

[1] The so-called ΛK_1° and ΛK^+ distributions are the observed $\Lambda_+ K_{1+}^\circ$ and $\Lambda_+ K^+$ distributions.

[2] All angular distributions presented are in the laboratory system.

[3] See Section 4.1.1.

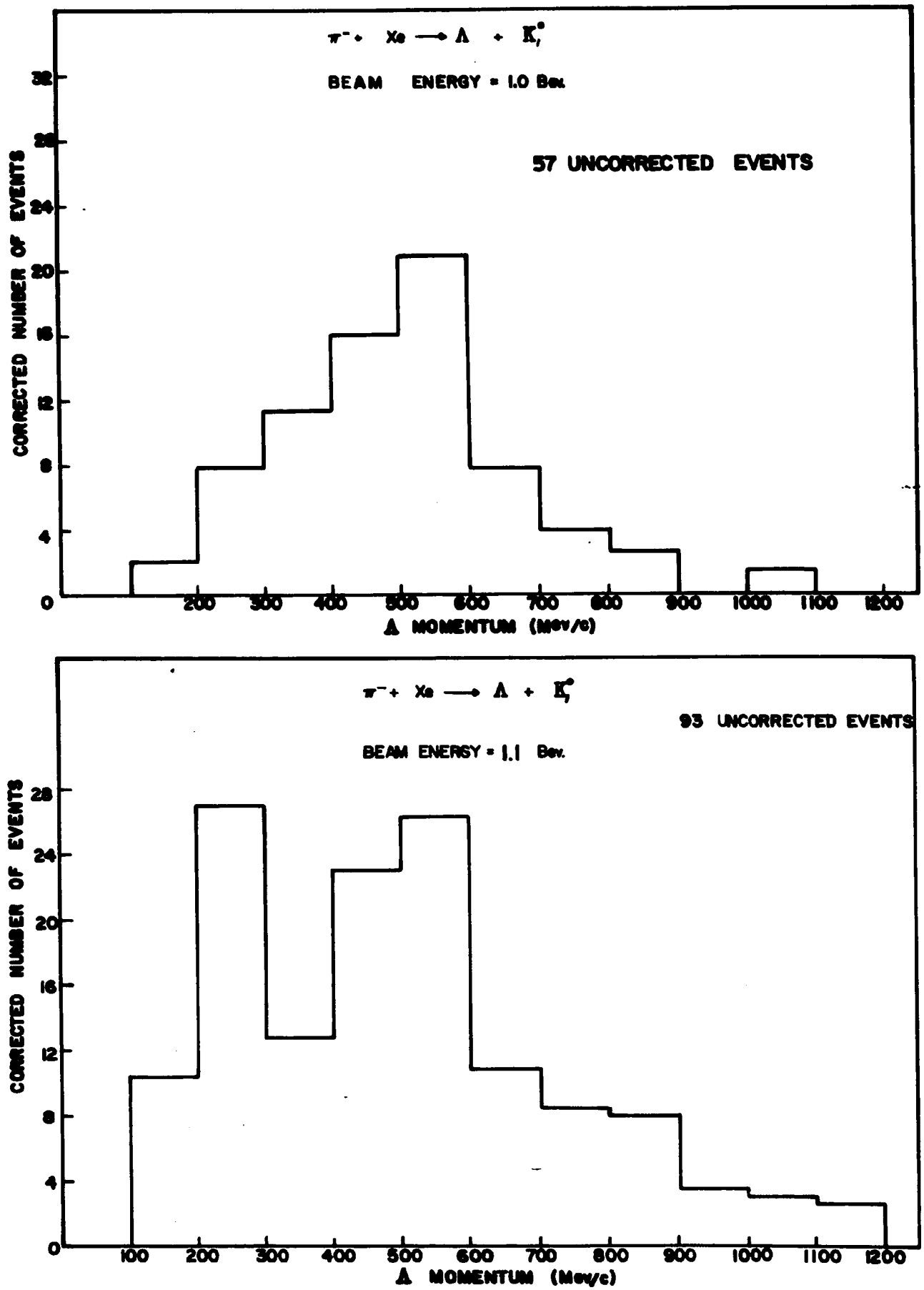


Figure 5. Corrected Λ Momentum Distributions for ΛK_1° from 1.0 and 1.1 Bev. π^- Mesons

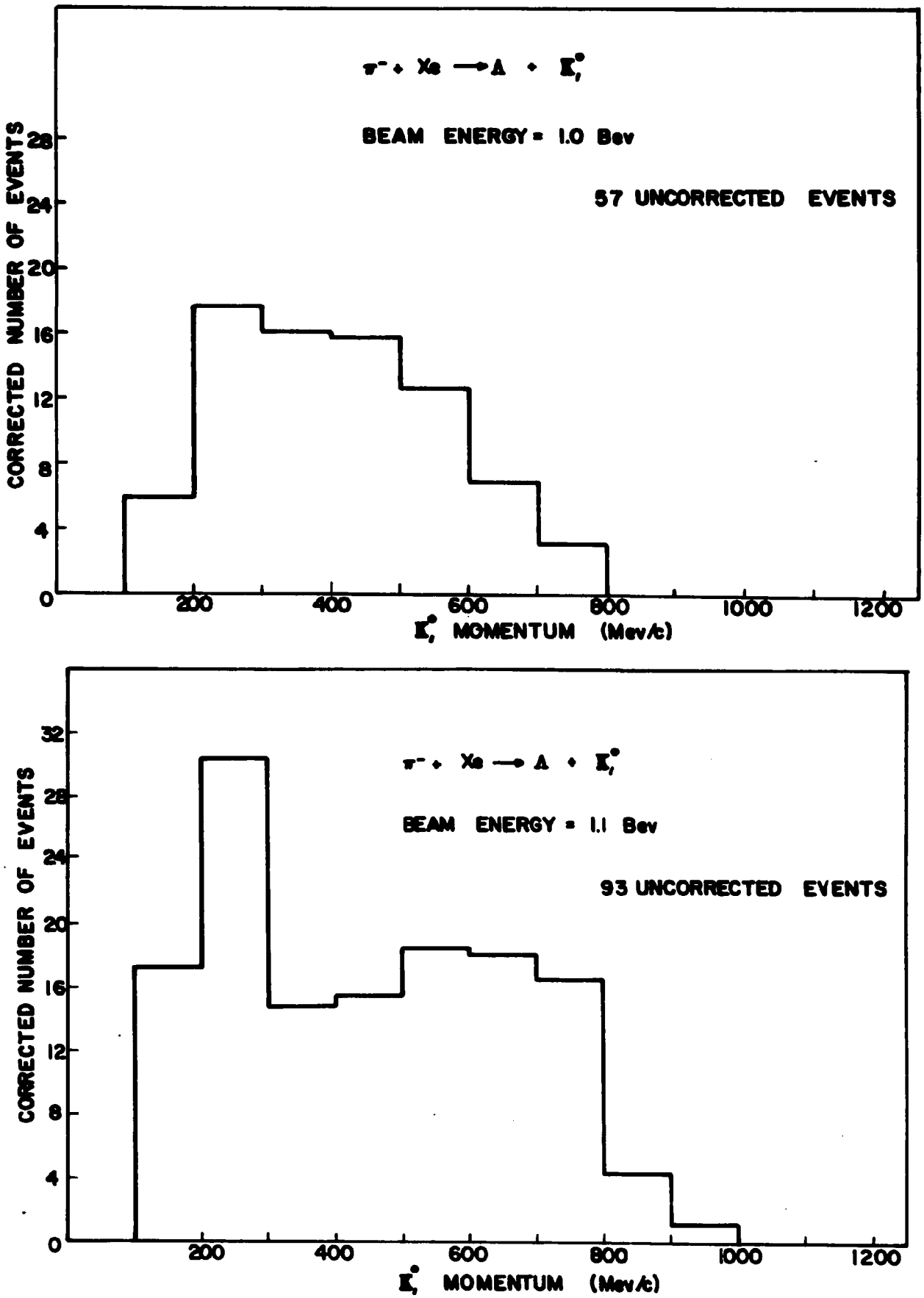
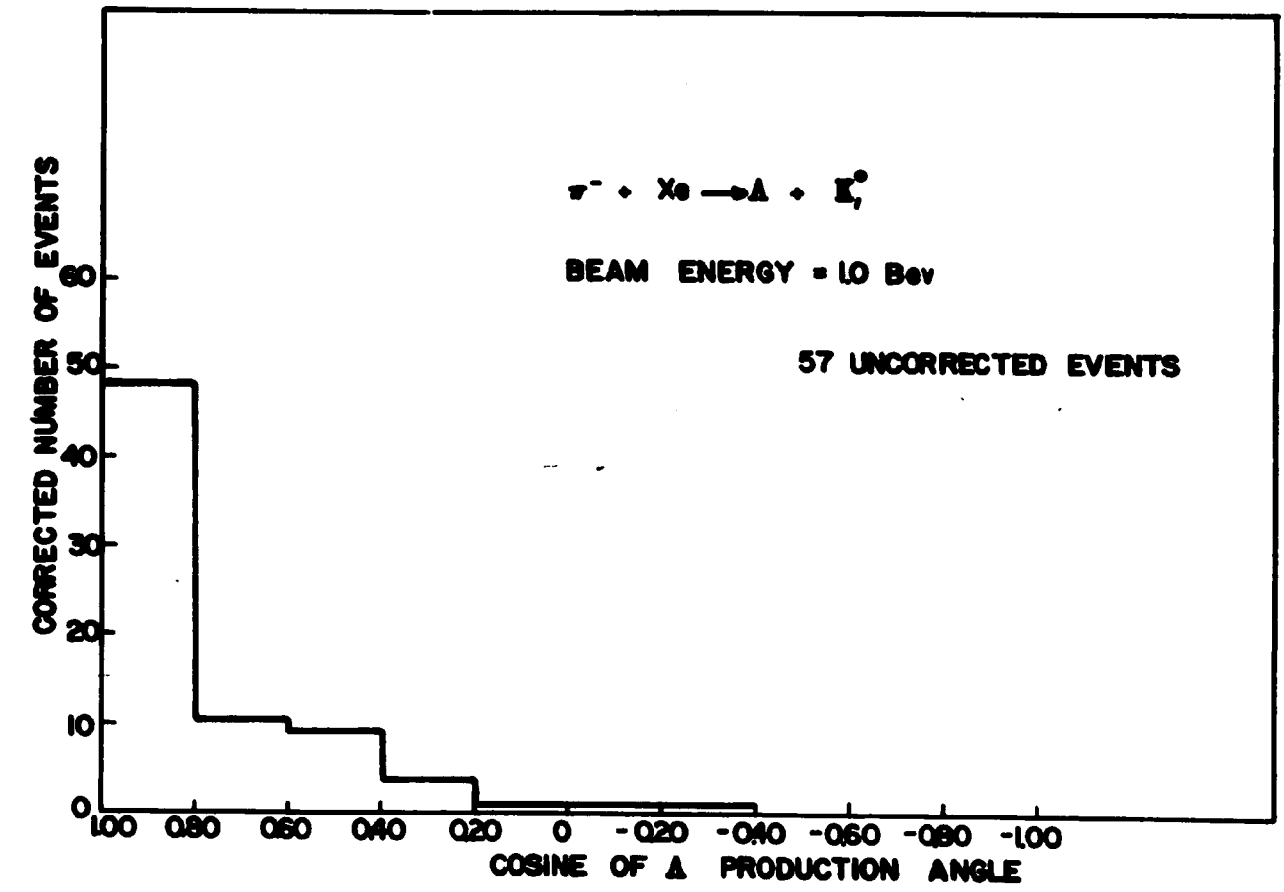


Figure 6. Corrected K_1° Momentum Distributions for ΛK_1° from 1.0 and 1.1 Bev. π^- Mesons



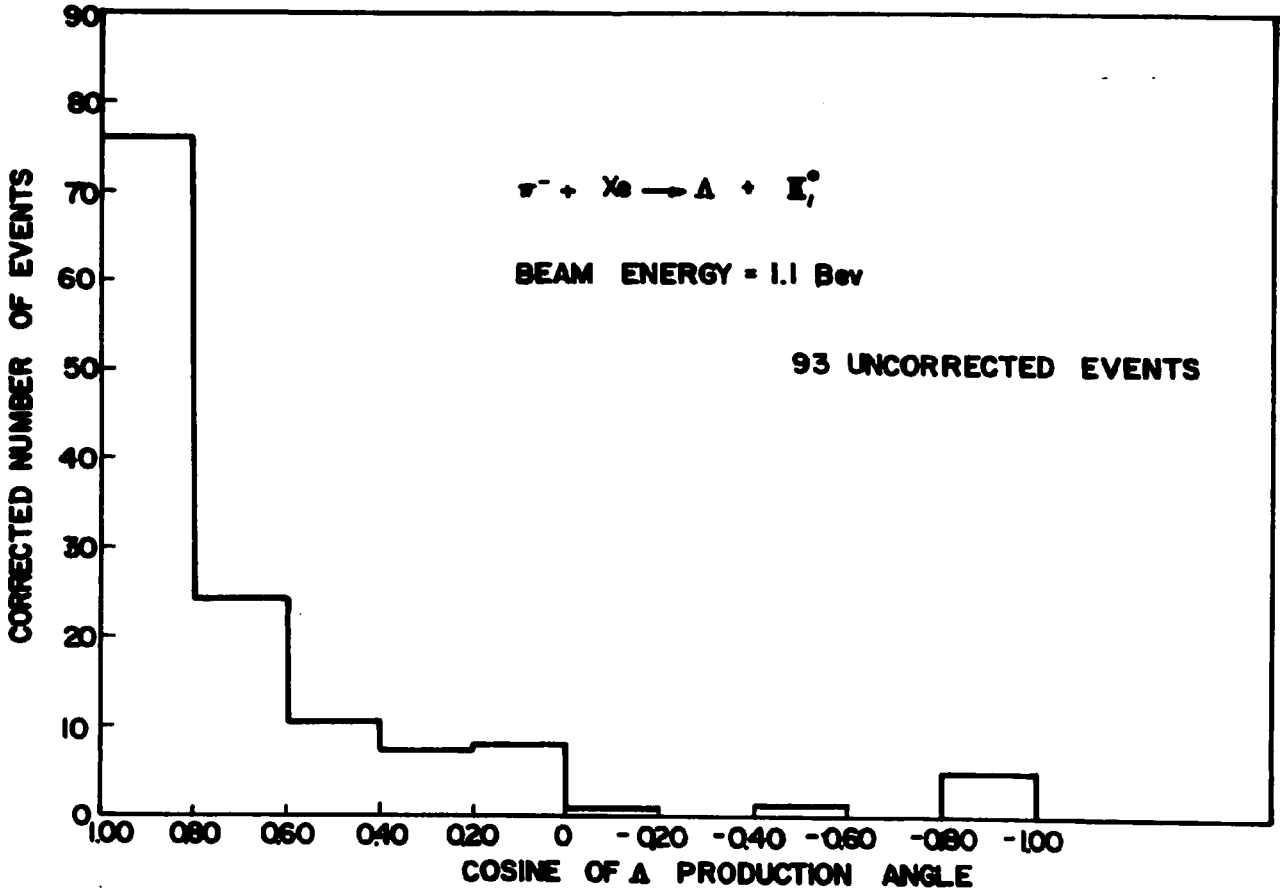


Figure 7. Corrected Λ Angular Distributions for ΛK_1° from 1.0 and 1.1 Bev. π^- Mesons

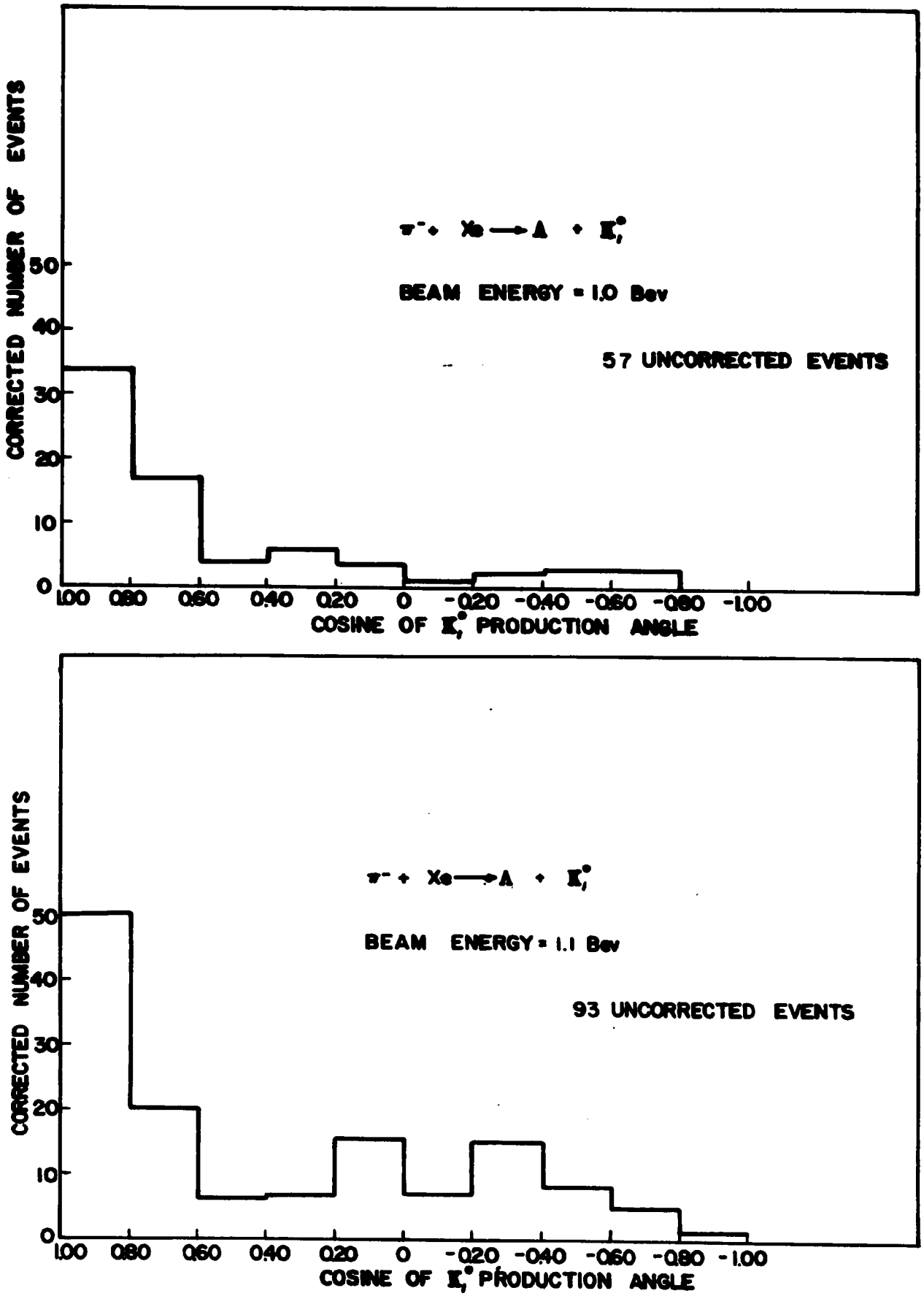


Figure 8. Corrected K_1° Angular Distributions for ΛK_1° from 1.0 and 1.1 Bev. π^- Mesons

5.2.2 Corrected Momentum and Angular Distributions of ΛK^+

The ΛK^+ sample which satisfied the cross-section criteria was used for obtaining the distributions of ΛK^+. If the K^+ meson left the chamber before decaying, the momentum was based on the observed range in the chamber; this would represent an absolute lower limit on the K^+ momentum.

In Figure 9 the corrected momentum distributions of Λ and K^+ from ΛK^+ production are displayed for a π^- beam kinetic energy of 1.0 Bev. The K^+ mesons which escaped the chamber were included and noted.

The angular distributions of Λ and K^+ from ΛK^+ are plotted in Figure 10. The K^+ mesons which left the chamber were included and noted.

In all displays the geometric corrections and corrections for one-legged Λ decays have been included.

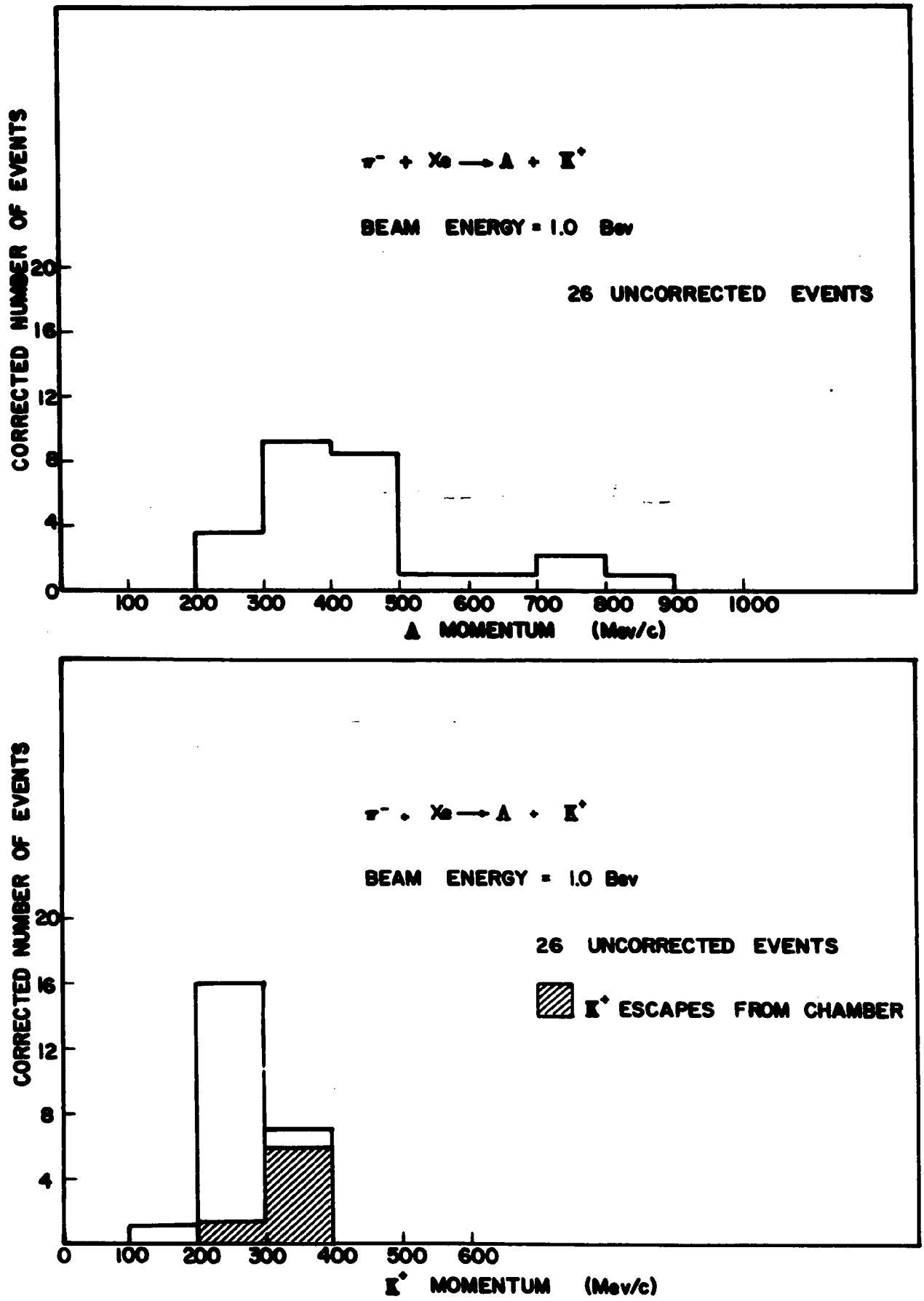
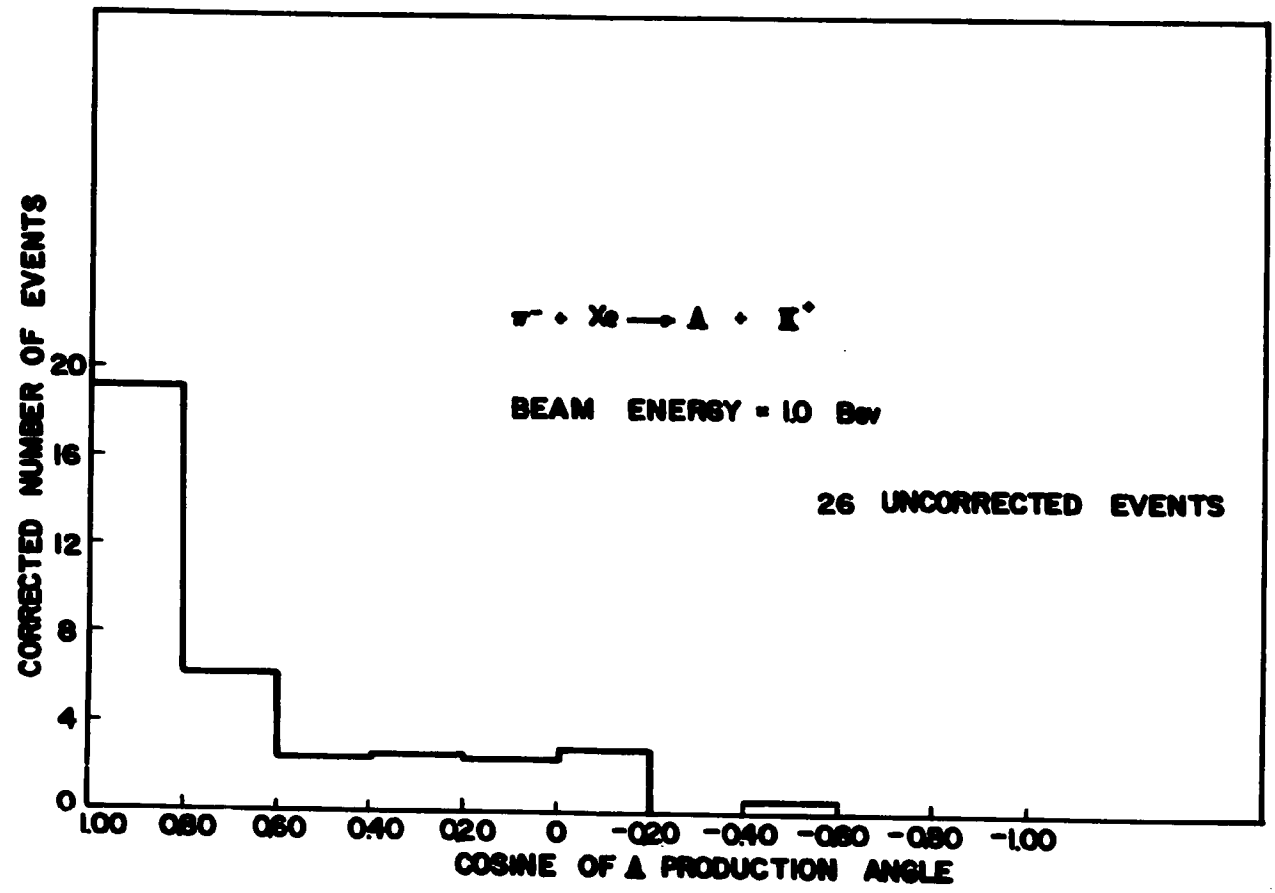


Figure 9. Corrected Λ and K^+ Momentum Distributions for ΛK^+ from 1.0 Bev. π^- Mesons



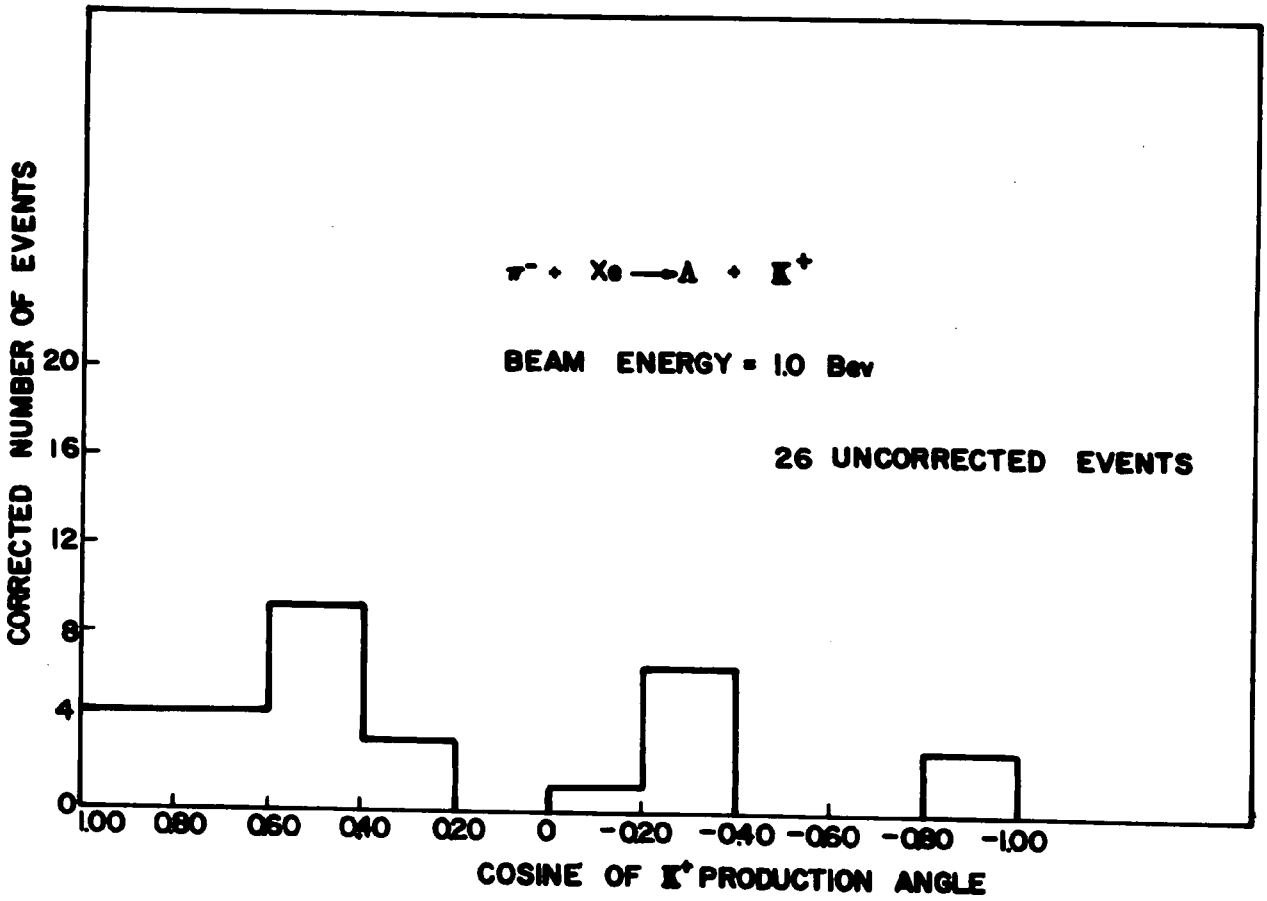


Figure 10. Corrected Λ and K^+ Angular Distributions from ΛK^+ for 1.0 Bev.

5.3 Energy and Momentum Balance in ΛK_1^0 and ΛK^+

Energy and momentum balance considerations have been applied to the same samples that were used for the momentum and angular distribution determinations of Section 5.2.

From the application of the principle of conservation of energy, the associated production of strange particles, we found that

$$E_\pi' + E_N = E_\Lambda + E_K + \Delta E$$

where

E_π' = total energy of the π^- meson in Mev

= beam energy in Mev corrected for energy loss in the beam window and in the xenon traversed

E_N = total energy of struck bound nucleon in Mev

= rest energy - 8 Mev binding energy $\simeq$ 930 Mev

$E_\Lambda + E_K$ = sum of total observed energies of Λ hyperon and K_1^0 meson in Mev

ΔE = energy unbalance in Mev

$$\Delta E = (E_\Lambda + E_K) - E_\pi' - 930 \text{ Mev}$$

Figure 11 displays the corrected distribution of ΔE for ΛK_1^0 events at each of the beam energies. The significance of ΔE is that it was a measure of the energy that strange particles lost through inelastic interactions within the parent production nucleus.

Figure 12 presents the corrected distribution of ΔE for ΛK^+ produced by the 1.0 Bev π^- beam.

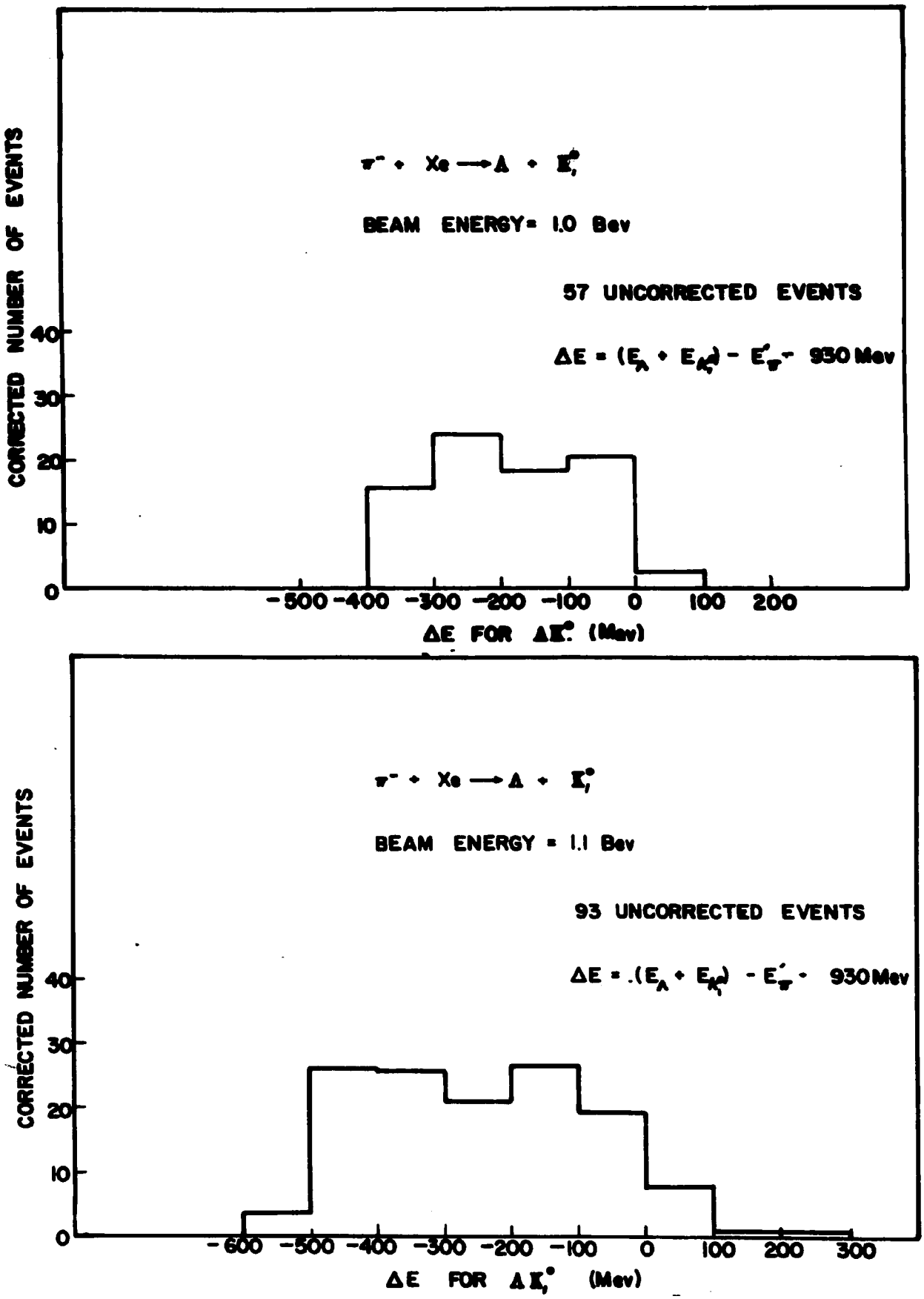


Figure 11. Corrected ΔE Distributions for ΛK_1° for 1.0 and 1.1 Bev. π^- Mesons

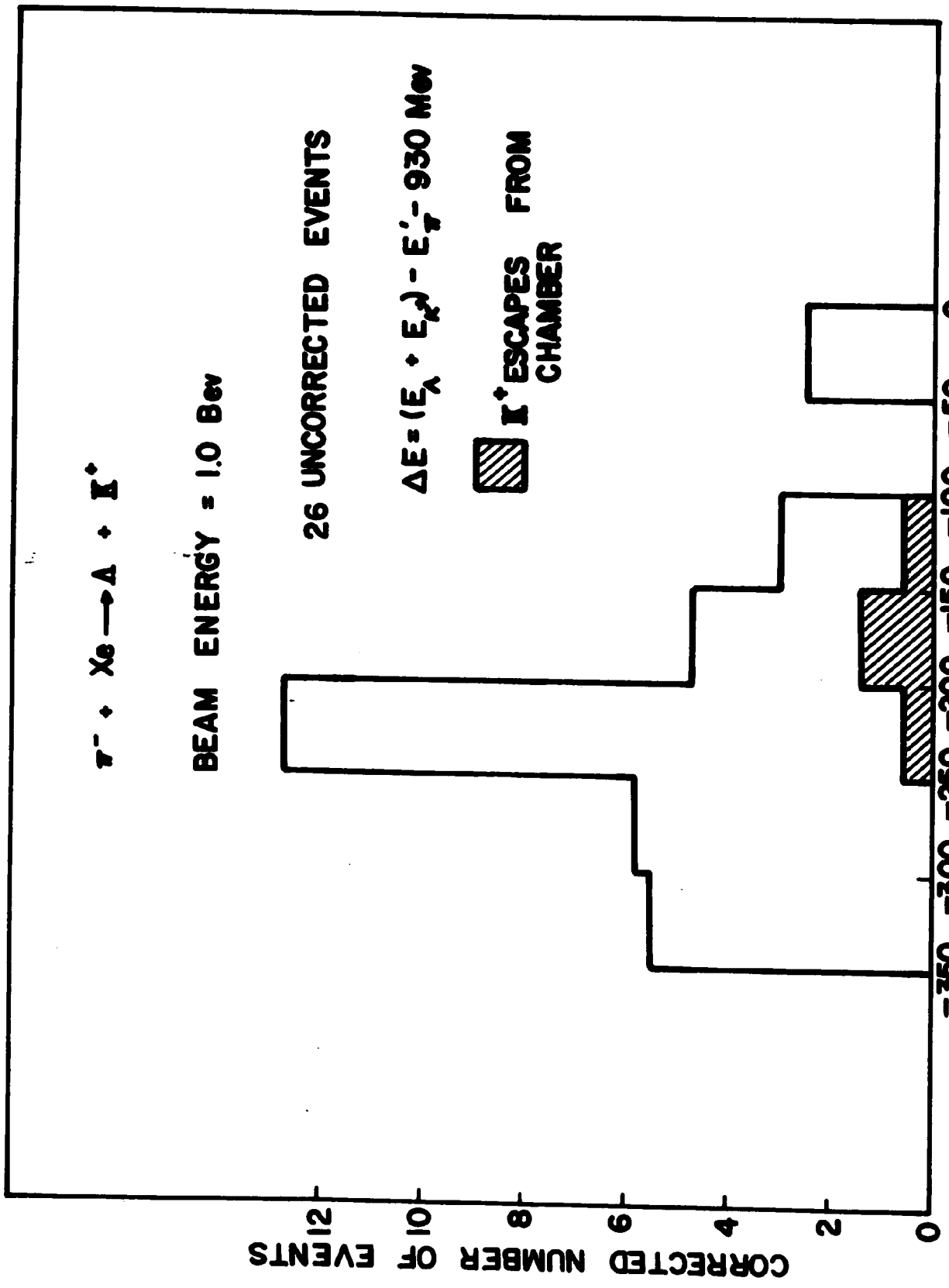


Figure 12. Corrected ΔE Distribution for ΛK^+ from 1.0 Bev. π^- Mesons

From the application of momentum conservation to associated production of strange particles

$$\vec{p}_{\pi} + -\vec{p}_{F} = \vec{p}_{\Lambda} + \vec{p}_{K}$$

where

$\vec{p}_{\pi}'$ = momentum of the π^- meson[1]

= incident beam momentum, corrected for momentum losses in the beam window and xenon

$-\vec{p}_{F}$ = momentum of the struck nucleon

$\vec{p}_{\Lambda} + \vec{p}_{K}$ = sum of the observed momenta of the Λ hyperon and the K_1° meson

$$\vec{p}_{F} = \vec{p}_{\pi} - (\vec{p}_{\Lambda} + \vec{p}_{K})$$

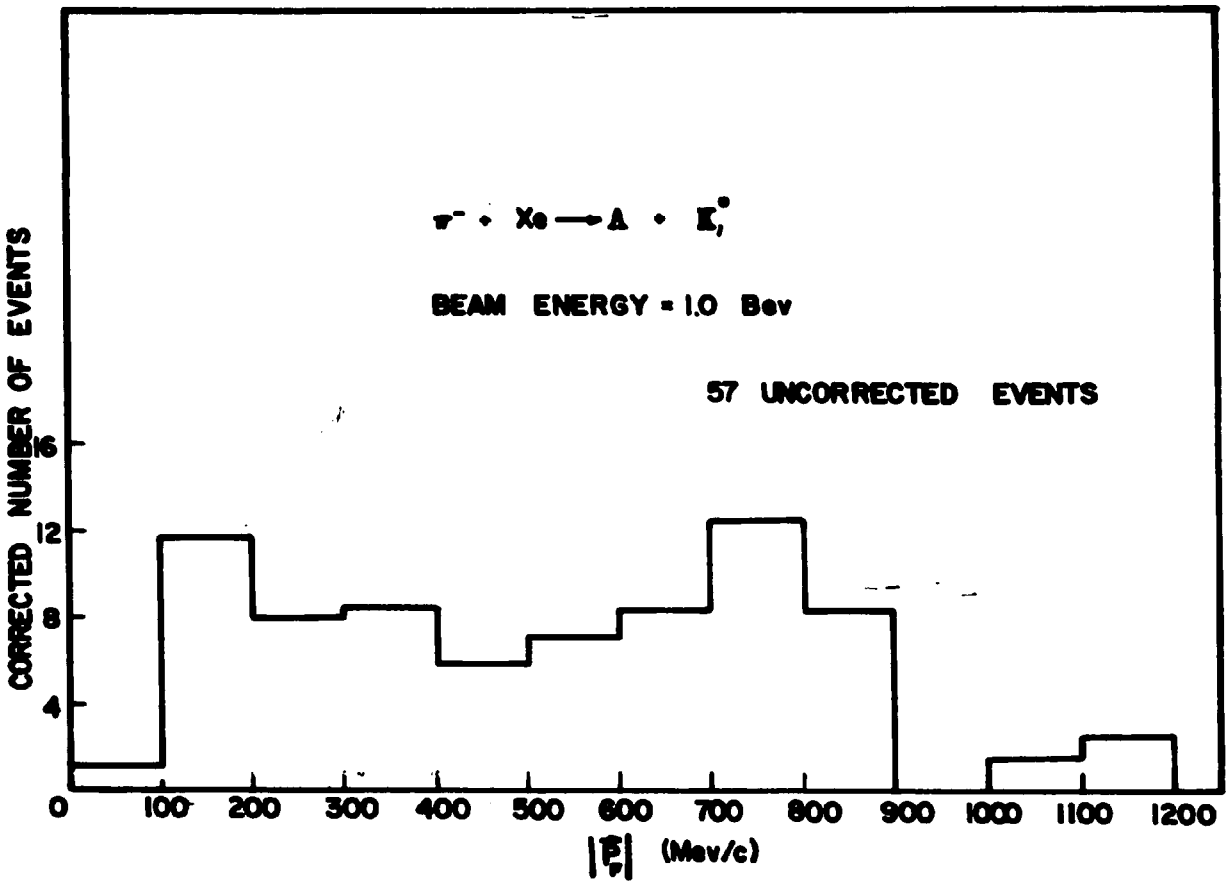
In those cases where both strange particles escaped from the nucleus without interacting, then $\vec{p}_{F}$ represented the momentum of the struck nucleon. If the strange particles had interacted inside the nucleus after production, then $\vec{p}_{F}$ was a measure of the momentum unbalance. The component of the momentum $\vec{p}_{F}$ along the beam direction was also examined.

$$p_{Fx} = \vec{p}_{F} \cdot \hat{x}$$

These corrected distributions for the quantities $|\vec{p}_{F}|$ and p_{Fx} are displayed for the ΛK_1° samples at both beam energies in Figures 13 and 14. The high values of $|\vec{p}_{F}|$ and $\vec{p}_{F} \cdot \hat{x}$ were evidence that the strange particles were interacting after production inside the parent xenon nucleus.

---

[1] All momenta are in the units Mev/c.



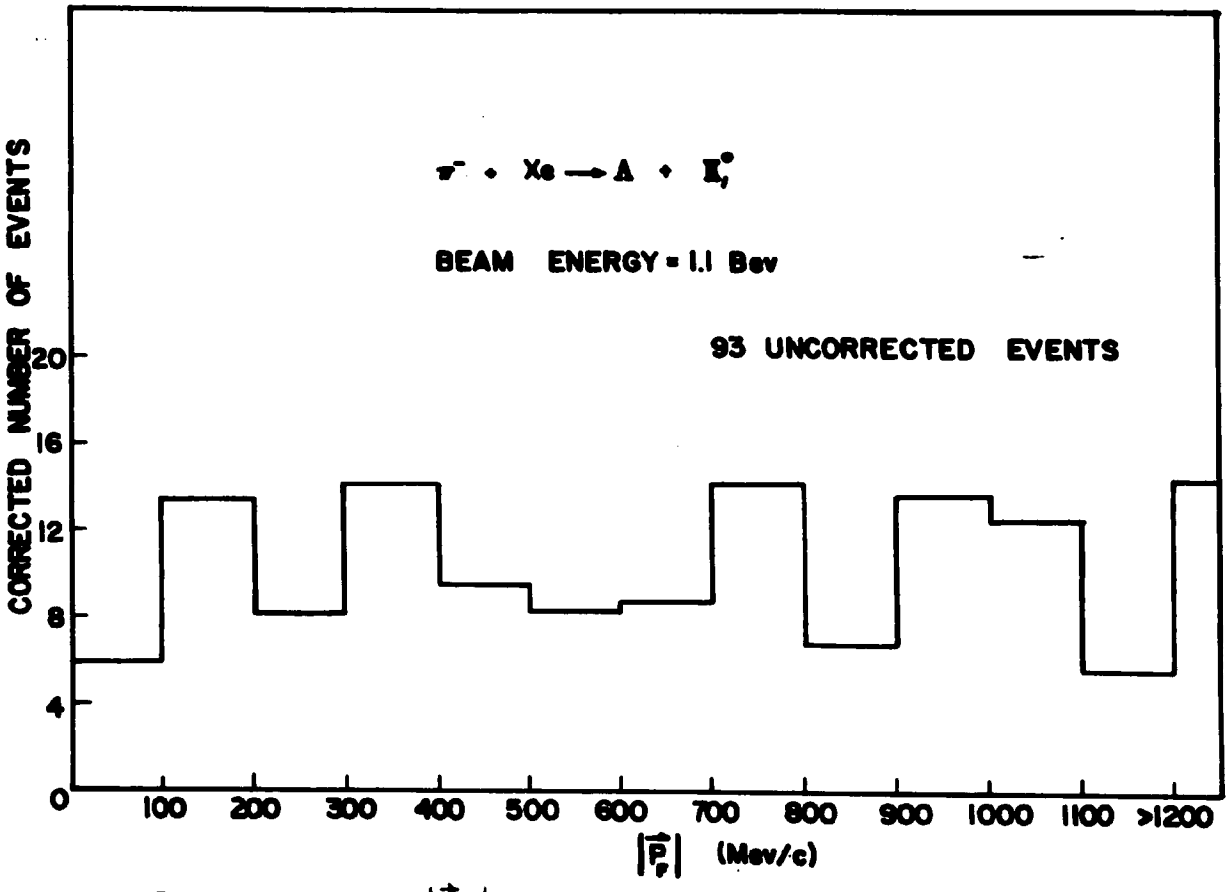
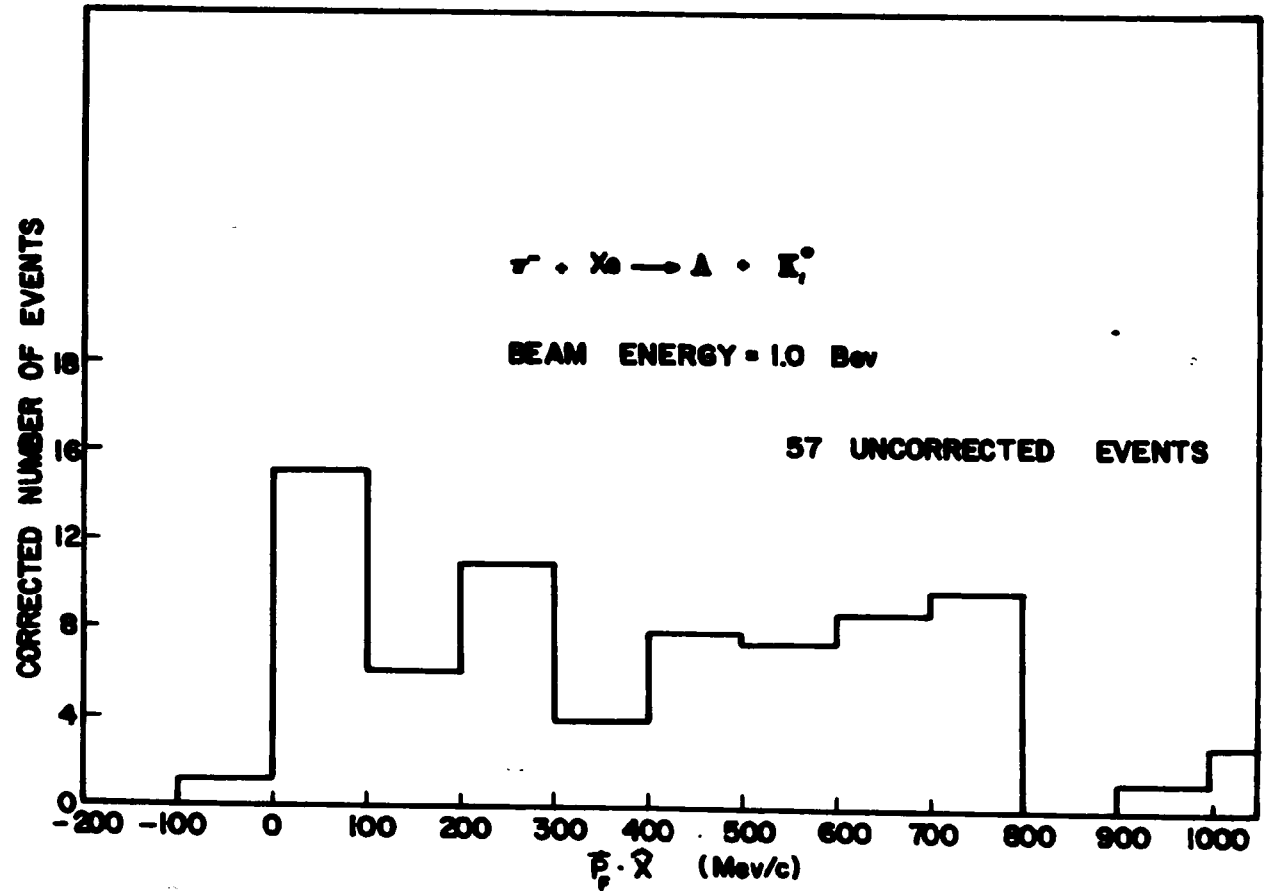


Figure 13. Corrected $|\vec{p}_F|$ Distributions from ΛK_1^0 for 1.0 and 1.1 Bev. π^- Mesons



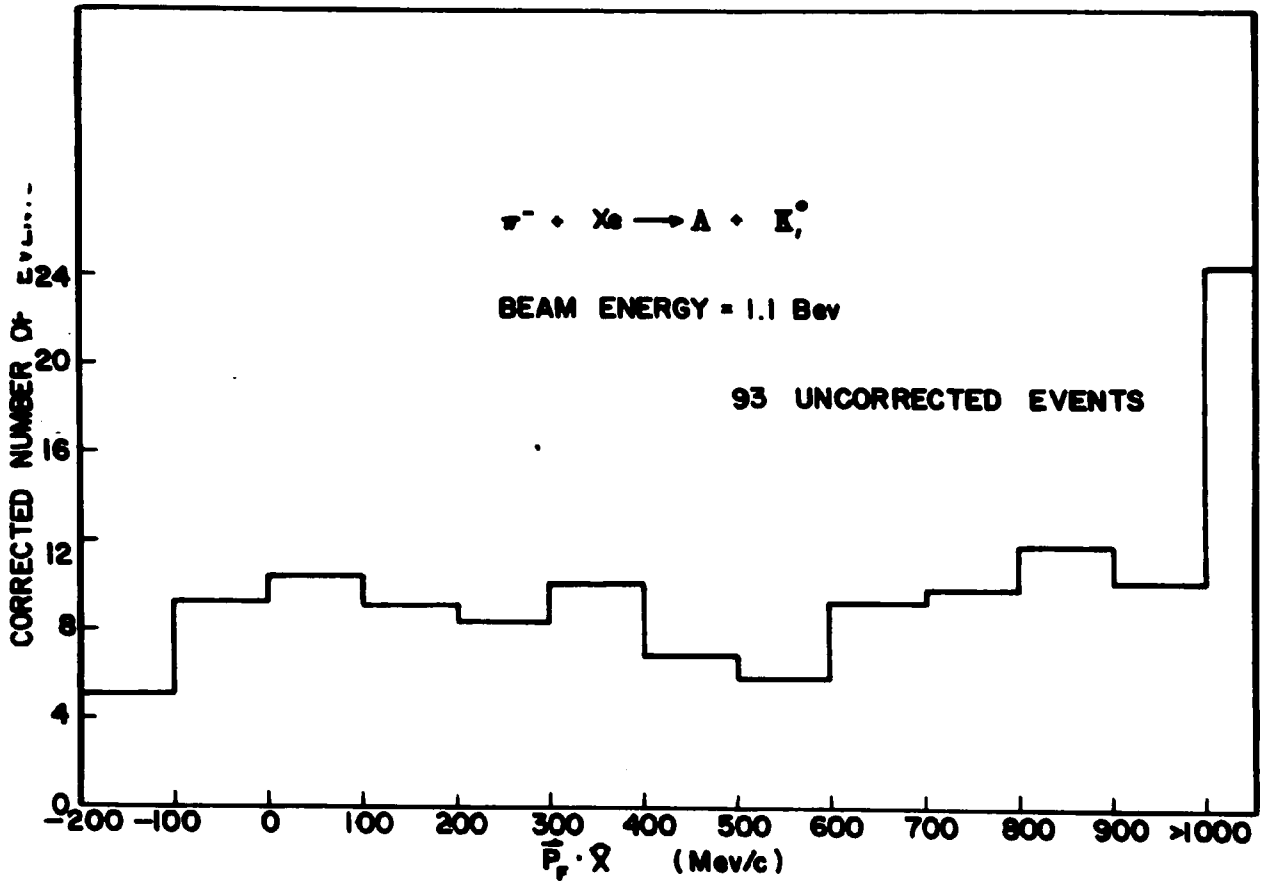


Figure 14. Corrected $\vec{p}_F \cdot \hat{x}$ Distributions from ΛK_1^0 for 1.0 and 1.1 Bev. π^- Mesons

5.4 Interactions of K° Mesons

The observation of a Λ decay in the bubble chamber consistent with being produced at an interaction origin marked by the disappearance of a π^- meson, was the signature that a K° or K^+ particle of strangeness +1 had been simultaneously produced. For events with this signature, we have searched the entire illuminated volume of the xenon bubble chamber for visible manifestations of the interactions of K° mesons.

Figure 15 is an example of a Λ_+ signature and an associated interaction of a K° meson. In this case the charge exchange reaction was observed

$$K^\circ + p \rightarrow K^+ + n$$

Figure 16 is an example of a Λ_+ signature and a second V° particle in the same picture. From the ranges of the secondaries of this V° particle and its opening angle, it has been unambiguously identified as a Λ hyperon. Furthermore, measurements indicated that it was emitted from the neutral star[1] (labeled on the photograph). This event has been interpreted as an example of a Λ hyperon being produced by the interaction of a K° meson. We have found nine additional examples of neutral stars which produced Λ hyperons and contained simultaneous Λ signatures from beam origins in the same photograph. In eight of these nine cases both of the secondaries from the Λ_+ decay stopped by ionization in the

[1] A neutral star is an interaction produced by a neutral particle; that is, an interaction not produced by a charged particle.

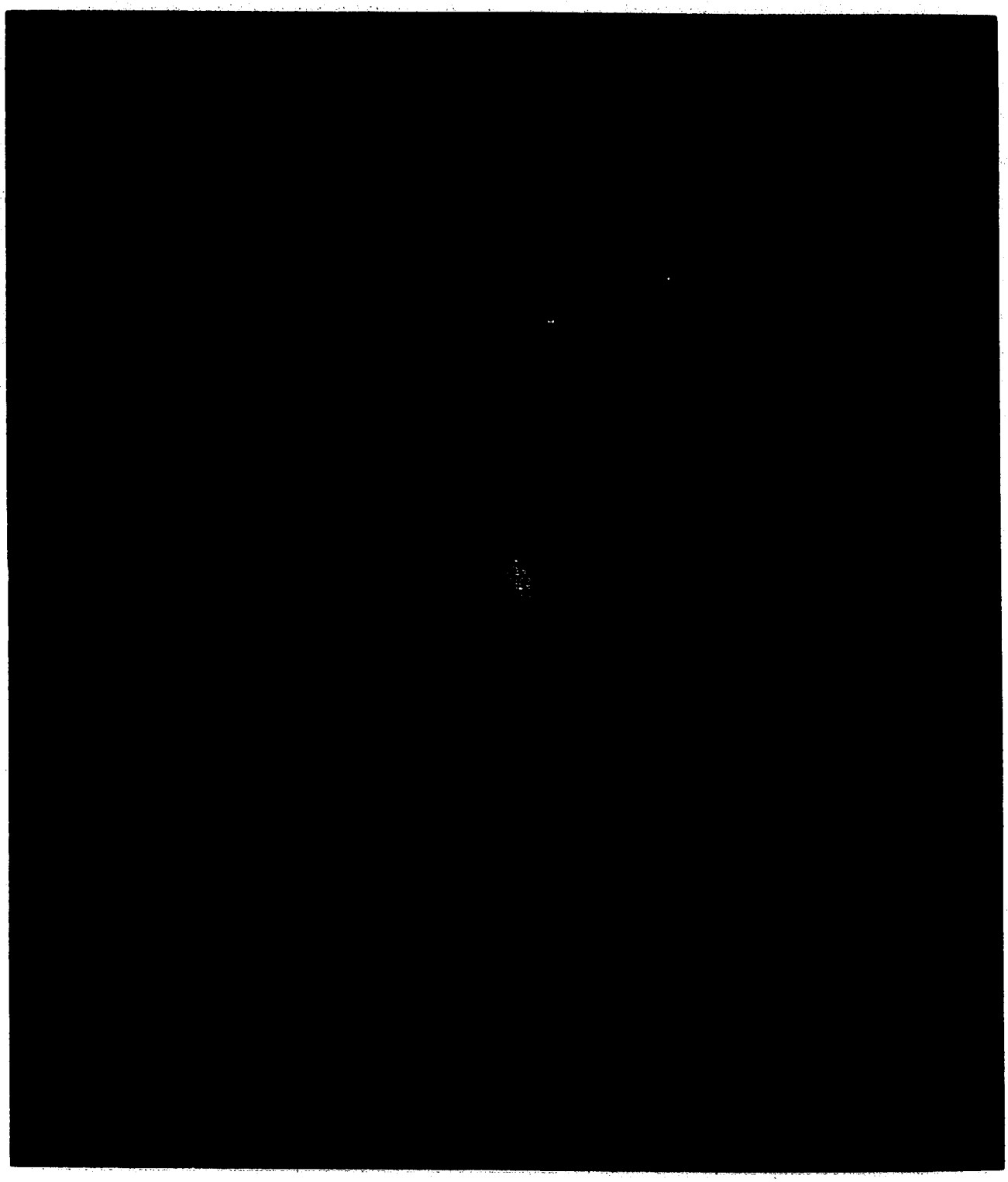


Figure 15. K° Interaction as Seen on Film

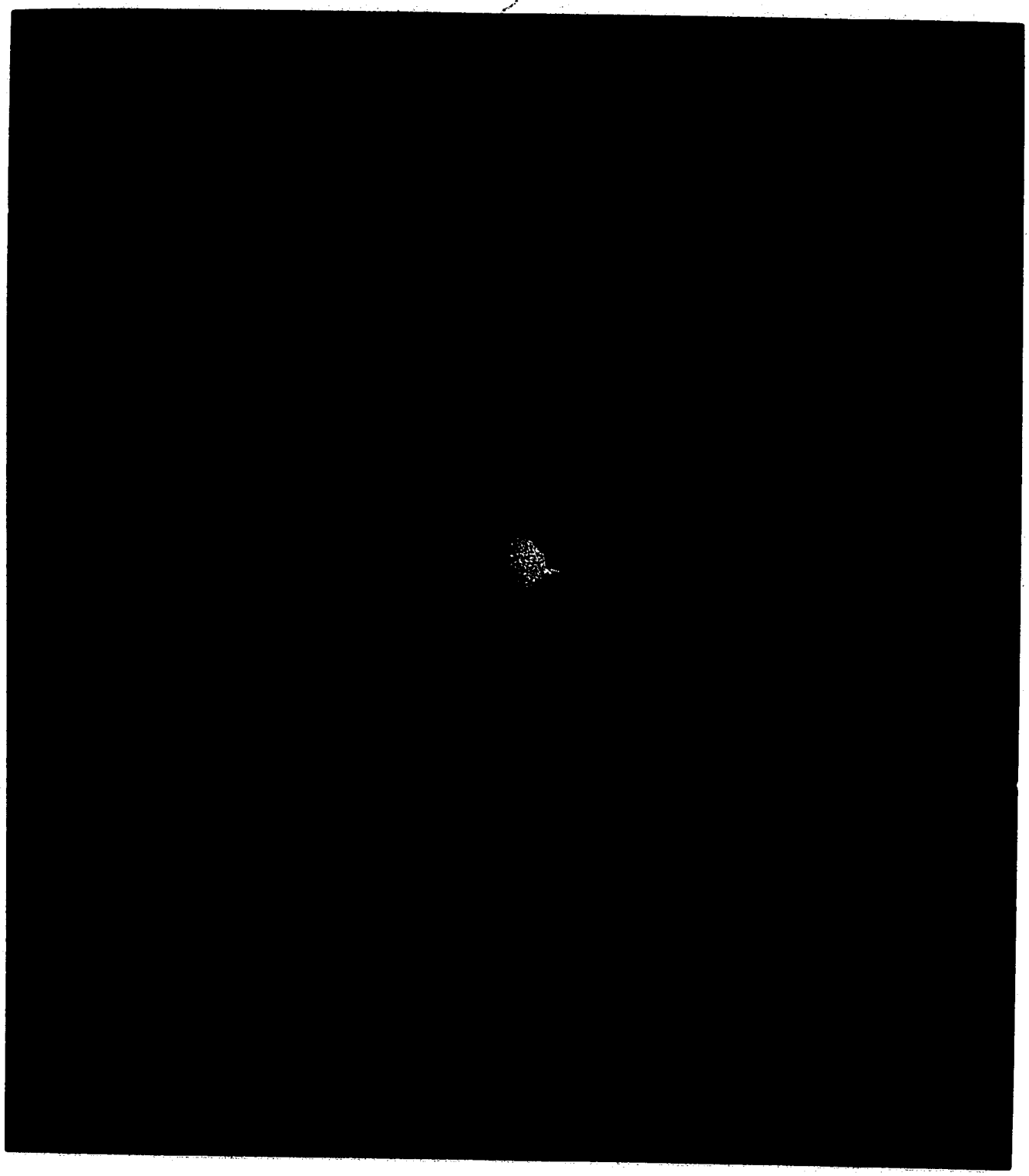


Figure 16. $\bar{K}^{o}$ Interaction as seen on Film

chamber, and therefore these V° particles from the neutral stars were unambiguously identified as Λ hyperons.

It was quite clear then that these neutral stars did produce Λ hyperons. We had to establish, however, the extent to which these neutral stars could be attributed to the interactions of K° mesons. The production of a K° meson was established by the appearance of a Λ signature. In order to prove that these Λ signatures were not accidents, we had to determine the probability of finding a sample of nine neutral stars which produced Λ_+ and contained a simultaneous associated Λ hyperon from a beam origin.

Since we were assuming that the two processes were independent

$$P(\Lambda\bar{K}^\circ) = p(\Lambda)\, p(\bar{K}^\circ)$$

where

$p(\Lambda)$ = probability of observing a Λ hyperon (either charged or neutral) decay per picture

$p(\bar{K}^\circ)$ = probability of observing a neutral star which produced Λ_+ hyperon per picture

We used the experimental data available for frames 4,000 - 86,000 to determine $p(\bar{K}^\circ)$. For that section of the film, every two prong V° with both legs stopping in the chamber was measured. A total of twelve Λ_+ which came from neutral stars were found.

$$p(\bar{K}^\circ) = \frac{12}{82{,}000} = 1.5 \times 10^{-4} \text{ events/picture}$$

$$p(\Lambda) = \frac{171}{82{,}000} = 2.1 \times 10^{-3} \text{ events/picture}$$

$$p(\Lambda K^\circ) = 3 \times 10^{-7} \text{ events/picture}$$

We defined

$\bar{N}(\Lambda\bar{K}^\circ)$ = average counting rate for $\Lambda\bar{K}^\circ$ events for 1.36×10^5 pictures

$\bar{N}(\Lambda\bar{K}^\circ) = 1.36 \times 10^5 \times p(\Lambda\bar{K}^\circ)$

$\bar{N}(\Lambda\bar{K}^\circ) = 4 \times 10^{-2}$ counts

The probability of observing the chance coincidence of nine Λ and nine $\bar{K}^\circ$ events in 136,000 pictures was found from the Poisson distribution

$$P(\Lambda\bar{K}^\circ) = P(n,\bar{N}) = \frac{\bar{N}^n}{n!} e^{-\bar{N}}$$

where

$P(n,\bar{N})$ = Poisson distribution

n = number of events = nine

$\bar{N}$ = "true" counting rate = average observed counting rate for $\Lambda\bar{K}^\circ$ events = 4×10^{-2}

$$\ln P(n,\bar{N}) = n \ln \bar{N} - \bar{N} - \ln n! \cong n \ln \bar{N} - \bar{N} - n \ln n + n$$

$$\ln P(n, \bar{N}) \cong -64.7$$

$$P(\Lambda\bar{K}^\circ) \cong e^{-65}$$

It was very unlikely, therefore, that the Λ signature and the neutral stars were chance associations. In fact, we now consider it established that they were associated.

The K° mesons were the mesons of strangeness +1. By the $\Delta S = 0$ rule for strong interactions, they were forbidden to produce hyperons. The particle mixture theory for neutral K mesons[15] explains hyperon

production by K° mesons and predicts for an initially produced K° meson, a $\bar{K}^\circ$ amplitude which would grow as a function of time. The $\bar{K}^\circ$ mesons could produce hyperons according to the elementary reactions

$$\bar{K}^\circ + n \rightarrow Y + \pi^{\circ}_{\pm}$$

$$\bar{K}^\circ + p \rightarrow Y^{+}_{\circ} + \pi^{+}_{\circ}$$

where Y is the symbol for a hyperon.

The rate of growth of the $\bar{K}^\circ$ amplitude was sensitive to the $K_1^\circ - K_2^\circ$ mass difference where K_1° and K_2° are the short-lived and long-lived K° decay modes. For various values of this mass difference, the rate of growth of $\bar{K}^\circ$ would reflect itself in different distributions in the distance of the hyperon producing interactions from the beam origins which produced the K°.[15,16]

$$F(\mu,t) = \left|\bar{K}^\circ(\mu,t)\right|^2 = \text{intensity of } \bar{K}^\circ \text{ component at time t after birth of } K^\circ$$

$$F(\mu,t) = \left|\bar{K}^\circ(\mu,t)\right|^2 = \frac{1}{2} e^{\frac{-(\delta+1)t}{2\gamma\tau_1}} \times \left[\cosh\frac{t}{2\gamma\tau_1} - \cos\frac{\mu t}{\gamma\tau_1}\right]$$

where

μ = $K_1^\circ - K_2^\circ$ mass difference in dimensionless units

$\gamma = \frac{E_\kappa}{M_\kappa}$ where E_κ = total energy of K° meson in Mev, and M_κ = rest energy of K° meson in Mev

τ_1 = lifetime of K_1° meson

t = time measured from birth of K_1° meson in laboratory system

δ = attenuation factor for K° in xenon = 0.1

Figure 17 presents sample curves of $F(\mu,t)$ for various values of the $K_1^\circ - K_2^\circ$ mass difference. The formulas were evaluated for a definite K° momentum of 421 Mev/c.[1]

A maximum likelihood calculation of the $K_1^\circ - K_2^\circ$ mass difference based on these principles has been devised. Starting from the observed spatial distribution of hyperon producing $\bar{K}^\circ$ interactions listed in Table 17 in Appendix C, a normalized likelihood function $L(\mu)$ was evaluated for various trial values of the $K_1^\circ - K_2^\circ$ mass difference. The calculation averages over an observed K_{1+}° momentum distribution of arbitrary length[2] after correcting the observed K_{1+}° distribution for escape and short decay. The entire calculation was performed by the IBM 704 computer and the details of this computation are discussed in Appendix B. This computation is easily adaptable for use with other experiments and, for a larger number of events, may result in a good estimate of the $K_1^\circ - K_2^\circ$ mass difference.

In this experiment we have found 12 $\bar{K}^\circ$ interactions with an associated Λ signature clearly present in the same photograph. In three of these 12 cases the neutral star emitted charged particles which were

[1] This was the average momentum of 36 K_{1+}° mesons randomly selected from the observed $\Lambda_+ K_{1+}^\circ$ cross section sample.

[2] The present computer program limits the K_{1+}° distribution to 500.

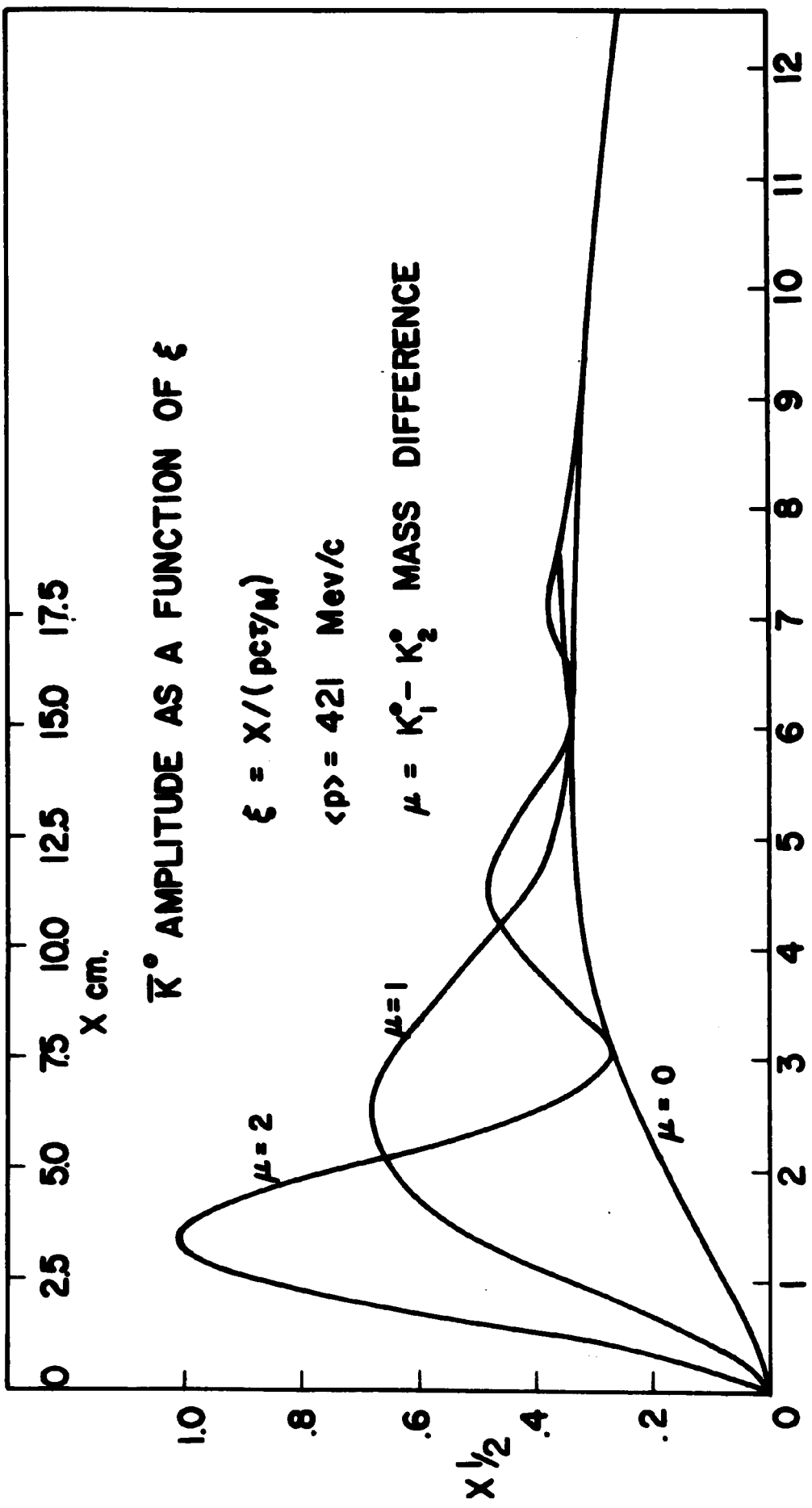


Figure 17. $\bar{K}^0$ Amplitude as Function of Distance from Beam Origin

interpreted as $\Sigma^{\pm}$ hyperons which decayed in the chamber. One additional $\bar{K}^{\circ}$ interaction was found where the neutral star emitted a Λ hyperon but where the beam origin hyperon was a Σ^{-} instead of a Λ. We have added these four events to our original sample of nine events.

The results of the mass difference computation for these 13 events is presented in Figure 18. The K° momentum distribution averaged over, consisted of 36 charged K_1° events chosen randomly from the ΛK_1° cross section sample.[1]

The likelihood function exhibits its peculiar behavior due to the presence of one event[2] where the $\bar{K}^{\circ}$ interaction occurred 0.56 cm from the beam origin. This result displayed in Figure 18 does not seem to be meaningful.

In the case that this event were a fluctuation, we have removed it from the sample by not considering $\bar{K}^{\circ}$ interactions less than 1.0 cm from the beam origin. On the other hand, we have correspondingly corrected the likelihood function to take this change in normalization into account.

$$f_i(\mu,t) = \text{normalized probability function for } i^{th} \text{ event}$$

$$= \frac{F_i(\mu,t)}{\int_{t_{min}}^{t_{max}} F_i(\mu,t)\ dt}$$

---

[1] We have limited the distribution to 36 events in order to conserve computer time.

[2] Frame number 121537.

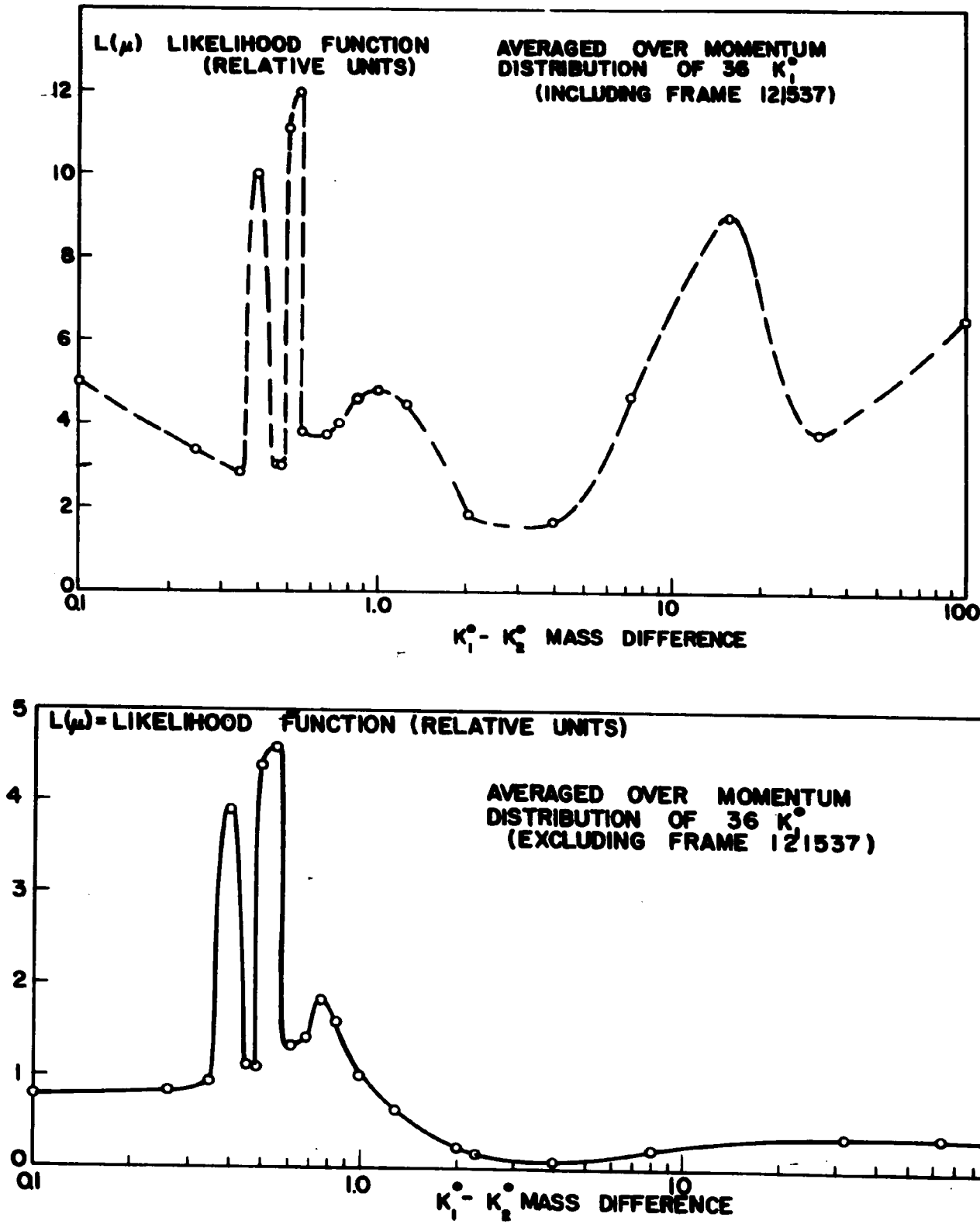


Figure 18. Likelihood Functions for Observed $\bar{K}^{\circ}$ Interactions

$$t_{max} = \frac{\text{potential path}}{pc/M_{\kappa}}$$

and

$$t_{min} = \frac{x_{min}}{pc/M_{\kappa}}$$

where

x = distance of $\bar{K}^{\circ}$ interaction from beam origin.

If we set x_{min} = 1.0 cm then the results of this new calculation of the K_1° - K_2° mass difference are displayed in Figure 18.

This likelihood function does seem to exhibit a definite maximum in the vicinity of mass difference one-half. It would be interesting to examine the results of this calculation with a K_1° momentum distribution of greater length to determine the effect of the size of the distribution on the result.

We have investigated the observed $\bar{K}^{\circ}$ interactions in order to determine whether the number seen was in accord with the expected number.

The total probability of a $\bar{K}^{\circ}$ interaction was obtained by the integration of the $\bar{K}^{\circ}$ probability function

$$N_i(\mu) = \frac{1}{\lambda} \int_0^{t_{max}} \left| \bar{K}_i^{\circ}(\mu,t) \right|^2 \frac{p_i c}{\gamma_i M_{\kappa}} \, dt_i$$

where

$N(\mu)$ = total probability of the i^{th} $\bar{K}^{\circ}$ interacting in an observation time, $t_i max$.

$t_i max$ = potential time of i^{th} $\bar{K}^{\circ}$ in the chamber

λ = mean free path for $\bar{K}^{\circ}$ interaction in cm of xenon = 60.4 [17]

$$\sum_{i=1}^{N_{K^\circ}} N_i(\mu) = \frac{1}{\lambda} \sum_{i=1}^{N_{K^\circ}} \int_0^{t_i^{max}} |\bar{K}_i^\circ(\mu,t)|^2 \frac{p_i c}{\gamma_i M_K} dt_i$$

where N_{K° = total number of K° corrected for escape.

The right hand side of the above equation has been empirically evaluated by using the observed spatial and momentum distributions of 124 K°_{1+} from the double V sample.

$\lambda < N(\mu) >$ = average number of expected $\bar{K}^\circ$ interactions per K°

The results were a function of the $K_1^\circ - K_2^\circ$ mass difference, and for $K_1^\circ - K_2^\circ$ mass differences between 0 and 1, $\lambda < N(\mu) >$ ranged between 2.0 - 3.5.

We estimated that there were 790 K° based on a total number of 250 observed $\Lambda_+ K^\circ_{1+}$ and by using an escape correction of 1.05.

The results of the expected number of $\bar{K}^\circ$ interactions for mass differences 0 and 1 are displayed in Table 14.

TABLE 14

EXPECTED NUMBER OF $\bar{K}^\circ$ INTERACTIONS

MASS DIFFERENCE	EXPECTED NUMBER
0	16
1	28

We observed 10 events with a Λ_+ to a beam origin and an associated $\bar{K}^\circ$ interaction star. In addition, since neutral decays from $\bar{K}^\circ$ stars could not be detected efficiently, the observed number of $\bar{K}^\circ$ interactions, which lead to Λ_+ (seven events), was corrected accordingly.

$N_c(\Lambda_+\bar{K}^\circ)$ = corrected number of observed $\bar{K}^\circ$ interactions

$N_c(\Lambda_+\bar{K}^\circ) = \left(\frac{7}{1 - B_\Lambda}\right)$ (escape correction for Λ from $\bar{K}^\circ$) + 3 [1]

$N_c(\Lambda_+\bar{K}^\circ) = 17.7$

This number of observed interactions has to be regarded as a lower limit on the number of $\bar{K}^\circ$ produced since it was possible that a certain fraction of the $\bar{K}^\circ$ interaction stars in xenon did not lead to an observable hyperon such as a Λ or $\Sigma^{\pm o}$ and instead produced hyperfragments or perhaps ordinary stars in xenon.

However if this loss of $\bar{K}^\circ$ interactions through reactions which do not produce hyperons is small, then these results could be interpreted to indicate that the K_1° - K_2° mass difference is less than 1.

---

[1] These are events where a $\bar{K}^\circ$ interaction produces a $\Sigma^\pm$.

5.5 Polarization of Λ from ΛK° and ΛK^+

Experiments with the hydrogen bubble chamber have established that Λ produced by the interaction of 1.0 - 1.1 Bev π^- mesons in the reaction

$$\pi^- + p \rightarrow \Lambda + K^\circ$$

were polarized.[19] This result was based on the observation of an up-down asymmetry of the Λ decay pion with respect to the Λ production plane where up was defined as $\cos \xi > 0$ and where $\cos \xi$ was

$$\cos \xi = (\hat{\pi}_{beam} \times \vec{\Lambda}) \cdot \hat{\pi}_{decay}^{1}$$

$$W(\xi^*, \eta^*)\, d\Omega^* = \frac{1}{4\pi} (1 + \alpha \bar{P} \cos \xi^*)\, d \cos \xi^*\, d\eta^*$$

where

$W(\xi^*, \eta^*)$ = intensity of decay pions from charged Λ decay

$\bar{P}$ = polarization averaged over all production angles

α = parameter of up-down asymmetry

η^* = azimuthal angle in Λ center of mass

By integration

$$\alpha\bar{P} = \frac{2 (N_{up} - N_{down})}{N_{up} + N_{down}}$$

Some information concerning the polarization of Λ produced in complex nuclei by 1.5 Bev π^- mesons was published but these results were uncertain.[20]

We therefore present the results of a study of the polarization of Λ produced by 1.0 and 1.1 Bev π^- mesons in the complex nucleus of xenon.

---

1 $\hat{\pi}$ decay in Λ center of mass.

The largest possible samples of Λ were assembled in order to decrease the statistical errors. The usual limitations on the number of tracks in a picture, the requirements on the origins for events, and fiducial volume limitations were relaxed in order to increase the number of events. The following criteria were retained.

Criteria for Double V Sample

(1) The charged decay was in reasonable agreement with the kinematics graphs for the Λ_+ decay.

(2) The measured coplanarity of the $\Lambda_+ \leq 7°$.

(3) The decay distance was ≥ 0.50 cm.

(4) No origin prongs left the visible volume of the chamber.[1]

(5) There was a possible K°_{1+} decay in the picture associated with the same beam origin as the Λ_+.

The result for the total $\Lambda_+ K^\circ_{1+}$ sample of 222 events (1.0 - 1.1 Bev) was

$$\alpha\bar{P} = +0.32 \pm 0.11$$

The probability that an unpolarized sample could give this result was 0.003.

Criteria for Single Λ Sample

(1') Same as (1) of Double V Sample

(2') Same as (2) of Double V Sample

(3') Same as (3) of Double V Sample

(4') Same as (4) of Double V Sample[1]

[1] This was to remove possible $\Lambda_+ K^+$ events.

(5') There was no K°_{1+} decay associated with a Λ_+ from the same beam origin. In addition, no more than one possible electron pair was associated with the beam origin; that is, there was no evidence of a K°_{1} decay either charged or neutral in the picture.

The result for the total $\Lambda_+ K^{\circ}_{2}$ sample of 233 events was

$$\alpha\bar{P} = +0.05 \pm 0.11$$

If the double V and single Λ samples had the same value of $\alpha\bar{P}$ and the observed results were due to statistical errors, then the probability that the result of $\alpha\bar{P} = +0.32 \pm 0.11$ was consistent with the result $\alpha\bar{P} = +0.05 \pm 0.11$ was 0.07.

As a check that our samples were not biased, control asymmetry parameter calculations were performed. Samples of K°_{1+} which appeared with Λ_+ were selected according to criteria similar to those used for selecting Λ_+ from double V. In this control sample a preferential orientation of the faster pion from the K°_{1+} decay was looked for but not detected. A similar control check was performed for single K°_{1+}, also with negative results.

These samples, double V and single Λ have been further subdivided according to beam energy and momentum. The division according to beam energy was made between the events at 1.0 Bev and the events at 1.1 Bev. The momentum separations were made into events with Λ momentum above or below 0.500 Bev/c.

The fast Λ's(defined as Λ with momentum greater than 0.500 Bev/c), were thought more likely to have been unscattered after production than slow Λ (defined as Λ with momentum less than 0.500 Bev/c). There was evidence from those double V events, where both strange particles escaped from the nucleus with small or no energy loss, that the momentum was greater than for these Λ's.

The results of all asymmetry parameter runs are displayed in Table 15 together with errors and the number of events in each sample.

For the calculations of Table 15, the simple computation for $\alpha\bar{P} = \frac{2\,(N_{up} - N_{down})}{N_{up} + N_{down}}$ has been replaced by a maximum likelihood calculation which for the same number of events yielded results with smaller statistical errors.[1]

The apparent difference in polarization between the $\Lambda_+K^\circ_2$ and $\Lambda_+K^\circ_{1+}$ samples was a puzzling result. The samples were rechecked to ensure that the criteria were applied in a uniform and unbiased manner. One difference between the double V and single Λ_+ samples was that in one case a K°_1 mode was present and in the other the K°_2 mode. Since the K°_{1+} showed a positive asymmetry, we determined $\alpha\bar{P}$ for the sample of Λ_+ with neutral K°_1 decays. The result was $\alpha\bar{P} = +.32 \pm 0.27$ for $\Lambda_+K^\circ_{1^\circ}$. This measurement was consistent within the statistical errors of $\alpha\bar{P} = +.32 \pm 0.11$ for the double V sample.

---

[1] This useful calculation was originally programmed for the IBM 704 computer by G. Trilling.

TABLE 15

ASYMMETRY PARAMETER DETERMINATIONS

TYPE OF SAMPLE	ASYMMETRY AND ERRORS	NO. OF EVENTS
Double V° Samples		
K°_{1+} with Λ_+ - control sample 1.0 Bev	-0.13 ± 0.15	140
$\Lambda_+ K^{\circ}_{1+}$ (1.0 - 1.1 Bev)	+0.32 ± 0.11	222
$\Lambda_+ K^{\circ}_{1+}$ (1.0 Bev)	+0.34 ± 0.16	86
$\Lambda_+ K^{\circ}_{1+}$ (1.1 Bev)	+0.32 ± 0.14	136
$\Lambda_+ K^{\circ}_{1+}$ (1.0 - 1.1 Bev) $\lvert\vec{p}_\Lambda\rvert < 0.500$ Bev/c	+0.26 ± 0.14	126
$\Lambda_+ K^{\circ}_{1+}$ (1.0 - 1.1 Bev) $\lvert\vec{p}_\Lambda\rvert > 0.500$ Bev/c	+0.38 ± 0.14	96.
Single V° Samples		
Single K°_{1+} - control sample 1.0 Bev	-0.10 ± 0.19	80
Single Λ_+ (1.0 - 1.1 Bev)	+0.05 ± 0.11	233
Single Λ_+ (1.0 - 1.1 Bev) $\lvert\vec{p}_\Lambda\rvert > 0.500$ Bev/c	+0.17 ± 0.15	118
Single Λ_+ (1.0 - 1.1 Bev) $\lvert\vec{p}_\Lambda\rvert < 0.500$ Bev/c	-0.05 ± 0.14	115
Other Samples		
$\Lambda_+ K^+$ (decay or escape) (1.0 - 1.1 Bev)	+0.29 ± 0.16	130
Λ_+ (and 2, 3, or 4 γ rays) (1.0 - 1.1 Bev)	+0.32 ± 0.27	60

APPENDIX A

DENSITY OF LIQUID XENON

A.1 Direct Measurement of the Density

In the interval since the discovery of xenon in 1898 by Ramsey and Travers only one measurement of the density of liquid xenon as a function of temperature had appeared in the literature. The accuracy of this measurement[21], performed in 1912, was questioned since the quantity of xenon used was small and the purity uncertain.

For this reason, the density of highly pure xenon[1] was measured over the entire range of the liquid phase. The mean value of the density fitted the empirical equation

$$\frac{\rho_L + \rho_V}{2} = 1.149 - 2.95 \times 10^{-3} \; t$$

where

ρ_L = the liquid density in gms/cm.^{3},

ρ_V = the vapor density in gms/cm.^{3}, and

t = the temperature in °C.

The critical density found from the preceding equation was 1.100 gms/cm.^{3}

---

[1] The maximum total impurities did not exceed 0.01%, based on mass spectrometric analysis of the sample by Linde Air Products Company. before use.

The experiment also yielded data concerning the densities of the liquid and vapor phases.

Experimental Method

The density of liquid xenon was determined by a method chosen to satisfy the following conditions:

(1) The total amount of xenon used was to be relatively small, 2-3 grams

(2) Measurements were to be performed throughout the temperature range of the liquid phase

(3) Measurements were to be accurate to ±1%

The method consisted of condensing and sealing xenon into a 0.3 cm (nominal) heavy wall pyrex capillary tube which was approximately 20 cm in length. A large enough mass of xenon was introduced into the capillary tube so that the liquid phase would be present up to the critical point. Two such capillary tubes were prepared containing different masses of xenon.[1] When both of these tubes were immersed completely in a bath at the same temperature, t,

$$m_1 = [\rho_L g h_1 + \rho_V g(L_1 - h_1)] A_1$$

$$m_2 = [\rho_L g h_2 + \rho_V g(L_2 - h_2)] A_2$$

[1] The two masses of xenon were approximately 1.1 and 1.5 gms.

where

m = total mass of xenon,

h = height of the liquid phase,

L = total inside length of the capillary,

A = average cross-sectional area of capillary,

ρ_V = density of xenon vapor, and

ρ_L = density of xenon liquid.

The simultaneous solution of the above equations together with a knowledge of the constants specified both the liquid and vapor densities at a particular temperature, t.

The actual measurement was performed with one capillary tube immersed at a time in an unsilvered cylindrical Dewar vessel, 35 cm long and 5 cm inside diameter. The Dewar was filled with an isopentane bath which was initially chilled to -130°C. Incident radiant energy warmed up the bath at the rate of approximately 15° per hour. As the temperature changed, the relative proportions of xenon in the liquid and vapor phases changed. The length of the column of liquid in the vapor phase was measured with a precision cathetometer every two degrees. In this way data for the determination of the density could be obtained anywhere in the region between the melting point and the critical point (-112 to 16.6°C). Difficulties in the measurement of the density occur at the extremes of this range. At temperatures close to the melting point, the mass of xenon in the vapor phase was small and therefore the

vapor density could not be determined accurately. At temperatures near the critical point the density changed too rapidly to be measured.

The mass of xenon trapped in the capillary was determined by weighing the capillary filled with xenon and then weighing the capillary empty, after cracking the capillary open at low temperature and allowing the xenon to vaporize. Weights were measured to 0.001 gms with a precision balance. The average cross-sectional area of the capillary was found by filling the capillary with mercury, measuring the height of the column of mercury with the cathetometer and then determining the mass of mercury by a difference weighing. Lengths were measured to ± 0.02 cm. with the cathetometer. Temperature measurements were made ± 0.2°C with a thermometer calibrated at the ice point ± 0.2°C.

Systematic Errors

The best check for overall accuracy and lack of systematic error would have been to measure the density of liquid ethylene. The physical properties of ethylene are so similar to xenon that the measurement would have been carried out over the identical temperature range. However, a simpler, although not as good control measurement was performed. The density of reagent grade carbon tetrachloride was measured by the same method as the xenon except that the measurement was performed at room temperature. The value of the density of carbon tetrachloride for each of two measurements compared with the value printed on the bottle within 1/2%.

A.2 Measurements of the Critical Density

We can rewrite the mean value of the density as

$$\frac{\rho_L + \rho_V}{2} = \rho_c + \beta (t - t_c)$$

where

β = constant in units of gm/cm ^{3} °C

ρ_c = critical density of xenon in gm/cm ^{3}

t = temperature in °C, and

t_c = critical temperature in °C

In this form the present determination gave the result

$$\frac{\rho_L + \rho_V}{2} = 1.100 + 2.95 \times 10^{-3} (t - t_c)$$

while the measurement of Patterson gave[21]

$$\frac{\rho_L + \rho_V}{2} = 1.155 + 3.055 \times 10^{-3} (t - t_c)$$

solving for the liquid density

$$\rho_L = 2\rho_c + 2\beta (t - t_c) - \rho_V$$

The liquid density is most sensitive to the value of the critical density; β and ρ_V are known to within 5% so that their uncertainty contributes a total error of about 1%.

A number of recent measurements of the critical density of pure xenon have been published[22, 23, 24], these results are

$\rho_c = 1.105$ [22]

$\rho_c = 1.110 \pm 0.002$ [23]

$$\rho_c = 1.099 \pm 0.002 \qquad [24]$$

$$\langle \rho_c \rangle = 1.105 \pm 0.005$$

where an error was inserted as a measure of the spread of these measurements.

The average critical density of 1.105 gms/cm^3 was in accord with our measurement of 1.100 ± 0.015 gms/cm^3. None of these measurements agreed with the higher and less recent value of 1.155 gms/cm^3.

We accepted the more recent measurements of the critical density and took the value ρ_c = 1.105 gms/cm^3. Once this value of the critical density was accepted, then values of the liquid density for all temperatures could be obtained to an accuracy of about 1%. The original value given for the density of xenon in the bubble chamber at the operating temperature ρ_L = 2.17 gms/cm^3. was based on the value of ρ_c = 1.100 gms/cm^3.

A.3 Range Energy Relations and the Density of Xenon

In the π^- experiment, five events were found where the entire range of the π^+ secondary from the $K_{\pi 2}$ decay was observed in the bubble chamber. Events were carefully checked for absence of inelastic interactions so that the observed pion range was due to ionization loss only. These observed ranges are given in Table 16.

TABLE 16

π^+ RANGE FROM $K_{\pi 2}$ DECAY

Frame Number	Observed Pion Range in cm
022151	23.72
085622	24.39
088657	23.19
096238	23.95
101869	23.71

A correction to the observed mean range of 23.79 cm for the error in measuring chords, raised the value of the mean range to 24.2 ± 0.3 cm, where possible measuring and straggling errors of the order of 0.3 cm were assumed. The calculated range from latest range energy calculations of Trilling[25] was 55.55 gm/cm^2, which implied a density of xenon of 2.30 ± 0.03 gm/cm^3.

This value of the density of xenon made the range energy relations self-consistent and therefore should be used to determine particle ionization losses in xenon.

In the analysis of the π^- experiment, the value of the density of xenon used in evaluating a different set of range energy relations was

2.167 gm/cm^3. For this set of range energy relations, differen . and considerably lower values of the ionization potential were used. The predicted $K_{\pi 2}$ range was 24.5 cm for this set of range energy relations. The observed range was found to be 24.2 cm. This comparison implied that the range energy relations used in the analysis of the π^- experiment were to a high degree self-consistent.

Nevertheless, a question remains concerning the correct value of the density of xenon nuclei for nuclear interaction estimates. We have used, for the density of xenon, the average of the value from the direct measurement and the value of 2.30 gm/cm^3 from the range energy relations.

APPENDIX B

$K_1^\circ - K_2^\circ$ MASS DIFFERENCE CALCULATION

The normalized probability function describing the chance of the i^{th} $\bar{K}^\circ$ interacting in a time interval in the laboratory between $t_{i\ max}$ and $t_{i\ min}$ was given in Section 5.4 as[1]

$$f_i(\mu,t) = \frac{F_i(\mu,t)}{\int_{t_{min}}^{t_{max}} F_i(\mu,t)\, dt}$$

with $F_i(\mu,t)$ defined as

$$F_i(\mu,t) = \frac{1}{2}\left(e^{\frac{-(\delta+1)\ t}{2\gamma\tau_1}}\right)\left(\cosh\ \frac{t}{2\gamma\tau_1} - \cos\ \frac{\mu t}{\gamma\tau_1}\right)$$

in terms of x, the distance of the $\bar{K}^\circ$ interaction from the beam origin

$$F_i(\mu,t) = \frac{1}{2}\left(e^{\frac{-(\delta+1)\ x}{pc\tau_1/M_K}}\right)\left(\cosh\ \frac{x}{2pc\tau_1/M_K} - \cos\ \frac{\mu x}{pc\tau_1/M_K}\right)$$

The Likelihood Function $L(\mu)$ for n events was

$$L(\mu) = \prod_{i=1}^{n} f_i\left(\mu, \frac{\gamma_i x_i}{p_i c\tau_1/M_K}\right)$$

where

x_i = distance of i^{th} $\bar{K}^\circ$ interaction from beam origin in cm

p_i = momentum of i^{th} $\bar{K}^\circ$ in Mev/c

---

[1] The notation used is the same as in Section 5.4.

In the xenon bubble chamber the momentum of the $\bar{K}^\circ$ which caused a particular interaction cannot be determined. However, we can evaluate the likelihood function if we integrate over the $\bar{K}^\circ$ momentum distribution, G(p).

$$L(\mu) = \prod_{i=1}^{n} \int_0^\infty f_i \left(\mu, \frac{\gamma x_i}{pc\tau_1/M_\kappa} \right) G(p) \, dp$$

In practice, we replaced this integration of G(p) by an averaging procedure and used the observed charged K_1° momentum distribution as the $\bar{K}^\circ$ momentum distribution. In addition, the observed charged K_1° momentum distribution was corrected for the geometric observational biases - for short decays and escape.

$$L(\mu) = \prod_{i=1}^{n} \frac{1}{r} \sum_{j=1}^{r} f_i \frac{\left(\mu, \frac{\gamma_j x_i}{p_j c\tau_1/M_\kappa} \right)}{\left(e^{-\frac{0.5}{p_j c\tau_1/M_\kappa}} - e^{-\frac{\text{pot. path}}{p_j c\tau_1/M_\kappa}} \right)}$$

where

r = number of charged K_1° in the momentum distribution

M_κ = rest mass of K° meson in Mev

The normalization integral, which appears in the following expression:

$$f_i \left(\mu, \frac{\gamma_j x_i}{p_j c\tau_1/M_\kappa} \right) = \frac{F_i \left(\mu, \frac{\gamma_j x_i}{p_j c\tau_1/M_\kappa} \right)}{\int_{\frac{x_{min}}{p_j c\tau_1/M_\kappa}}^{\frac{x_{max}}{p_j c\tau_1/M_\kappa}} F_i \left(\mu, \frac{\gamma_j x_i}{p_j c\tau_1/M_\kappa} \right) dx}$$

has been evaluated in closed form

$$I(\mu,\xi_{ij}) = \frac{p_j c\tau_i}{M_\kappa \lambda} \left[\frac{e^{a\xi_{ij}}}{4} \left(\frac{e^{\xi_{ij}/2}}{a + \frac{1}{2}} + \frac{e^{-\xi_{ij}/2}}{a - \frac{1}{2}} - \frac{2a \cos \mu\xi_{ij}}{a^2 + \mu^2} - \frac{2\mu \sin \mu\xi_{ij}}{a^2 + \mu^2} \right) \right]_{\xi_{min}}^{\xi_{max}}$$

where

$$\xi_{ij} = \frac{x_i}{p_j c\tau_1 / M_\kappa}$$

$$a = \frac{\delta + 1}{2}$$

APPENDIX C

LISTS OF DATA

TABLE 17

K° INTERACTION DATA**

Frame	Distance of Interaction From Origin	Potential Path Length of K° *	Star Products	Beam Origin Hyperon
008243	11.70	17.81	Λ_+, p_Λ=370	Λ_+, p_Λ=325
012247	12.76	19.21	$\Sigma^\pm$	Λ_+, p_Λ=240
025379	12.25	13.70	$\pi^\pm$, Λ_+, p_Λ=100	Λ_+, p_Λ=580
042690	02.42	18.43	$\Sigma^\pm$	Λ_+, p_Λ=580
047435	06.32	13.89	Λ_+, p_Λ=580	Λ_o (2γ)
070412	06.93	08.33	Λ_+, p_Λ=150	Λ_+, p_Λ=185
073011	04.90	17.38	Λ_+, p_Λ=448	Λ_+, p_Λ=745
083182	08.59	20.24	Λ_+, p_Λ=260	Λ_o (2γ)
085343	10.32	20.97	π°, Λ_+, p_Λ=370	Σ^-
102773	05.36	12.71	π^+, Λ_+, p_Λ=480	Λ_+, p_Λ=1300
103560	08.36	16.26	$\Sigma^\pm$	Λ_+, p_Λ=1120
107389	11.36	16.66	$\pi^\pm$, Λ_+, p_Λ=825	Λ_+, p_Λ=450
121537	00.56	10.38	Λ_+, p_Λ=390	Λ_+, p_Λ=625
036052	05.49	13.38	K^+, p_{K^+}=265	Λ_+, p_Λ=700
102033	02.54	15.01	K^+, p_{K^+}=365	Λ_+, p_Λ=760

* Potential path lengths were calculated for a chamber of radius 12.5 cm and $1 \leq z \leq 24$.

** Momenta are given in Mev/c and distances in cm.

TABLE 18

CROSS-SECTION SAMPLES

ΛK° Cross Section

Frame	p_Λ	Λ Prod. Angle	p_K	K° Prod. Angle	Total Correction
004348	220	31.1	420	52.3	2.22
004391	940	34.2	150	123.1	2.35
005601	730	24.3	330	48.3	1.93
009029	605	35.4	620	26.2	1.38
009655	290	93.1	440	18.0	1.67
012662	400	54.4	250	67.9	1.39
015353	580	13.1	260	22.8	1.67
017538	365	12.7	360	50.8	1.38
018435	340	20.0	490	68.6	1.50
019737	540	30.9	310	65.9	1.56
021006	410	63.1	430	51.1	2.33
023432	520	24.1	310	66.8	1.56
024016	520	106.8	610	25.7	1.53
026311	450	86.6	340	09.4	1.53
026838	1030	34.5	280	43.3	1.91
027324	500	36.6	210	70.2	3.84
028556	590	40.3	400	74.6	1.51
032080	400	46.0	590	25.1	1.21
033843	540	49.7	540	22.6	1.44
037193	430	38.6	360	88.8	1.51
039355	690	49.4	330	30.4	1.66
039660	180	20.9	780	04.5	2.68
039882	770	48.5	300	31.7	1.59
039898	240	61.0	230	123.7	2.37
041301	570	32.8	190	112.4	1.92
042184	480	31.7	510	61.2	2.77
047051	485	16.9	580	14.9	2.08
050456	300	68.3	540	19.6	1.52
051870	460	23.7	430	32.1	1.63
051975	590	21.1	160	97.3	2.04
052293	220	53.3	670	08.4	2.60
057303	610	31.4	580	15.6	1.54
059311	630	17.3	490	37.3	1.47
059541	840	18.4	410	50.0	1.62
059569	560	32.0	570	16.6	1.40
059574	250	61.9	280	46.9	2.22
061458	590	28.0	580	24.9	1.42
064511	510	19.7	580	12.2	1.41
066193	820	11.9	400	57.0	1.68
066501	520	12.7	650	18.5	1.44

TABLE 18 (Continued)

ΛK° Cross Section

Frame	p_Λ	Λ Prod. Angle	p_K	K° Prod. Angle	Total Correction
068417	540	77.5	650	47.9	2.20
070772	485	23.9	715	33.4	1.96
071029	490	65.1	460	82.4	1.51
071469	275	43.6	260	102.1	2.03
075718	640	07.3	270	27.5	1.64
076281	460	31.2	460	13.7	1.43
076421	650	26.1	400	96.6	4.78
077638	1090	32.5	500	36.3	1.78
080965	550	17.9	650	23.3	1.74
081167	1050	27.0	170	27.9	2.13
081347	270	65.3	380	36.9	3.44
081591	230	33.3	750	16.3	2.02
082767	700	09.4	190	89.9	2.51
083416	460	09.3	380	127.1	1.51
084008	340	148.4	500	22.9	1.48
084126	480	40.7	460	27.7	1.47
087785	170	53.8	220	81.6	3.82
088319	750	01.8	720	02.8	1.42
088508	740	78.9	180	09.8	2.06
088601	550	62.3	280	70.5	1.61
089270	240	42.9	240	160.7	2.33
089321	250	167.7	330	51.0	2.08
089794	750	23.1	240	108.4	2.14
091372	150	81.3	215	104.5	4.55
092872	1100	11.2	270	44.0	1.61
095854	280	27.6	410	28.5	1.73
096876	270	68.4	840	08.5	1.73
097016	440	17.3	340	102.5	1.66
097063	390	29.5	760	16.2	1.26
097840	550	58.0	360	49.0	1.53
099001	490	83.3	150	124.6	2.08
099655	800	20.1	640	30.7	1.34
101202	810	40.3	270	41.5	1.64
101573	275	36.1	650	85.7	4.09
101997	485	18.6	670	06.8	1.59
102465	380	75.9	505	35.6	1.35
102485	830	32.5	675	38.8	1.41
104013	850	20.5	330	35.3	2.35
107442	480	113.4	215	160.6	1.74
107774	490	47.0	520	49.2	1.41
108103	560	11.9	390	86.8	1.51

TABLE 18 (Continued)

ΛK° Cross Section

Frame	p_Λ	Λ Prod. Angle	p_K	K° Prod. Angle	Total Correction
108567	190	32.8	200	89.8	3.32
108839	440	08.2	530	09.7	1.41
110004	590	23.8	680	28.8	3.14
110852	890	22.2	570	23.5	1.41
111751	230	114.0	740	23.9	2.18
111916	375	67.4	410	52.4	1.29
112110	250	75.5	270	42.1	2.15
113887	500	25.2	730	14.4	12.47
114503	660	29.3	730	42.2	1.37
115971	530	41.6	460	43.8	1.43
116779	270	45.4	670	22.5	1.89
116789	680	27.7	270	123.1	2.00
117513	400	69.5	660	17.6	2.17
118712	260	43.7	530	65.9	1.90
120258	520	29.4	634	26.9	1.44
121400	420	73.9	290	40.7	1.69
122063	570	33.8	720	30.2	1.45
124106	200	31.6	210	107.3	3.05
126193	350	87.0	150	143.0	1.95
128182	880	17.1	440	39.2	1.72
128540	200	37.4	810	37.3	2.42
128591	980	09.6	160	127.7	3.31
129228	340	51.8	650	37.3	1.91
129707	650	53.2	550	39.4	1.69
129728	500	29.1	180	112.2	2.09
130724	630	29.8	465	101.4	1.54
134718	350	148.8	700	25.7	1.34
135120	430	41.0	100	80.0	2.89
136418	620	29.4	800	22.3	1.41
137873	740	13.0	280	113.5	1.64
139599	485	47.0	690	14.0	1.38

TABLE 18 (Continued)

$\Lambda - K^+$ Cross Section

Frame	p_Λ	Λ Prod. Angle	p_K	K° Prod. Angle	Total Correction
8992	250	94.5	200	155.2	1.58
16759	410	46.2	290	65.2	1.32
20715	367	33.2	285	95.3	1.22
23968	420	08.3	314	138.5	1.20
24713	350	10.4	285	57.9	1.24
27748	800	21.3	262	35.7	1.19
29229	337	122.7	230	109.7	1.26
30742	415	33.0	>350	35.0	1.21
32898	570	36.1	>208	105.5	1.26
34627	450	34.8	317	107.3	2.69
35873	560	19.7	235	66.3	1.24
36348	500	61.2	364	61.1	1.21
43147	470	26.2	>362	26.7	1.26
44054	850	04.9	348	126.7	1.23
44270	520	91.9	324	57.1	1.29
50242	200	23.4	337	73.2	2.06
51916	380	41.4	375	29.0	1.22
52069	930	19.0	169	104.1	1.34
52252	455	59.1	317	49.1	1.20
53007	320	76.6	215	65.5	1.43
53578	330	78.2	200	78.9	1.29
57317	670	43.8	>328	44.5	1.22
61133	430	84.6	>325	29.0	1.22
61269	700	14.3	206	144.4	1.19
64595	500	40.9	206 -	59.3	1.52
65872	340	90.0	242	42.8	1.26

TABLE 18 (Continued)

$\Sigma^{\circ}K^{\circ}$ Cross Section

Frame	p_{Λ}	Λ Prod. Angle	p_K	K° Prod. Angle	Total Correction
14971	275	92.8	440	13.3	2.20
15401	540	17.1	220	80.3	2.26
22215	250	08.7	390	72.4	2.60
67634	600	48.6	200	78.1	2.30
90106	440	40.0	420	85.7	1.72
112059	680	09.0	450	140.3	2.10
117549	900	06.0	350	22.9	1.86
136404	830	29.9	320	29.4	1.92

BIBLIOGRAPHY

1. Alikhanian, et al., Zh. eksper. teor. Fiz., 31, 955 (1956).
2. Yamanauchi, Phys. Rev. Letters, 3, 480 (1959).
3. Brown, et al., Phys. Rev. Letters, 3, 51 (1959).
4. Brown, et al., Phys. Rev. Letters, 3, 653 (1959).
5. Morris, Fowler, and Garrison, Physical Review, 103, 1472 (1956).
6. Brown, J. L., thesis, The University of Michigan, 1958 (unpublished).
7. Hartung, R. W., private communication.
8. Cronin, Cool, and Abashian, Physical Review, 107, 1121 (1957).
9. Cool, Cork, Cronin, and Wenzel, Physical Review, 114, 912 (1959).
10. Wilcox, UCRL Report - 3475 (1956).
11. Sartori, Werbrouck, Wooten, and Bivins, private communication.
12. 1958 International Conference on High Energy Physics at CERN, Proceedings, IUPAP, 174 (Geneva, 1958).
13. Crawford, et al., Phys. Rev. Letters, 2, 361 (1959).
14. Bowen, et al., "Production of Strange Particles by 1.5 Bev π^- Mesons in C, Fe, and Pb," in press.
15. Gell-Mann and Pais, Physical Review, 97, 1387 (1955).
16. Bolt, Caldwell, and Pal, Physical Review, 150 (1958).
17. Fry and Sachs, Physical Review, 109, 2212 (1958).
18. Freden, Gilbert, and White, Physical Review, 118, 564 (1960).
19. Crawford, et al., Physical Review, 108, 1102 (1957).

20. Bowen, et al., Phys. Rev. Letters, 1, 11 (1958).

21. Patterson, Cripps, and Whytlaw-Gray, Proc. Royal Soc., A 86, 579 (1912).

22. Weinberger and Schneider, Canadian Journal of Chemistry, 30, 422 (1952).

23. Habgood and Schneider, Canadian Journal of Chemistry, 32, 98 (1953).

24. Whiteway and Mason, Canadian Journal of Chemistry, 31, 569 (1952).

25. G. Trilling, private communication.